

Dissertation zur Erlangung des Doktorgrades
der Fakultät für Chemie und Pharmazie
der Ludwig-Maximilians-Universität München



Oligonucleotides for enhancing intracellular
delivery and monitoring intracellular stability of
synthetic RNAi nanoagents

Philipp Michael Heißig

aus

Erlenbach am Main

2017

Erklärung

Diese Dissertation wurde im Sinne von § 7 der Promotionsordnung vom 28. November 2011 von Herrn Prof. Dr. Ernst Wagner betreut.

Eidesstattliche Versicherung

Diese Dissertation wurde eigenständig und ohne unerlaubte Hilfe erarbeitet.

München, 16.01.2017

.....
Philipp Heißig

Dissertation eingereicht am 16.01.2017

1. Gutachter: Prof. Dr. Ernst Wagner

2. Gutachter: Prof. Dr. Don C. Lamb

Mündliche Prüfung am 28.02.2017

Table of contents

1. Introduction	1
1.1. DNA as a tunable adaptor for siRNA polyplex stabilization and functionalization	1
1.1.1. RNA interference.....	1
1.1.2. siRNA as a therapeutic tool.....	4
1.1.3. Sequence-defined cationic oligomers.....	6
1.1.4. DNA as building block	7
1.1.5. siRNA extension.....	8
1.2. Localization and integrity of small single-stranded RNA.....	9
1.2.1. Single-stranded oligonucleotide therapeutics.....	9
1.2.2. Unspecific RNases	10
1.2.3. Chemical modification of RNA	11
1.2.4. Localization and stability of small RNA.....	12
1.3. Aims of the thesis	13
2. Materials and Methods	15
2.1. Materials	15
2.1.1. Oligonucleotides.....	15
2.1.1.1. eGFP siRNAs.....	15
2.1.1.2. CTRL siRNAs.....	15
2.1.1.3. Modified RNA single-strands.....	16
2.1.1.4. DNA extensions/adaptors	16
2.1.2. Cationic oligomers	17
2.1.3. Reagents	17
2.1.4. Buffers.....	18
2.1.5. Cell lines	19
2.2. Methods	20
2.2.1. Conjugation and assembly of oligonucleotides and DNA nanostructures	20
2.2.1.1. Assembly of the siRNAs and the DNA nanostructures	20
2.2.1.2. Coupling of the DNA extensions to the siRNA passenger strands with disulfide chemistry.....	20

2.2.1.3.	Coupling of DNA extension strands to INF7	21
2.2.1.4.	Labelling of the RNA oligonucleotides with Atto488 and tetramethylrhodamine	21
2.2.1.5.	Purification with high performance liquid chromatography	21
2.2.1.6.	Native polyacrylamide gel electrophoresis	22
2.2.2.	Polyplex formation and analysis	22
2.2.2.1.	Polyplex formation.....	22
2.2.2.2.	Dynamic light scattering	22
2.2.2.3.	siRNA binding assay.....	23
2.2.3.	Cell culture	23
2.2.3.1.	Cultivation of cells	23
2.2.4.	Transfection of N2A/eGFPluc and KB/eGFPluc cells for downregulation of eGFPluc	23
2.2.4.1.	MTT assay.....	24
2.2.4.2.	Transfection of HeLa cells in chamber slides	24
2.2.5.	RNA stability and localization measurements	24
2.2.5.1.	HeLa whole cell extracts	24
2.2.5.2.	Cell extract measurements	25
2.2.5.3.	FLIM measurements on fixed cells.....	25
3.	Results and Discussion.....	27
3.1.	DNA adaptors for siRNA polyplex formation.....	27
3.1.1.	Design of the basic DNA nanostructure and the delivery agent.....	27
3.1.2.	Variables in transfection efficiency.....	29
3.1.3.	More complex structures	31
3.1.4.	Simpler structures.....	33
3.1.5.	Single-stranded versus double-stranded	34
3.1.6.	Optimal length of DNA sequence per siRNA.....	35
3.1.7.	Reducible vs. non-reducible siRNA attachment.....	36
3.1.8.	Challenging the constructs	39
3.1.9.	Luciferase knockdown is mediated by eGFP siRNA.....	40
3.1.10.	Stability and particle sizes	42
3.1.11.	Different polycations for siRNA transfection	44

3.1.12. Attachment of functional domains to siRNA	46
3.2. Localization and integrity of small single-stranded RNA	50
3.2.1. Oligonucleotide Design	50
3.2.2. Stability evaluation in cell extracts.....	52
3.2.2.1. Fluorescence correlation spectroscopy	52
3.2.2.2. Fluorescence cross-correlation spectroscopy	54
3.2.2.3. Förster resonance energy transfer	55
3.2.3. Measurements in cells	57
3.2.3.1. Transfection.....	57
3.2.3.2. Fluorescence intensity.....	58
3.2.3.3. Fluorescence lifetime in cells.....	61
4. Conclusions	68
4.1. DNA as a tunable adaptor for siRNA polyplex stabilization and functionalization ..	68
4.2. Localization and integrity of small single-stranded RNA.....	71
5. Summary.....	74
6. Appendix.....	76
6.1. Abbreviations	76
6.2. Additional methods.....	78
6.2.1. Intensity FRET analysis	78
6.2.2. Lifetime FRET analysis	78
6.2.3. FCS and FCCS analysis.....	79
6.2.4. FLIM analysis.....	80
6.3. Appendix figures.....	81
6.4. Publications	83
6.5. Poster presentations.....	83
7. References.....	84
8. Acknowledgments	89

1. Introduction

1.1. DNA as a tunable adaptor for siRNA polyplex stabilization and functionalization

1.1.1. RNA interference

The first mention of RNA interference was in 1993, when Ambros and co-workers discovered that LIN-14 protein downregulation in *C. elegans* is not mediated by proteins [1]. The *lin-14* locus was found to code for RNA transcripts complementary to short repeats in the 3' untranslated region (3' UTR) of the *lin-14* mRNA, which turned out to be responsible for this phenomenon. With the discovery of other regulatory RNAs in *C. elegans* and various organisms in the early 2000s [2, 3], it became apparent that this was not a single case. The effectors were 21- to 23-nucleotide double-stranded RNAs mediating gene silencing on the mRNA level, termed microRNAs.

In the meantime, it was discovered that introduction of artificial small double-stranded RNA (termed siRNA) could mediate knockdown of a gene of interest guided through complementary base pairing to the coding mRNA as demonstrated separately by Mello [4] and Tuschl [5].

Soon after, the catalytic mechanism behind the RNA interference process was elucidated. The major effector machinery was the RNA induced silencing complex (RISC), consisting of the complementary short RNA and multiple proteins with different functions in RNA loading, anchoring and target mRNA processing [6].

The discovery of RNA interference opened the door for therapeutic intervention in various directions. Artificial introduction of siRNA or microRNA is utilized to regulate gene expression on the mRNA level and interference with the endogenous microRNA machinery is achieved through antisense approaches.

Despite their different origins, siRNAs and microRNAs have in common that they are processed from longer double-strands by the RNase III family endonuclease Dicer into 21 to 23 base pairs double-strands, leaving a two nucleotides 3' overhang and 5' monophosphates (Figure 1) [7]. This active form is loaded into the RISC complex. An

Argonaute family protein, which is part of the RISC complex, anchors the siRNA/microRNA [8]. The strand with the least thermostable base pairs at the 5' end is selected as guide strand, which directs the RISC complex to the target site through complementary base pairing [9]. The passenger strand is removed and either degraded or incorporated as a new additional guide strand [10]. For target mRNA processing, two cases have to be distinguished. Either the mRNA is cleaved at a defined position between nucleotide 10 and 11 counted from the 5' end of the guide strand, followed by exonucleolytic degradation, or the RISC complex remains associated to the target mRNA leading to translational repression. Prerequisites for the prior case are a perfect sequence match between the guide strand and the target mRNA and the presence of Argonaute 2 as part of the RISC complex. Argonaute 2 is the only protein of the Argonaute family executing RNase H activity [11]. In any other case, gene silencing is accomplished by translational repression.

Differences between siRNA and microRNA can be found in their origin. siRNAs are part of the defense mechanism against invasive nucleic acids from viruses, transposons or centromeres. Long double-stranded RNA is directly processed by Dicer and directed against the nucleic acids from which it is derived. Therefore siRNA guide strands are typically perfectly complementary to their target RNA which is processed *via* the Argonaute 2 dependent cleavage mechanism [8].

In contrast, microRNAs are endogenous regulatory elements. They are transcribed in the nucleus from non-coding regions commonly in clusters of several different microRNAs. These so-called pri-microRNAs are further processed by the RNase III family protein Drosha to pre-microRNAs, which are hairpin structures including only one microRNA [12]. After the protein exportin 5 mediates their translocation to the cytosol [13], the mature microRNA is generated by Dicer as described above (Figure 1). In mammalian cells, microRNAs mediate silencing almost exclusively through translational repression. Target sequences lie in the 3' UTR of the open reading frame and have several mismatches for pairing with the microRNA guide strand. A perfect match is only required for the seed region which comprises nucleotides 2 to 8 counted from the 5' end of the microRNA guide strand [14]. This implies that a single microRNA can have several targets and regulates expression of a set of proteins.

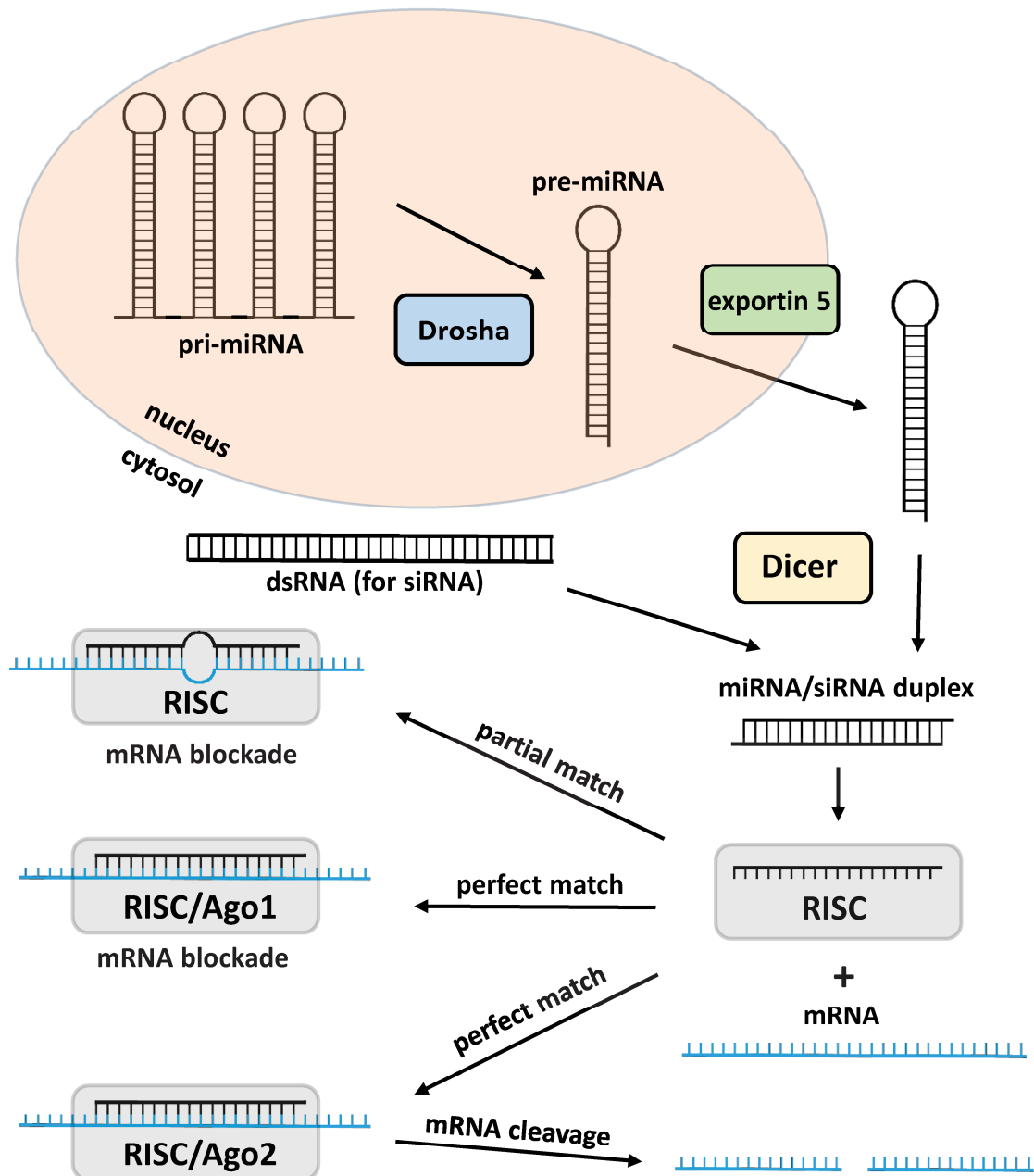


Figure 1. microRNA/siRNA biogenesis. The pri-microRNA is transcribed in the nucleus and trimmed by Drosha to pre-microRNA, which is a hairpin structure including one microRNA. The pre-microRNA is transported to the cytosol by exportin 5. This is where the pathway of microRNA and siRNA maturation come together. Long double-stranded RNA from exogenous origin (which is the precursor of siRNA) and pre-microRNA are both processed to their 21- to 23-base pair mature forms by the endonuclease Dicer. After incorporation into the RISC complex, mRNA downregulation is achieved by two different mechanisms. In case of a perfect sequence match to the target sequence and the presence of endonucleolytically active Argonaute 2 (Ago2) in the RISC complex, the mRNA is cleaved at a defined position (siRNA, microRNA in plants). Upon imperfect sequence match or presence of any other Argonaute protein (Ago1, Ago3, Ago4), the outcome is translational repression by mRNA blockade (microRNAs in mammals).

1.1.2. siRNA as a therapeutic tool

At a first glimpse, siRNA seems to be the perfect drug to conquer a huge variety of diseases associated with genetic dysregulation. The sequence can be designed complementary to any target mRNA, leading to knockdown of a protein of interest and interference with any cellular process. Once incorporated into the RISC complex, the siRNA guide strand is stable for weeks and able to recognize and cleave multiple mRNAs in a catalytic manner. Therefore only a few hundred siRNAs in the cytosol are sufficient to provide efficient downregulation of the target [15]. Nevertheless only a couple of siRNA based drugs have proceeded to late clinical phases so far. The utilization of siRNA as a therapeutic agent faces various obstacles, which are the subject of current research.

First of all, one has to differentiate between local and systemic administration. Local administration is less challenging as the delivery to the target tissue is not an issue here [16]. This is the reason why the only clinically approved RNA therapeutic is the aptamer Macugen against macular degeneration, which inhibits the vascular endothelial growth factor in the eye [17]. But as only few target sites like eye, skin or lung are accessible by local administration, systemic delivery *via* intravenous injection is required to access a broader spectrum of target tissues. The potential of this strategy is demonstrated by a recent boost in RNAi formulations in clinical trials targeting various cancers, the liver, the gastrointestinal tract and infectious diseases [18].

When entering the bloodstream, the siRNA molecule is exposed to a variety of molecules and blood cells. Recognition by Toll-like receptors and uptake by phagocytes leads to activation of the innate immune system [19, 20] and nucleases may rapidly degrade the siRNA. Some of these issues can be addressed by chemical modification of the siRNA itself. In addition, the siRNA can be packed into nanoparticles and shielded with hydrophilic molecules like polyethylene glycol to prevent interaction with the environment (Figure 2a).

After crossing the endothelial barrier and diffusing through the extracellular matrix, the siRNA has to enter the target cell. As both the siRNA and the cell membrane are negatively charged, a promising strategy has been to complex the siRNA with cationic polymers like polyethylenimine (PEI) to obtain nanoparticles with a positive surface charge and facilitated interaction (Figure 2b) [21]. One can further include a

ligand for a cell-type specific receptor to increase interaction and specificity. Once the siRNA has entered the cell through endocytosis, the next hurdle is the release to the cytosol, which is its site of action (Figure 2c).

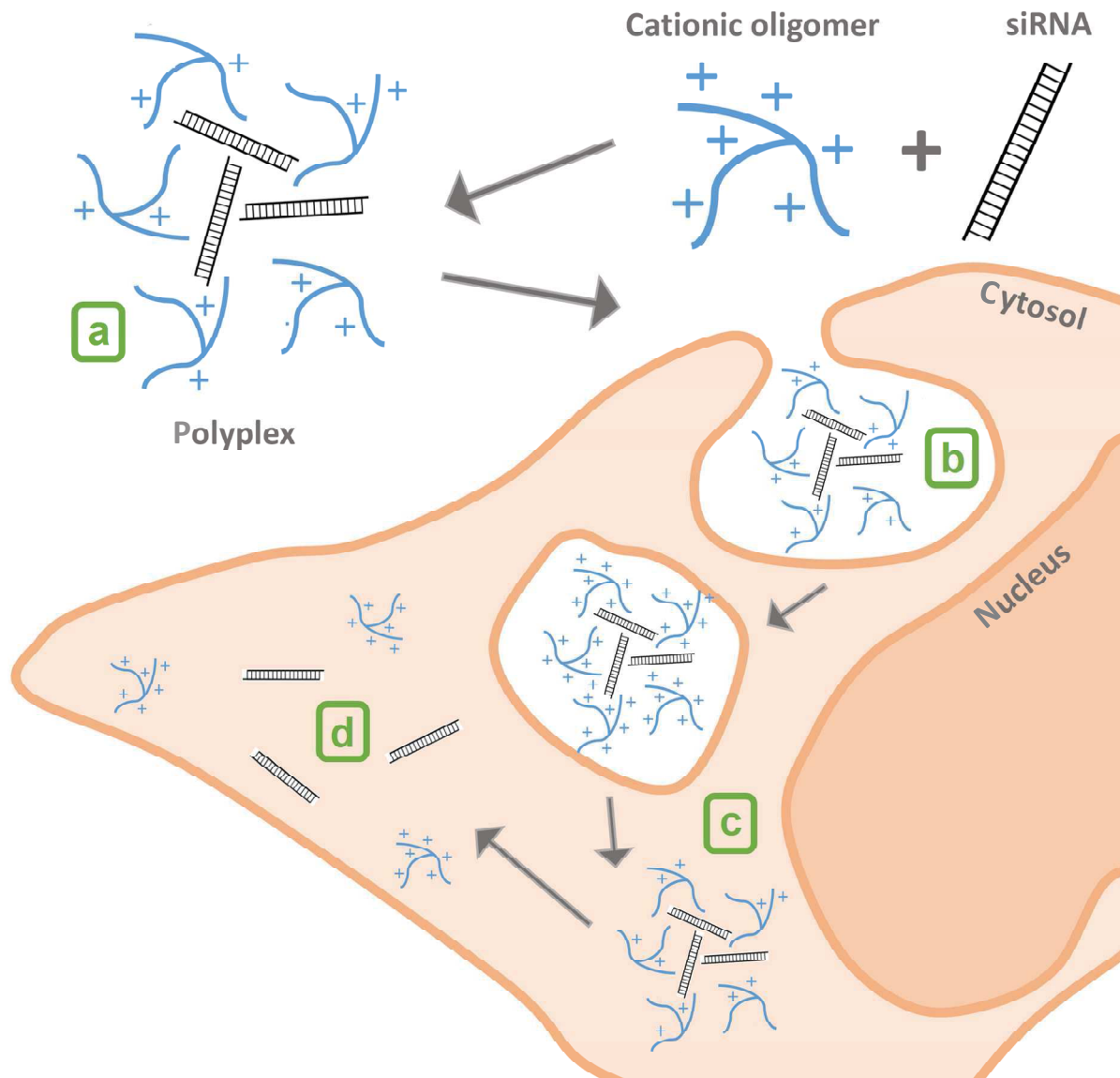


Figure 2. Barriers in siRNA delivery can be overcome with functionalized cationic oligomers.

(a) The siRNA is formulated into a nanoparticle. (b) Association and internalization of the polyplex into the target cell is facilitated by a positive zeta-potential and cell type-specific receptor binding. (c) Endosomal escape can be mediated by the proton sponge effect and membrane interacting peptides and fatty acids. (d) Including bioreducible disulfides facilitates dissociation of the siRNA from the oligomer. Finally the free siRNA can be incorporated into the RISC complex and exert its function.

Cationic carriers with a high buffer capacity can counteract the acidification of the endosome, leading to an increased influx of H^+ and Cl^- ions. Osmotic pressure

increases and the carrier becomes increasingly cationic and membrane-destabilizing. The endosome bursts and releases its cargo to the cytosol (proton sponge effect) [22, 23]. Membrane destabilizing peptides and membrane interacting fatty acids can promote liberation to the cytosol as well [24, 25]. A final step, before the siRNA can be incorporated into the RISC complex and guided to the mRNA of interest, is its release from the delivery vehicle. The reducing environment of the cytosol can be exploited by including disulfides which are stable in the extracellular environment, but reduced in the cytosol, leading to destabilization of the nanoparticle (Figure 2d) [26]. Even after functionally incorporated into the RISC complex, the siRNA can still exert toxicity through off-target effects. Seed region pairing to sequences in distinct mRNAs can lead to unwanted translational repression similar to the microRNA mechanism. This unspecific knockdown has shown to be reduced by 2'-O-Methyl ribose modification of the second nucleotide counted from the guide strand 5' end [27].

Taking all the above mentioned barriers into account, our working group is designing sequence defined carriers based on an oligoethan amino amide core conjugated to various functional entities to enable delivery of the siRNA to the target site [28].

1.1.3. Sequence-defined cationic oligomers

Our group has created a library of over 1000 sequence defined cationic oligomers by solid phase peptide synthesis (SPPS) to figure out how the abovementioned barriers can be overcome by combining functional entities in different ways (Figure 2). The core of the oligomers are SPPS-compatible oligoethan amino amide units like Stp (succinoyl-tetraethylene pentamine), Sph (succinyl-pentaethylene hexamine) or Gtp (glutaryl-tetraethylene pentamine) [29]. These artificial amino acids gain additional positive charges upon endosomal protonation. They can be combined to differently shaped structures (U-shaped, T-shaped, i-shaped, comb-like, dendrimers) by incorporation of branching lysines [30, 31].

Fatty acids or tyrosines can be included to provide stabilization through hydrophobic interaction [32]. Terminal cysteines stabilize the polyplex further in extracellular environment through disulfide bridging. Disulfides are reduced in the cytosol and promote the release of the siRNA from its carrier [33].

As the positive surface charge of nucleic acid/oligomer nanoparticles might promote aggregation with serum proteins, we use hydrophilic molecules like polyethylene glycol (PEG) for shielding. Also the particle size can be tuned by selecting PEG chains of different length [34]. In general, size is an issue that has to be considered carefully. Plain siRNA, for example, would be prone to rapid renal clearance due to its small size of only 2 x 7 nm [35]. Too large particles or aggregates however trigger toxicity in an *in vivo* setting. Interaction with the target cell can be facilitated by incorporating targeting ligands. Each cell type expresses a characteristic pattern of membrane proteins on their surface. A couple of receptors have been identified to be highly overexpressed in certain cancer types, representing attractive starting points for targeting ligand selection. Folic acid (targeting the folic acid receptor) [36], GE11 (targeting the EGF-receptor) [37] or transferrin (targeting the transferrin receptor) [38] were already successfully incorporated into the oligomers.

To circumvent endosomal entrapment, our group uses the endosomolytic peptide INF7, which is a synthetic analog of the influenza virus N-terminus of the hemagglutinin subunit HA-2 that in natural conditions triggers fusion with the endosomal membrane [39]. Including histidines increases the buffer capacity of the polyplex, promoting the proton sponge effect and the endosome to burst [22].

When optimizing the carrier, its nucleic acid cargo has to be taken into account. Polyplexes formed with plasmid DNA are generally more stable than those with siRNA [40]. The large size and high charge density of plasmid DNA promotes formation of robust interelectrolyte complexes, which is a requirement for an efficient delivery agent. siRNA is constrained to only 21 to 23 base pairs in its mature form and hence less suitable for stable polyplex formation. Therefore, better complexation can be achieved by direct modification of the siRNA. With its high charge density, good biocompatibility and inexpensive synthesis, DNA is an attractive option to extend siRNA for improved polyplex formation [41].

1.1.4. DNA as building block

In 1982, Seeman could demonstrate that DNA can be used to form structures that differ from the conventional linear double-strands by introducing junctions and assembling them into lattices [42]. In the following years, the utilization of DNA as a building block and not as a carrier of genetic information, has expanded peaking in

the invention of the DNA origami strategy in 2006 by Paul W. K. Rothemund [43]. By using a long backbone strand and numerous short staple strands, it was possible to design and assemble complex three-dimensional structures by Watson Crick base pairing. The design of such structures is facilitated by computational tools like CADnano [44] for complex DNA origamis or NUPack [45] for small assemblies. At the time, the toolbox of DNA nanostructures ranges from simple assemblies such as polyhedrons [46-48] up to very complex designs like tubes and boxes using the abovementioned DNA origami approach [41, 49, 50].

An attractive feature of DNA nanostructures is that functional domains can be placed at defined positions with high precision. As high definition is a prerequisite for reproducible therapeutic application, DNA is a highly suitable backbone for therapeutic cargo delivery. Despite additional favorable properties, like biocompatibility and easy synthesis, only a couple of them have been tested in siRNA delivery so far [51].

1.1.5. siRNA extension

The strategy of increasing the charge density of siRNA for better complexation with polycations has been pursued in several approaches during the past few years. An evident possibility is siRNA multimerization *via* sticky ends [52] or disulfide chemistry [53, 54]. A disadvantage of this strategy is that the number of siRNAs per structure is not uniform, which is a serious drawback when defined formulations are required. In this respect, the design of defined nanostructures came into focus. This can be achieved by utilizing chemical [55] or DNA based backbones, the latter being a key aspect of this work. This strategy has already demonstrated to improve transfection efficiency for small, medium-sized and large DNA backbones. Even short DNA overhangs increased transfection efficiency after complexation with polyethylenimine [56]. A few star-shaped structures [57-60] and a folate-targeted DNA tetrahedron hybridized to a defined number of siRNAs provided efficient uptake [61]. Furthermore, a DNA nanotube, also conjugated to folate, could successfully be delivered to folate receptor bearing cells [62]. However none of these studies sets a focus on which characteristics of the DNA extension/backbone are really necessary to improve delivery. For therapeutic administration, the nanostructure has to be

formulated into a drug agent that can be synthesized reproducibly in large scale. It is advisable to keep the construct as simple as possible.

1.2. Localization and integrity of small single-stranded RNA

1.2.1. Single-stranded oligonucleotide therapeutics

Apart from the double-stranded, canonical siRNA and microRNA formats, a huge variety of therapeutic approaches exist that utilize single-stranded RNA. Even the guide strands of siRNA and microRNA have shown to work without their passenger strands. In detail, a 2'-F/2'-O-Me/PS modified single-stranded siRNA guide strand was used to efficiently silence mutant Huntingtin allele in a HD model mice [63] (for detailed explanation of stabilizing RNA modification see chapter 1.2.3). A metabolically stable 5' phosphate (E-vinylphosphonate) is essential for *in vivo* activity [64]. Also single-stranded microRNA-mimics could guide gene silencing in cells in culture [65]. Advantages of the single-stranded format include the smaller size, the reduction of off-target effects as no passenger strand has to be co-delivered and the possibility to functionally deliver the siRNA without the need for formulation [64, 66].

A second class of therapeutic single-stranded RNAs is antisense oligonucleotides [67]. The sequences are designed to bind to mRNA at various positions and processing stages through complementary base pairing. In that respect, the specificity of RNase H for cleavage of RNA/DNA duplexes can be exploited by applying DNA strands complementary to the mRNA sequence, which should be inactivated [68].

Furthermore, antisense oligonucleotides can block cellular processes by binding to the mRNA. Miss-splicing diseases are especially suitable for antisense mediated therapy. Non-functional proteins are produced by wrong assembly of exons during splicing. Antisense oligonucleotides can bind to the regions responsible for the dysregulation and induce exon skipping or inclusion of exons to restore the correct protein variant [69, 70]. While an antisense preparation against Duchenne muscular dystrophy failed in clinical phase III [71], studies on spinal muscular atrophy are still

ongoing [72, 73]. Additional points for intervention by antisense oligonucleotides include inhibition of translation initiation, translational arrest and inhibition of polyadenylation by blocking the responsible region in the mRNA [74].

When antisense oligonucleotides are used to target microRNAs by complementarity to the guide strand, they are called antagomirs [75]. This class of small RNAs has been subject to extensive research in the past years. Various different backbone modifications have been evaluated for microRNA downregulation efficiency. A seminal work from 2006 demonstrates that PS/2'-O-Me modified oligonucleotides can be used to silence several microRNAs in mice [76]. Another interesting approach is locked nucleic acid modified oligonucleotides. The oxygen at 2' and the carbon at 4' position of the ribose are bridged leading to a rigid 3' endo conformation. Due to their high double-strand melting temperature, only a stretch of 8 nucleotides that targets the seed region of the microRNA is sufficient to provide its downregulation *in vivo* [77]. A promising candidate for HCV infection therapy in late clinical phases is miravirsen. The mir122 targeting 15-nucleotide sequence is composed of DNA nucleotides, locked nucleic acids and PS linkages [78].

An approach that is not based on complementary base pairing is CpG oligodeoxynucleotides. They are single-stranded DNA oligonucleotides containing an unmethylated cytosine/guanine motif, which act as immunostimulants through the Toll-like receptor 9 [79, 80].

1.2.2. Unspecific RNases

The cell has developed many pathways for RNA processing and degradation [81]. As this work focuses on the fate of single-stranded RNA, our interest is concentrated on unspecific ribonucleases (RNases) capable of cleaving single-stranded RNAs in mammalian cells. In general, RNases can be divided into three categories, namely endonucleases, 3'-5' exonucleases and 5'-3' exonucleases.

The most prominent mammalian endonucleases are part of the RNase A or RNase T2 family. The RNase A superfamily comprises RNase 1 to 8, which share a highly thermostable disulfide bonded structure, a pH optimum of around 8 and a specificity for cleavage of single-stranded RNA 3' of pyrimidines [82, 83]. RNase T2 family members have a broader range of substrates and are able to cleave next to all four bases. With a pH optimum of 4-5, they are most active in lysosomes [84].

Exonucleases either cleave in 3'-5' or in 5'-3' direction. The exosome is a multi-enzyme complex residing in the cytosol and the nucleus, which is responsible for 3'-5' degradation. The catalytically active domains are mammalian analogues to the bacterial polynucleotide phosphorylase (PNPase) [85]. In the cytoplasm, degradation from the 5'-3' direction can be accomplished in p-bodies. These are small cytoplasmic foci containing various enzymes involved in mRNA processing including exonuclease Xnr1 [86]. The Xnr1 paralogue Xnr2 is involved in RNA degradation in the nucleus [87].

1.2.3. Chemical modification of RNA

Single-stranded RNA oligonucleotides are especially susceptible to degradation by unspecific RNases. Apart from packaging the oligonucleotides into nanoparticles it has proven to be highly effective to chemically modify the RNA backbone.

During the past years a huge variety of internucleotide, sugar and base modifications have been developed, that can be implemented to increase stability, binding affinity and immunostimulatory properties. In the following, the chemical modifications used in this work are discussed in detail.

As internucleotide modification, phosphorothioate bonds were used instead of phosphodiester bonds (Figure 3). Replacing the oxygen with sulfur introduces chirality at the phosphate. In R conformation, the linkage is still susceptible to nucleolytic degradation. The S conformation however disturbs the active site of the nuclease, leading to the increased resistance. Apart from that favorable property, phosphorothioates reduce complement binding affinity compared to unmodified RNA [88]. Other internucleotide modifications commonly used to counteract nuclease susceptibility include N3-phosphoramidate, boranophosphate, morpholino or phosphonoacetate modifications [89].

Ribose modifications are typically introduced at the 2' position. 2'-O-Methyl (2'-O-Me) and 2'-Fluoro (2'-F) modifications were used in this work (Figure 3). Both keep the oligonucleotide in a 3' endo conformation, mimicking the RNA structure. 2'-F modification and to some extent also 2'-O-Me modification have shown to increase the binding affinity to their complementary sequence and can therefore be used to counteract the detrimental properties of the phosphorothioate linkages [90]. Fluorine is highly electronegative leading to an enthalpy driven stabilization of the duplex. The

decreased hydration compared to the unmodified form leads to enhanced base stacking [91, 92].

The 2'-O-Me modification provides additional nuclease resistance and reduces recognition by the immune system, which to a lesser extent applies to the 2'-F modification. Other commonly used ribose modifications include locked nucleic acids or 2'-O-(2-methoxyethyl) modification.

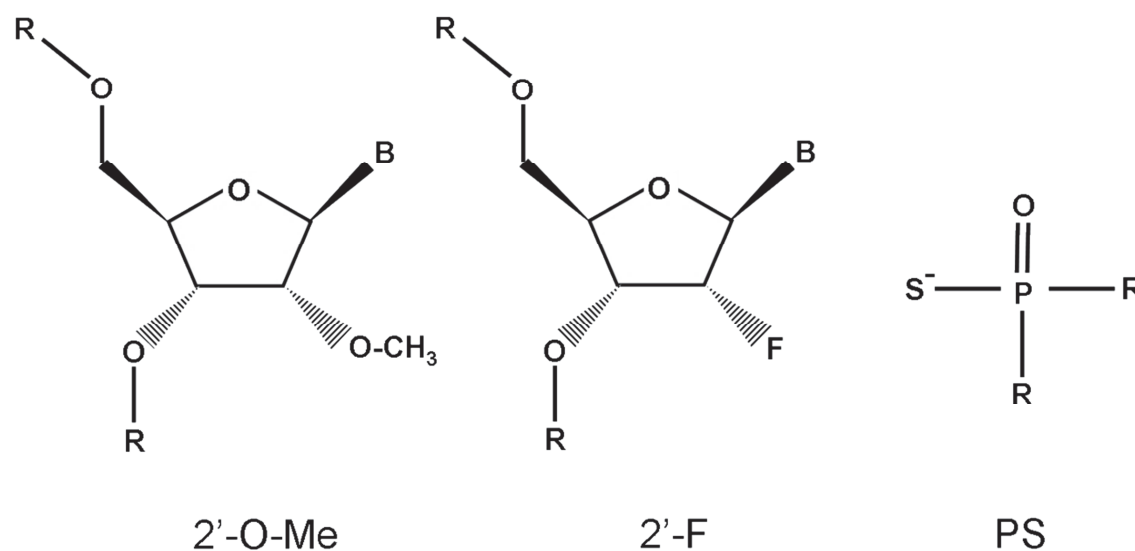


Figure 3. Chemical backbone modifications used in this work. 2'-O-Me and 2'-F modification increases the nuclease resistance and double-strand melting temperature. Phosphorothioate modification increases the nuclease resistance.

All chemical modifications discussed above are already part of a FDA approved formulation and represent a realistic approach for improving nucleic acid therapy [89].

1.2.4. Localization and stability of small RNA

Most studies on the impact of chemical modifications on bioactivity of small RNA therapeutics rely on quantitative readouts like reporter gene knockdown efficiency [4, 93] or in case of antagomirs on microRNA target upregulation [94, 95]. Nevertheless, sophisticated designs can only be accomplished if the fate of such modified oligonucleotides is elucidated after their introduction into the target cell. A few studies are available dealing with intracellular stability and localization of chemically modified small RNA.

An early work compares localization and stability of microinjected phosphodiester and phosphorothioate oligonucleotides by fluorescence microscopy. Both show fast nuclear translocation. While phosphodiester oligonucleotides were degraded already after 20 min, phosphorothioate oligonucleotides displayed stability over 24 h [96]. Later on, the formation of nuclear bodies was observed after delivery of phosphorothioate modified antisense oligonucleotides by transfection and microinjection [97].

Another study demonstrates that the rate of false-positives for 2'-O-Me molecular beacons can be reduced by including phosphorothioate linkages. Cytosolic retention by conjugation to NeutrAvidin also decreases non-specific hairpin opening and degradation [98]. Furthermore, the stability of a malachite green aptamer was monitored by the increased fluorescence of malachite green after binding [99] and the fate of chemically modified antagomirs was elucidated after *in vivo* delivery, indicating a RNAi independent degradation mechanism as the antagomirs do not localize in p-bodies [100]. Eventually, the duplex stability and localization of siRNA was monitored by Hirsch *et al.* by intensity based FRET [101].

1.3. Aims of the thesis

The aim of the first part of the thesis was to provide an overview of how DNA adaptor molecules can be used to improve cellular delivery of siRNA in polyplexes with sequence defined cationic oligomers. Different aspects of siRNA extension with DNA had to be illuminated:

- multi-siRNA vs. single-siRNA constructs
- single vs. double-stranded DNA adaptors
- influence of DNA adaptor length
- reducible vs. non-reducible adaptor connection
- siRNA functionalization *via* DNA adaptors
- validity of the findings for different transfection agents

The aim of the second part of the thesis was to find a suitable setup for the examination of the fate of small RNAs after exposure to cellular environment. Dual-fluorophore labelled RNA oligonucleotides that differ in their extent of stabilizing backbone modifications had to be compared. The degradation rate of those

oligonucleotides was to be monitored in cell extracts and the localization dependent integrity to be recorded in cells in culture.

For the cell extract measurements, various ultrasensitive fluorescence methods like fluorescence correlation spectroscopy, fluorescence cross-correlation spectroscopy and Förster resonance energy transfer should be compared. The methods had to be examined with respect to their sensitivity and ability to distinguish unspecific effects from RNA degradation.

Fluorescence lifetime imaging microscopy was to be used to examine the fate of the chemically stabilized oligonucleotides when they are transfected with a sequence defined cationic carrier. Their localization, integrity and intracellular retention should be monitored with this approach.

2. Materials and Methods

2.1. Materials

2.1.1. Oligonucleotides

The following oligonucleotides were purchased from Axolabs (Kulmbach, Germany) except the DNA adaptors, which were purchased from Sigma Aldrich (Steinheim, Germany)

Nomenclature: **A** = 2'-H, **A** = 2'-OH, **a** = 2'-O-Me, **s** = phosphorothioate, **fA** = 2'-F
 C6SSC6 = symmetrical hexyl disulfide linker

2.1.1.1. eGFP siRNAs

siRNAs targeting the enhanced green fluorescent protein

Guide strand	UGC UUGUCGGC cAUG Au AUT sT
Passenger strand	AuAucAuGGccGAcAAGcAT sT
SS-passenger strand	(C6SSC6) AuAucAuGGccGAcAAGcAT sT
Passenger strand 5' extension	GCCGGATCGCCACATAAC- AuAucAuGGccGAcAAGcAT sT
Passenger strand 3' extension	AuAucAuGGccGAcAAGcAT sT-CGACGGATATACATGACG

2.1.1.2. CTRL siRNAs

siRNAs with a non-functional control sequence

Guide strand	CuAAuAcAGGCcAAuAcA UTsT
Passenger strand	AuGuAuuGGccuGuAuuAG TsT
SS-passenger strand	(C6SSC6) AuGuAuuGGccuGuAuuAG TsT

2.1.1.3. Modified RNA single-strands

Stable control	usfCscsfAsusfCsasfUsusfAscscscsgsgsfCsasfGsusfAsusfUsa
Instable control	UCCAUCAUUACCCGGCAGUAUUA
Construct 1	usfCscsfAsusfCsasfUsusfAscscs CsCGsGsf CsasfGsusfAsusfUsa
Construct 2	uscscsas UCAUUACCCGGCAGU sasususa

2.1.1.4. DNA extensions/adaptors

SS-extension 5'	GCCGGACGCCACATAAC (C6SSC6)
SS-extension 3'	(C6SSC6) CGACGGATATACATGACG
1bb2si	GTTATGTGGCGATCCGGCAGCATAACATCTTAGCTCTGCGCACGCGTTAGTCCCGATAACTCGTCATGTATATCCGTCG
4bb4si	GTTATGTGGCGATCCGGCAGCAGTAGTGATAAGAATGCTGCGCAGTACTTCGGCTCATAACGGCGTCATGTATATCCGTCG GTTATGTGGCGATCCGGCAGCAGTAGTGATAAGAATGCTGCGCAGAGCTAAGATGTTATCGGCGTCATGTATATCCGTCG CCGATAACATCTTAGCTCTGCGGCAGCATTCTTATCACTACGT CCGATAACATCTTAGCTCTGCGGCAGCATTCTTATCACTACGT
3bb6si	GTTATGTGGCGATCCGGCAGCATAACATCTTAGCTCTGCGCACGCGTTAGTCCCGATAACTCGTCATGTATATCCGTCG GTTATGTGGCGATCCGGCTGTTATCGGGACTAACGCGTGAGCAGCATTCTTATCACTACGGCGTCATGTATATCCGTCG GTTATGTGGCGATCCGGCAGCAGTAGTGATAAGAATGCTGCGCAGAGCTAAGATGTTATCGGCGTCATGTATATCCGTCG
5bb10si	GTTATGTGGCGATCCGGCAGCATAACATCTTAGCTCTGCGCACGCGTTAGTCCCGATAACTCGTCATGTATATCCGTCG GTTATGTGGCGATCCGGCAGCAGTAGTGATAAGAATGCTGCGCAGTACTTCGGCTCATAACGGCGTCATGTATATCCGTCG GTTATGTGGCGATCCGGCTCGTTATGAGCCGAAGTACTGACGCTACTATGGTCATCGTGCACGTCATGTATATCCGTCG GTTATGTGGCGATCCGGCAGCAGTAGTACCATAGTAGCGAGCAGAGCTAAGATGTTATCGGCGTCATGTATATCCGTCG GTTATGTGGCGATCCGGCTGTTATCGGGACTAACGCGTGAGCAGCATTCTTATCACTACGGCGTCATGTATATCCGTCG
Ext I	CGGCTCATGCGGCAGCTAGCACGTCATGTATATCCGTCG
Ext II	GCTAGCTGCCGCATGAGCCGTCGACGGAAGTCACGGGAACG
Ext III	GCACTCGAGGTGATCCATGCCCGTTCCCGTGACTTCCGTCG
Ext IV	GCATGGATCACCTCGAGTGACGAGCACGACATTTTCATGC
Ext V	TCCTCACTTAACTATCCACTGCATGAAATGTGCGTGCTCG

2.1.2. Cationic oligomers

<i>Oligomer ID</i>	<i>Structure</i>
188	C-Stp ₄ -K(PEG ₂₄ -A)-Stp ₄ -C
278	C-K(K-LinA ₂)-Stp ₃ -K(K-LinA ₂)-C
356	C-Stp ₄ -K(PEG ₂₄ -FolA)-Stp ₄ -C
454	C-Y ₃ -Stp ₂ -K(K-OleA ₂)-Stp ₂ -Y ₃ -C
689	C-(H-Stp) ₃ -H-K(H-(Stp-H) ₃ -C) ₂

C: cysteine; Stp: succinoyl-tetraethylene pentamine; K: lysine; PEG₂₄: polyethylene glycol consisting of 24 ethylene glycol units; A: alanine; LinA: linoleic acid; FolA: folic acid; Y: tyrosine; OleA: oleic acid; H: histidine.

2.1.3. Reagents

Acetonitrile	VWR Int, Darmstadt, Germany
Acrylamide/bis-acrylamide, 30% solution, 37.5:1	Bio-Rad, Munich, Germany
Agarose NEEO ultra-quality	Carl Roth, Karlsruhe, Germany
Ammonium persulfate	Sigma-Aldrich, Steinheim, Germany
Atto488-NHS ester	Atto-Tec, Siegen, Germany
Cell culture consumables	NUNC Langensfeld, Germany
Dimethylsulfoxide	Sigma-Aldrich, Steinheim, Germany
5,5'-Dithiobis-(2-nitrobenzoic acid)	Sigma-Aldrich, Steinheim, Germany
Dithiotreitol	Sigma-Aldrich, Steinheim, Germany
D-luciferin sodium	Promega, Mannheim, Germany
DMEM	Sigma-Aldrich, Steinheim, Germany
EDTA	Sigma-Aldrich, Steinheim, Germany
Ethanol	Sigma-Aldrich, Steinheim, Germany
Fetal bovine serum	Life Technologies, Darmstadt, Germany
GelRed 10000x solution	VWR Int, Darmstadt, Germany
HEPES	Biomol, Hamburg, Germany
INF7 peptide	Biosyntan, Berlin, Germany
Isopropanol	Sigma-Aldrich, Steinheim, Germany

Magnesium chloride	Sigma-Aldrich, Steinheim, Germany
MTT	Sigma-Aldrich, Steinheim, Germany
Paraformaldehyde	Sigma-Aldrich, Steinheim, Germany
PMSF	Sigma-Aldrich, Steinheim, Germany
Potassium chloride	Sigma-Aldrich, Steinheim, Germany
RPMI-1640	Life Technologies, Darmstadt, Germany
Sodium borate	Sigma-Aldrich, Steinheim, Germany
Sodium chloride	Sigma-Aldrich, Steinheim, Germany
Streptomycin	Life Technologies, Darmstadt, Germany
TEMED	Sigma-Aldrich, Steinheim, Germany
Tetramethylrhodamine-6-maleimide	Life Technologies, Darmstadt, Germany
Triethylamine	AppliChem, Darmstadt, Germany
Tris(2-carboxyethyl)phosphine	Sigma-Aldrich, Steinheim, Germany
Trizma base	Sigma-Aldrich, Steinheim, Germany
Trypsin/EDTA	Biochrom, Berlin, Germany

2.1.4. Buffers

Buffer A	10 mM HEPES, 10 mM KCl, 1.5 mM MgCl ₂ , 0.2 mM PMSF, 0.5 mM DTT, pH 7.9
Fixation buffer	PBS containing 4 % paraformaldehyde
HBG	20 mM HEPES, 5% glucose, pH 7.4
HEPES buffer	20 mM HEPES, pH 8.4
PBS	137 mM NaCl, 2.7 mM KCl, 12 mM phosphate, pH 7.4
SB buffer	100 mM sodium borate, 20 % Acetonitrile, pH 8.5
SP buffer	50 mM sodium phosphate, 20 % Acetonitrile, pH 7
TBE buffer	89 mM Trizma base, 89 mM boric acid, 2 mM EDTA-Na ₂ , pH 8
TEAA buffer	0.1 M TEAA (from acetic acid, triethylamine), pH 7
TM buffer	10 mM Tris-Cl, 5 mM MgCl ₂ , pH 7.5

2.1.5. Cell lines

HeLa	human cervical carcinoma cells
KB/eGFPluc	human cervical carcinoma cells stably expressing an eGFP-luciferase fusion protein
Neuro2A/eGFPluc	murine neuroblastoma cells stably expressing an eGFP-luciferase fusion protein

2.2. Methods

2.2.1. Conjugation and assembly of oligonucleotides and DNA nanostructures

2.2.1.1. Assembly of the siRNAs and the DNA nanostructures

All DNA nanostructures used in this work were designed with NUPACK [45]. The constructs were assembled in TM buffer (10 mM Tris-Cl; 5 mM MgCl₂, pH 7.5) to yield a concentration of 1-6 μM. The components were mixed in their respective molar amount, incubated at 95 °C for 5 min and cooled to RT at a rate of ca. 2 °C/min. The siRNA nanostructures were assembled with the oligonucleotides described in the materials part.

2.2.1.2. Coupling of the DNA extensions to the siRNA passenger strands with disulfide chemistry

Disulfide modified siRNA was reduced with buffered tris(2-carboxyethyl)phosphine (TCEP, 700 times molar excess, pH 7) for 2.5 h at RT. TCEP was removed by EtOH precipitation. The remaining pellet was activated with 2.5 mM 5,5'-dithiobis-(2-nitrobenzoic acid) (DTNB, 17 times molar excess) for 1 h at RT. The activated siRNA was purified by EtOH precipitation and dissolved in 20 mM HEPES pH 8.4. The absence of dimers was verified with native polyacrylamide gel electrophoresis. Disulfide modified DNA extensions were reduced with buffered TCEP (700 times excess, pH 7), purified by EtOH precipitation and dissolved in HEPES buffer. The activated siRNA and the reduced DNA extensions were combined at a concentration of 50 μM and incubated at RT for 1h. Reaction was completed upon standard freezing to -20 °C, presumably facilitated by the temporarily high concentrations in the mother liquor. The products were purified by EtOH precipitation and HPLC. Their correct size and purity was verified by native polyacrylamide gel electrophoresis.

2.2.1.3. Coupling of DNA extension strands to INF7

The cysteine of the INF7 peptide (GLFE AIEG FIEN GWEG MIDG WYGC) was activated with DTNB (17 times molar excess) and purified by HPLC. The product was incubated with the TCEP reduced DNA extension (see chapter 2.2.1.2) in 20 mM HEPES pH 8.4 for 1 h at RT and frozen to -20 °C. The product was again purified by HPLC and verified by agarose gel electrophoresis.

2.2.1.4. Labelling of the RNA oligonucleotides with Atto488 and tetramethylrhodamine

The 3'-amino and 5'-disulfide modified oligonucleotide was dissolved in 100 mM sodium borate buffer containing 20 % acetonitrile (pH 8.5) to a final concentration of 800 µM. Atto488-NHS ester was dissolved in anhydrous DMSO to a working concentration of 1 mM. Three molar equivalents of Atto488-NHS ester solution were added over 2 h every 15 min, following 3 h incubation at 25 °C. The resulting construct was purified by EtOH precipitation and redissolved in water to a concentration of 1 mM. The disulfide modified end was reduced with buffered TCEP (700 times molar excess, pH 7) for 2.5 h at RT. TCEP was removed by EtOH precipitation. The remaining pellet was redissolved in 50 mM sodium phosphate buffer 20 % acetonitrile pH 7 to a concentration of 800 µM. Tetramethylrhodamine-6-maleimide was dissolved in anhydrous DMSO to a working concentration of 1 mM. The tetramethylrhodamine-6-maleimide solution (1.3 equivalents) was added immediately to the oligonucleotide solution, following incubation of 2 h at 25 °C. The product was purified by EtOH precipitation and HPLC.

2.2.1.5. Purification with high performance liquid chromatography

Purification of the dual-labelled RNA oligonucleotide and the DNA extensions coupled *via* a disulfide bond to the siRNA passenger strand or INF7 was performed using high performance liquid chromatography (VWR Hitachi Chromaster consisting of 5430 Diode array detector and 5160 gradient pump, Darmstadt, Deutschland). The products were separated with a XTerra C8 column (5 µm, 4.6 x 150 mm, Waters,

Eschborn, Germany) and eluted with a 0.1 M triethylammonium acetate/acetonitrile gradient (95:5 to 35:65 in 30 min). Product containing fractions were identified by their retention, absorbance maxima and by native polyacrylamide gel electrophoreses, lyophilized and stored at -20 °C.

2.2.1.6. Native polyacrylamide gel electrophoresis

Gels for DNA nanostructure analysis were poured in TBE buffer containing 4 % (for large structures) to 15 % (for short oligonucleotides) acrylamide, ammonium persulfate and TEMED. They were run in TBE buffer at 130 V for 30 min. Staining was accomplished in 0.1 M NaCl solution supplemented with 2x GelRed solution.

2.2.2. Polyplex formation and analysis

2.2.2.1. Polyplex formation

Sequence-defined oligomers **188**, **278**, **356**, **454** and **689** were synthesized by solid-phase-assisted synthesis as described in our previous publications [24, 30, 32]. The siRNA and the required amount of oligomer were separately diluted in 20 mM HEPES-buffered 5 % glucose pH 7.4 (HBG) in a final volume of 10 - 30 μ l. Both solutions were pooled and incubated for 45 min at RT.

2.2.2.2. Dynamic light scattering

Polyplexes were formed with oligomer **689** in a total volume of 60 μ l as described in the method section for polyplex formation. After incubation, the solution was measured in a folded capillary cell (DTS1070) using a Zetasizer Nano ZS with backscatter detection (Malvern Instruments, Worcestershire, UK). The refractive index of the solvent was set to 1.330 and the viscosity to 0.8872. The refractive index of polystyrene latex (1.590) was used for polyplex analysis of the particles. Each sample was measured three times with 10 to 17 subruns.

2.2.2.3. siRNA binding assay

siRNA (500 ng) or siRNA/DNA conjugate and the amount of oligomer corresponding to the required N/P ratio were diluted separately in HBG in a volume of 10 μ L. The solutions were pooled and incubated at RT for 45 min. After addition of 4 μ L loading buffer (prepared from 6 mL of glycerol, 1.2 mL of 0.5 M EDTA, 2.8 mL of H₂O, 0.02 g of bromophenol blue) the polyplexes were run on a 1.5 % agarose gel supplemented with GelRed at 90 V for 45 min.

2.2.3. Cell culture

2.2.3.1. Cultivation of cells

Murine neuroblastoma (N2A/eGFPluc) or human cervix carcinoma (KB/eGFPluc) cells are each stably transfected with an enhanced green fluorescent protein GL3 firefly luciferase fusion protein [24, 25, 36]. HeLa cells were used as wild-type cells. They were cultured at 37 °C in Dulbecco's modified Eagle's Medium with 1 g/L glucose (for N2A), or folate free RPMI 1640 medium (for KB, HeLa), in both cases supplemented with 10 % fetal bovine serum (FBS), 4 mM glutamine, 100 U/mL penicillin and 100 μ g/mL streptomycin. For maintenance the cells were detached with a trypsin-EDTA solution (0.25 %) and seeded at the desired concentration.

2.2.4. Transfection of N2A/eGFPluc and KB/eGFPluc cells for downregulation of eGFPluc

N2A/eGFPluc and KB/eGFPluc cells were seeded in 96-well plates in 100 μ L medium (N2A/eGFPluc: 5000 cells per well in DMEM, 10 % FBS, KB/eGFPluc: 4000 cells per well in folate-free RPMI, 10 % FBS). After 24 h, the medium was exchanged with 80 μ L fresh medium. The formed polyplexes containing the eGFP siRNA for downregulation of the eGFPluc fusion protein were added in a volume of 20 μ L to each well. After the respective incubation time, the medium was exchanged with 100 μ L fresh medium. 48 h past the transfection the cells were incubated with 100 μ L lysis buffer (25 mM Tris, pH 7.8, 2 mM EDTA, 2 mM DTT, 10% glycerol, 1% Triton X-

100). 35 μL of the lysate was used for luciferase activity determination with a luciferase assay kit (100 mL Luciferase Assay Buffer, Promega, Mannheim, Germany) in a luminometer (Centro LB 960 plate reader luminometer, Berthold Technologies, Bad Wildbad, Germany).

2.2.4.1. MTT assay

The cells were transfected in 96-well plates as described above. 48 h post transfection 10 μL MTT solution was added to a final concentration of 0.5 mg/mL. The plate was incubated at 37 °C for 2 h for formation of the insoluble purple formazan. The medium was removed and the plate was stored at -80 °C for at least 1 h. 100 μL DMSO was added to each well which dissolved the formazan and was quantified through its absorbance at 530 nm using a microplate reader (TecanSpectrafluor Plus, Tecan, Männedorf, Switzerland). Results are presented relative to a buffer treated control.

2.2.4.2. Transfection of HeLa cells in chamber slides

HeLa wild-type cells were seeded in 8-well Nunc Lab-Tek chamber slides (Thermo Scientific, Germany) in 300 μL medium (25,000 cells per well). After 24 h, the medium was exchanged with 250 μL fresh medium. The formed polyplexes containing the oligonucleotide were added in a volume of 50 μL to each well. After 15 min incubation time at 37 °C, the medium was exchanged with 300 μL fresh medium. Fixation was accomplished by washing the wells twice with PBS (resuspending) at the desired time point, followed by 10 min incubation with 4% paraformaldehyde/PBS at RT. The wells were washed three times with PBS and stored at 4 °C up to 3 days.

2.2.5. RNA stability and localization measurements

2.2.5.1. HeLa whole cell extracts

HeLa cells were seeded in 150 cm^2 plates. After 48 h, the cells were detached with trypsin-EDTA solution and washed three times with PBS. The resulting pellet was resuspended in 4 packed cell volumes of buffer A (10 mM HEPES, 10 mM KCl, 1.5

mM MgCl₂, 0.2 mM PMSF, 0.5 mM DTT, pH 7.9) and sonicated three times for 5 s at 30 % amplitude with 30 s incubation on ice in between. Phenylmethylsulfonyl fluoride (PMSF) and dithiothreitol (DTT) were added to the buffer immediately before use. The cells were centrifuged for 20 min at 14,000 x g and the supernatant was collected. After aliquotation, the extract was frozen in liquid nitrogen and stored at -80 °C.

2.2.5.2. Cell extract measurements

Correlation and FRET measurements in cell extract (diluted 1/10) were performed on a home-built pulsed interleaved excitation laser scanning confocal microscope described previously [102, 103] in TM buffer (10 mM Tris-Cl; 5 mM MgCl₂, pH 7.5). For focusing the excitation light and collecting the fluorescence, a 60x water immersion objective with a numerical aperture (NA) of 1.27 was used (Plan Apo IR 60x WI, Nikon). This resulted in a diffraction limited lateral focus size ω_r of 210 nm for the green and 260 nm for the red channel, respectively. The laser power measured directly before the objective was set to 10 μ W for the blue 475 nm laser and 3 μ W for the yellow 565 nm laser. To prevent evaporation of the immersion liquid, an immersion oil with a refractive index of 1.33 was used.

During the measurements, the fluorescence intensity of the two channels was recorded at a single point in the solution. The experiments were performed at 37 °C for 3 h each, divided into individual measurements of 1 min. A home written software package PAM was used for FCS, FCCS and FRET analysis. The analysis methods are described in greater detail in the appendix (see chapter 6.2.1 to 6.2.3).

2.2.5.3. FLIM measurements on fixed cells

FLIM measurements on fixed cells were performed on the same microscope as the cell extract measurements. For single cell images, a 1.27 NA 60x water immersion objective (Plan Apo IR 60x WI, Nikon) was used. Areas of 100 μ m by 100 μ m were recorded as 300 x 300 images, resulting in a pixel size of 333 nm. In order to image larger areas, a 0.45 NA 10x air objective was used (CFI Plan APO 10x 0.45 NA, Nikon). This resulted in 600 μ m by 600 μ m sized images with a pixel size of 1.17 μ m for a resolution of 512 x 512 pixels.

For each region, 50-100 frames were recorded at a frame time of 5 s. The laser power of the 475 nm laser was set to 2-10 μW for the 60x objective and 10-90 μW for the 10x objectives to achieve a count rate between 50 kHz and 1 MHz. This guaranteed a high enough signal for the FLIM analysis while preventing artifacts from detector dead-time and photon pileup. The home written software package PAM was used for the phasor analysis of the FLIM data. A detailed description of the analysis method is given in the appendix (see chapter 6.2.4).

3. Results and Discussion

3.1. DNA adaptors for siRNA polyplex formation

This chapter has been partly adapted from:

Philipp Heissig, Philipp M. Klein, Philipp Hadwiger, Ernst Wagner, DNA as tunable adaptor for siRNA polyplex stabilization and functionalization, Molecular Therapy Nucleic Acids (2016), 5, e288

3.1.1. Design of the basic DNA nanostructure and the delivery agent

The basic structure used for this approach is composed of two siRNAs directed against eGFP linked by a 79 nucleotides DNA backbone strand. In detail, the siRNA consists of a guide strand and a complementary passenger strand with either a 5' or a 3' 18 nucleotides DNA extension. Both, the siRNA guide and passenger strand contain two 3' desoxythymidines linked by a phosphorothioate bond. In addition, all pyrimidines of the passenger strand and pyrimidines 5' of adenines of the guide strand are 2'-O-Methyl modified, ensuring protection against nucleases. *Via* the DNA extensions, the siRNAs are hybridized to both ends of the DNA backbone strand resulting in structure 1bb2si (= 1 backbone strand + 2 siRNAs) (Figure 4a). The construct is formed by mixing the components in their respective molar amounts, heating to 95 °C and slow cooling to room temperature. The verification of the assembly is accomplished by building the structure from its subunits and monitoring the retention of each by native polyacrylamide gel electrophoresis (PAGE). All assemblies were clean and showed the expected difference in migration (Figure 4b).

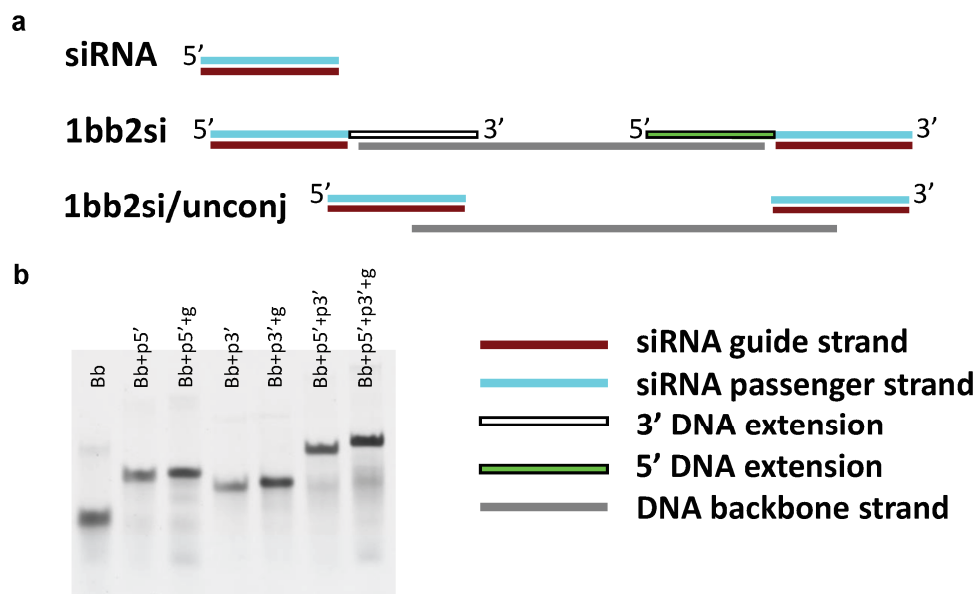


Figure 4. Assembly of DNA nanostructures for polyplex formation. (a) Basic building block consisting of two siRNAs with a DNA extension at the 3' or 5' terminus of the passenger strand used for hybridization to both ends of a DNA backbone strand (1bb2si). Unconjugated control consisting of two equivalents siRNA mixed with one equivalent backbone strand (1bb2si-unconj). (b) Assembly of 1bb2si from its subunits verified on a native polyacrylamide gel (Bb: DNA backbone strand; p5': passenger strand with 5' DNA extension; p3': passenger strand with 3' DNA extension; g: guide strand, gel cropped). Adapted from [104].

For transfection, the nanostructure was complexed with the three-armed cationic oligomer **689** [105]. Each arm contains three protonable succinoyl-tetraethylene pentamine units (Stp) for complexation of the negatively charged nucleic acids, four histidines which promote endosomal escape through the proton sponge effect [22] and terminal cysteines for polyplex stabilization through disulfide bond formation (Figure 5).

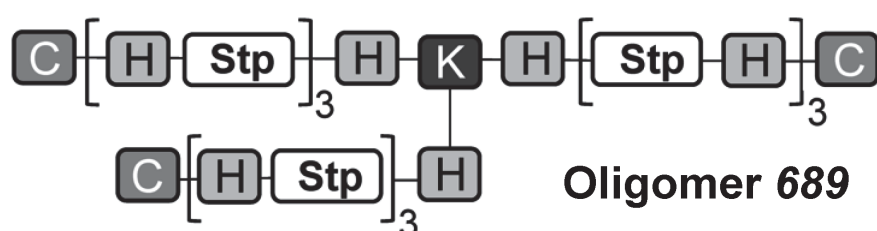


Figure 5. Oligomer 689 for complexation of the DNA nanostructures C: cysteine; H: histidine; Stp: succinoyl-tetraethylene pentamine; K: lysine, structure from N to C. Adapted from [104].

3.1.2. Variables in transfection efficiency

The next step was to test whether 1bb2si has already advantages over a canonical siRNA format in transfection-mediated gene silencing experiments. It was mixed with oligomer **689** at an amine to phosphate ratio of 6 (N/P 6, including all phosphates from siRNA and DNA) and transfected into murine neuroblastoma N2A/eGFPluc cells in medium supplemented with 10 % fetal bovine serum. As these cells stably express an eGFP-luciferase fusion protein, luciferase is downregulated upon gene silencing of the eGFPluc fusion mRNA and represents a convenient quantitative read-out for subsequent transfections.

The siRNA was used at a concentration of 0.36 μM and the polyplexes were incubated on the cells for 48 h. Luciferase knockdown is specified relative to a buffer treated control (Figure 6a). As expected, the canonical siRNA already exhibited a high gene silencing efficiency, but it was outperformed by 1bb2si. A control was included to verify that hybridization of the siRNA to the DNA backbone strand is necessary. siRNA without DNA extensions was mixed with the respective amount of the DNA backbone strand (1bb2si-unconj). Silencing by 1bb2si-unconj was comparable to that of the canonical siRNA. Thus the beneficial effect of the nanostructure cannot be achieved by mixing siRNA with DNA without prior conjugation of complementary DNA extensions. To challenge the effectiveness of 1bb2si, the incubation time was decreased to 1.5 h and the siRNA concentration was reduced to 0.2 μM . While gene silencing of 1bb2si remained as good as in the previous experiment, the efficiency of the canonical siRNA as well as of 1bb2si-unconj was significantly reduced.

The previous transfections were conducted at a constant N/P ratio of 6. As extension of siRNA with DNA comes along with an increase in phosphates per unit, the amount of oligomer used for complexation of 1bb2si was higher than for siRNA. To exclude that the positive effect is due to the increase in oligomer amount, the transfections were repeated at constant oligomer concentrations of 1.7 μM and 4.1 μM (corresponding to a N/P ratio of 6 for both, the canonical siRNA and 1bb2si) (Figure 6b). In both cases the prior results could be reproduced. Considering this fact, subsequent transfections were conducted at a constant oligomer concentration of 1.7 μM .

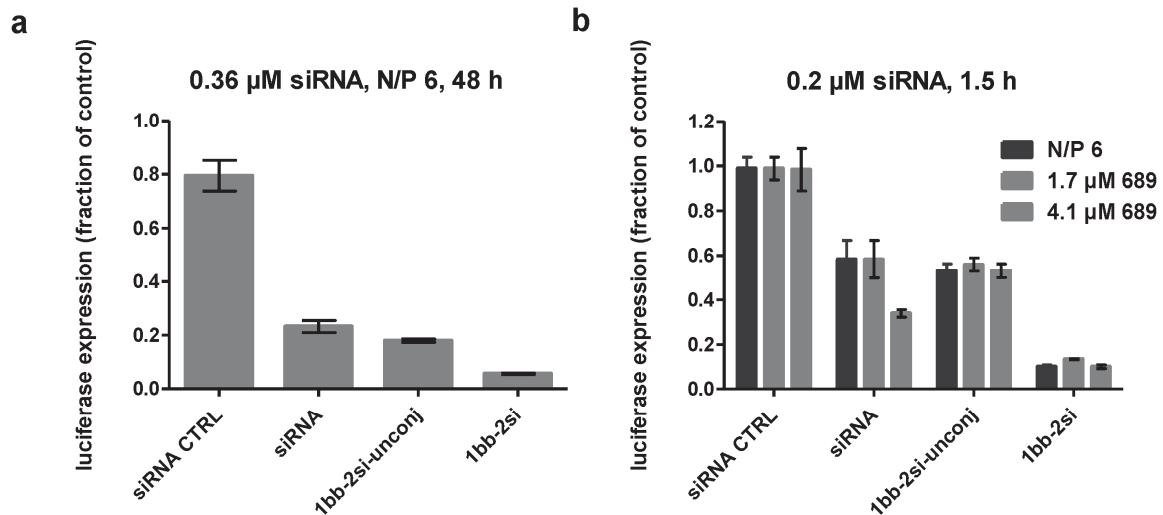


Figure 6. Transfection efficiency of polyplexes formed with oligomer 689 and siRNA, 1bb2si or 1bb2si-unconj. (a) Luciferase knockdown in N2A/eGFPluc cells with 0.36 μM eGFP siRNA at N/P 6 and 48 h incubation time. (b) Comparison of luciferase knockdown at constant N/P ratio and constant oligomer concentration of 1.7 μM and 4.1 μM with 0.2 μM siRNA and 1.5 h incubation time. Adapted from [104].

Furthermore the influence of the siRNA concentration with fixed oligomer concentration of 1.7 μM was investigated. The amount of 1bb2si and canonical siRNA was varied and transfection efficiency was compared (Figure 7).

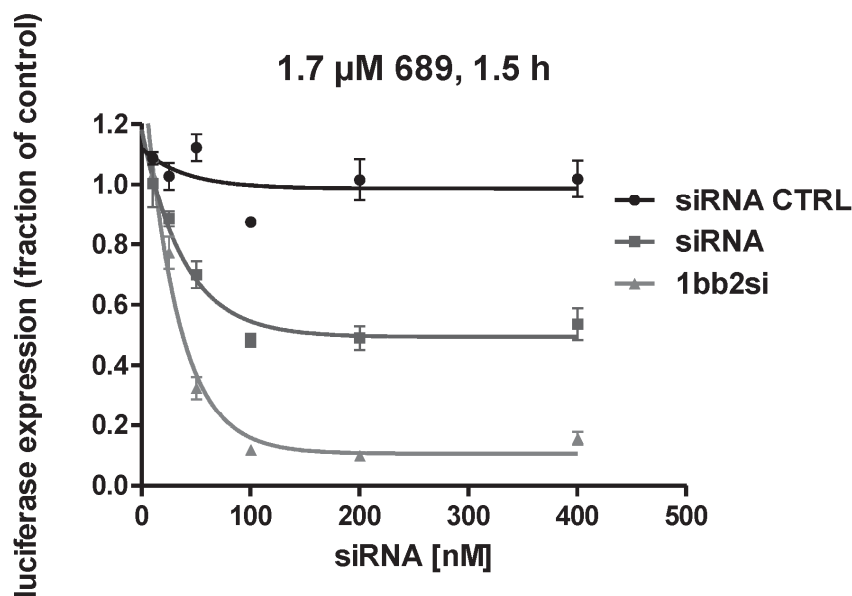


Figure 7. Correlation of gene silencing with siRNA concentration. Knockdown efficiency of siRNA CTRL, canonical siRNA and 1bb2si were compared at different concentrations, while the concentration of oligomer 689 was kept constant at 1.7 μM . Adapted from [104].

The maximal reduction of luciferase expression was achieved for both samples at 0.1 μM (siRNA 50 %, 1bb2si: 10 %). A further increase in concentration had no effect. This proves that the gene silencing efficiency of 1bb2si cannot be achieved by raising the siRNA concentration. Within the examined range, the advantage of 1bb2si over canonical siRNA is independent of N/P ratio, oligomer and siRNA concentration.

To examine if the enhanced transfection efficiency is due to the formation of more stable polyplexes, a comparative binding assay of canonical siRNA and 1bb2si at different N/P ratios was performed on an agarose gel. After complexation, charge neutralized particles remain in the pocket while free nucleic acids migrate into the gel (Figure 8). For 1bb2si the retention was nearly complete already at N/P 3 indicating that only a low oligomer excess is necessary to form stable polyplexes proofing complete binding of the construct. In contrast, with canonical siRNA even at a N/P ratio of 24, still free siRNA could be detected.

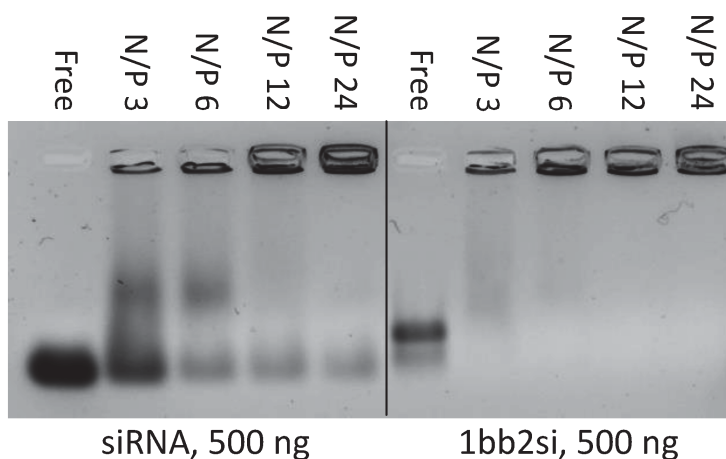


Figure 8. Binding assay for canonical siRNA and 1bb2si at different N/P ratios. Complexed nucleic acids remain in the loading pocket while free nucleic acids migrate into the gel (gel cropped). Adapted from [104].

3.1.3. More complex structures

More sophisticated multimeric siRNA structures can easily be formed with the building block 1bb2si. By annealing three of these constructs through their DNA backbone, a 3-armed structure containing 6 siRNA units was assembled (3bb6si). A

5-armed structure containing 10 siRNA units was constructed by the same strategy (5bb10si) and a 4-armed with only one siRNA per arm was assembled by linking two 1bb2si building blocks by two DNA backbone strands (4bb4si) (Figure 9).

The larger constructs were less defined on a native PAGE gel. Various strategies were tested to increase the purity of the resulting nanostructures. Cooling time, assembly concentration and buffer composition was varied. Building blocks were pre-annealed and assembled at a lower temperature, single-stranded domains were introduced at critical positions and the largest of the resulting bands was purified from a PAGE gel. Nevertheless, none of these approaches resulted in an increased purity.

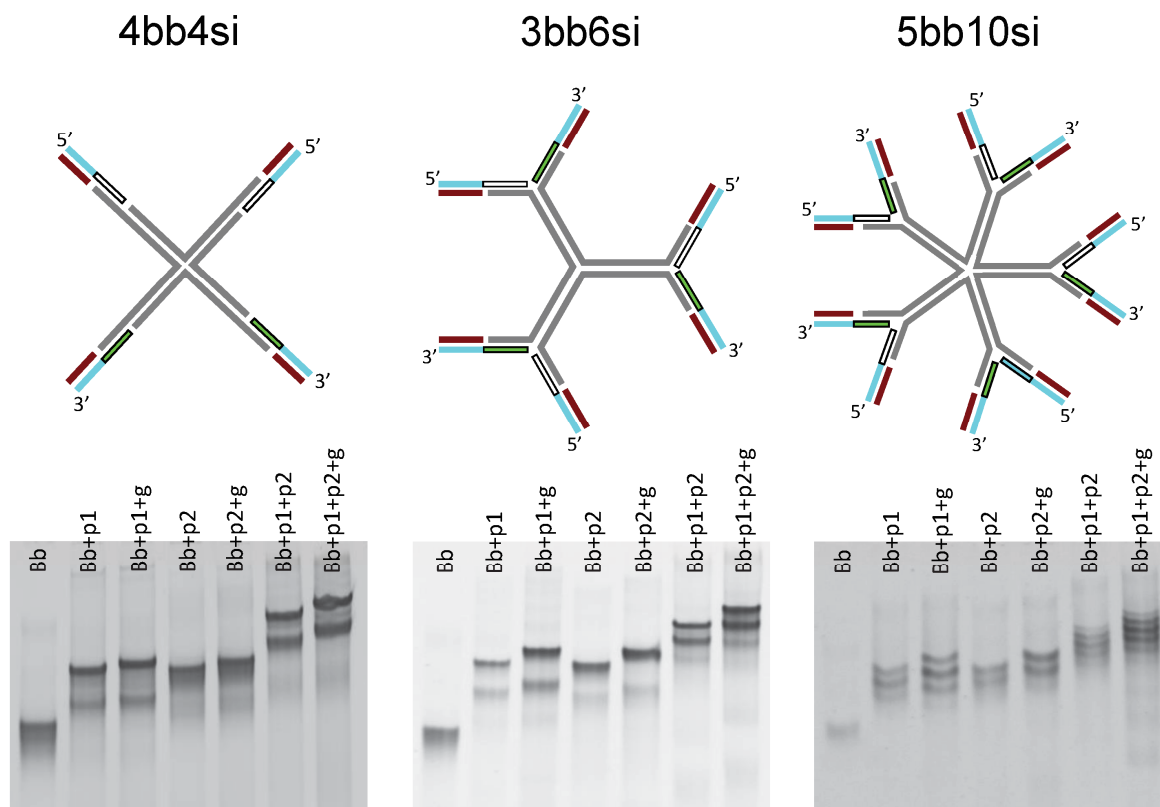


Figure 9. Assembly of star-shaped multi-siRNAs. Correctness of assembly assessed with native PAGE (Bb: backbone; p5': passenger strand with 5' DNA extension; p3': passenger strand with 3' DNA extension; g: guide strand, gels cropped). Adapted from [104].

Transfection efficiency decreased with increased number of siRNA units per structure. 4bb4si, unless a little less effective than 1bb2si, still exhibited a relatively high luciferase knockdown. In contrast 5bb10si had only minor advantages compared to canonical siRNA, indicating that there is no need to follow up the strategy of merging more than two siRNA units into one construct (Figure 10).

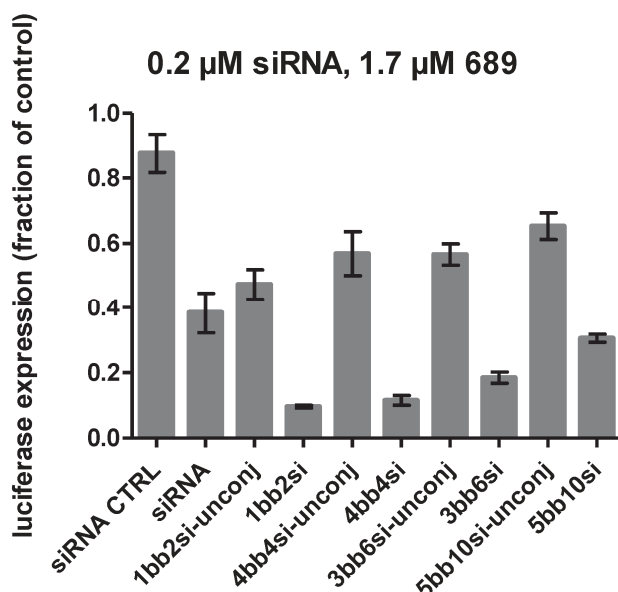


Figure 10. Gene silencing of the star-shaped multi-siRNAs. The structures were compared to the respective unconjugated controls (DNA backbone mixed with the corresponding equivalents siRNA). Adapted from [104].

3.1.4. Simpler structures

Hence, the next step was to consider more simple structures than 1bb2si, which can be achieved by testing the subunits of 1bb2si for gene silencing (Figure 11a). This provides also an insight into the possible cause of the enhanced transfection efficiency of 1bb2si. Constructs extended by 18 DNA nucleotides either at the 3'- or 5'-end of the passenger strand (siRNA/3'ov, siRNA/5'ov) are already slightly more efficacious compared to canonical siRNA. However, hybridizing either of the two constructs separately to the DNA backbone strand (1bb1si/3'ov and 1bb1si/5'ov, respectively) boosts transfection efficiency even more. Single siRNA construct 1bb1si/3'ov performs equally well as dimer siRNA construct 1bb2si (Figure 11b).

This indicates that attaching more siRNAs to one structure is not necessarily beneficial. It can even be detrimental as shown in the previous experiment. What seems to matter is an extension of a single siRNA by adaptor DNA. Regarding the attachment site of the DNA extension, the 3' extended structures exhibited an increased gene silencing efficiency compared to their 5' counterparts.

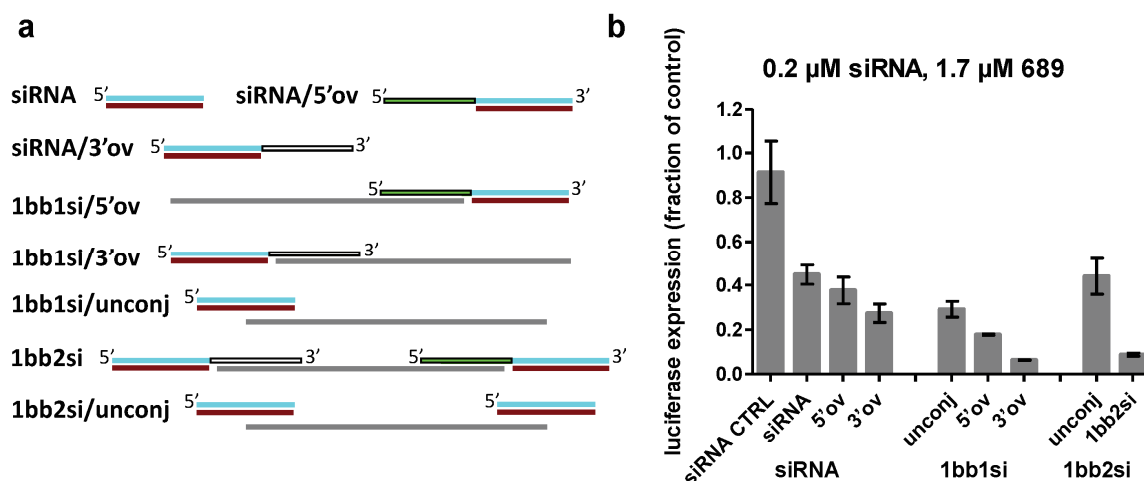


Figure 11. Transfection efficiency of the subunits of 1bb2si. (a) Schematic representation of the subunits of 1bb2si and (b) luciferase knockdown after complexation with oligomer **689**. Canonical siRNA and 1bb2si were compared to the 5' or 3' passenger strand extended constructs with and without hybridization to the DNA backbone strand. The unconjugated controls consist of siRNA lacking the DNA extensions and DNA backbone strand mixed in equimolar amounts. Adapted from [104].

3.1.5. Single-stranded versus double-stranded

All substructures of 1bb2si possess single-stranded DNA regions of different length (siRNA/3'ov: 18 bases, 1bb2si: 43 bases, 1bb1si/3'ov: 61 bases). As single-strands are more flexible than double-strands, this might be a requirement for stable particle formation and hence increased transfection efficiency. To test this hypothesis, the respective double-stranded equivalents were assembled and examined for luciferase knockdown with oligomer **689** (siRNA/3'ov-ds, 1bb1si/3'ov-ds, 1bb2si-ds) (Figure 12a). siRNA/3'ov-ds and 1bb2si-ds resulted in a similar silencing efficiency as their single-stranded counterparts, indicating that a single-stranded domain is not a requirement. In contrast, 1bb1si/3'ov-ds showed a reduced knockdown (Figure 12b). The stiffness of its long unnicked double-strand might disturb particle formation.

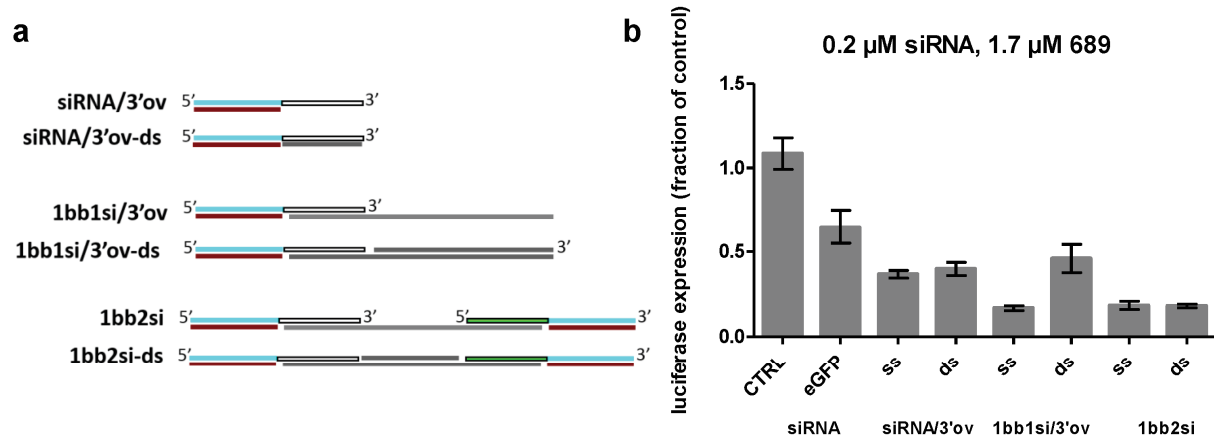


Figure 12. Influence of single-stranded (ss) and double-stranded (ds) domains on transfection efficiency. The double-stranded equivalents corresponding to siRNA/3'ov, 1bb1si/3'ov and 1bb2si were assembled, transfected and compared to their single-stranded counterparts. Adapted from [104].

3.1.6. Optimal length of DNA sequence per siRNA

Given the results above, the question was asked whether there is an optimum DNA sequence length connected to a single siRNA. Due to a better transfection efficiency of DNA extension at the passenger strand's 3'-terminus compared to the 5'-counterparts, it was decided to probe a potential DNA sequence length bias with a sequential DNA extension approach 3' of the passenger strand. DNA strands with a complementary part to the previous extension and a 20 nucleotides part for further extension were used to assemble the different sized defined structures (Ext I, Ext II, Ext III, Ext IV, Ext V) (Figure 13a). One single-stranded nucleotide was introduced between the extensions to facilitate assembly. The purity of the structures was verified by native PAGE (Figure 13b). A positive correlation of gene silencing efficiency and construct size was observed. siRNA/3'ov with a single-stranded DNA overhang displays improved silencing activity compared with canonical siRNA without overhang. Double-stranded DNA extensions up to Ext II resulted in a strong increase in potency. Larger constructs (Ext III to V) did not increase transfection efficiency further (Figure 13c).

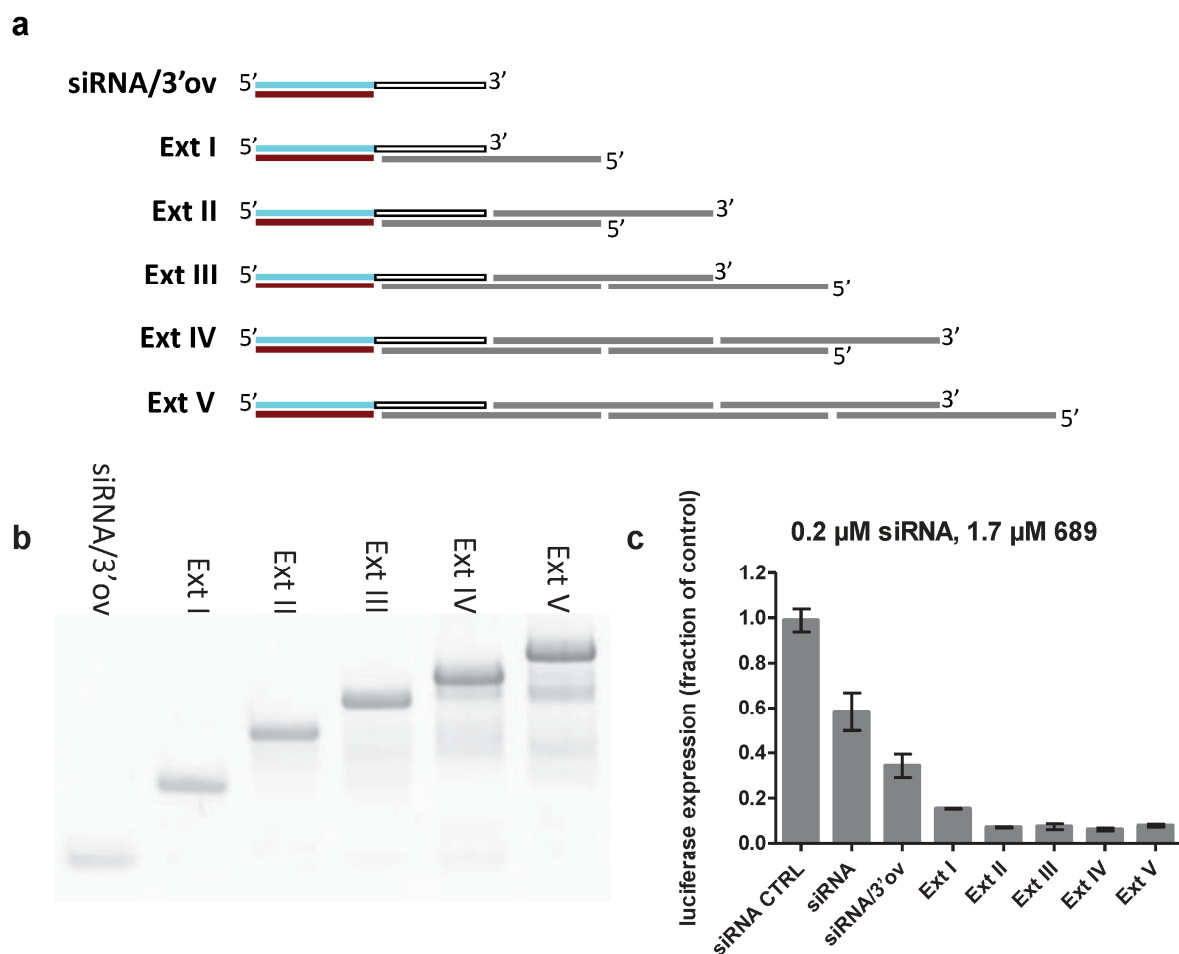


Figure 13. Optimal sequence length of DNA backbone. (a) Schematic representation of the stepwise DNA extended siRNA. Each extension step is accomplished by a DNA strand with one segment complementary to the previous extension and a 20 nucleotide segment for further extension. (b) Assembly (verified by native PAGE, gel cropped) and (c) transfection efficiency of the nanostructures. Adapted from [104].

This indicates that in this setup, hybridization of a single siRNA to an at least 99-nucleotide DNA extension provides the maximum silencing effect. As all constructs contain a similarly long stretch of 20-nucleotide single-stranded DNA, the positive effect of flexible single-strandedness on polycation complexation can be ruled out as major cause for the enhancement.

3.1.7. Reducible vs. non-reducible siRNA attachment

In all previous experiments, irrespective of the siRNA's terminus the DNA extension is covalently connected to the passenger strand *via* a phosphodiester linkage. It is possible that this chemistry prevents the siRNA from gaining full activity. This

assumption is supported by the difference in efficiency of the 5' and 3' extended passenger strand. To test this hypothesis a biocleavable disulfide linker was engineered between the RNA and the DNA extension sequence. The cytosol's reducing environment should be utilized to cleave the disulfide bond, which leaves the siRNA in a more accessible form for the RNA-induced silencing complex.

In order to implement this strategy two thiol modified 18 nucleotides DNA strands were used, each complementary to one end of the 79 nucleotides backbone strand that was used for the assembly of 1bb2si. An eGFP siRNA with a 5' thiolated passenger strand was activated with 5,5'-dithiobis-(2-nitrobenzoic acid), coupled to the thiolated DNA strand and purified with high-performance liquid chromatography (Figure 14a).

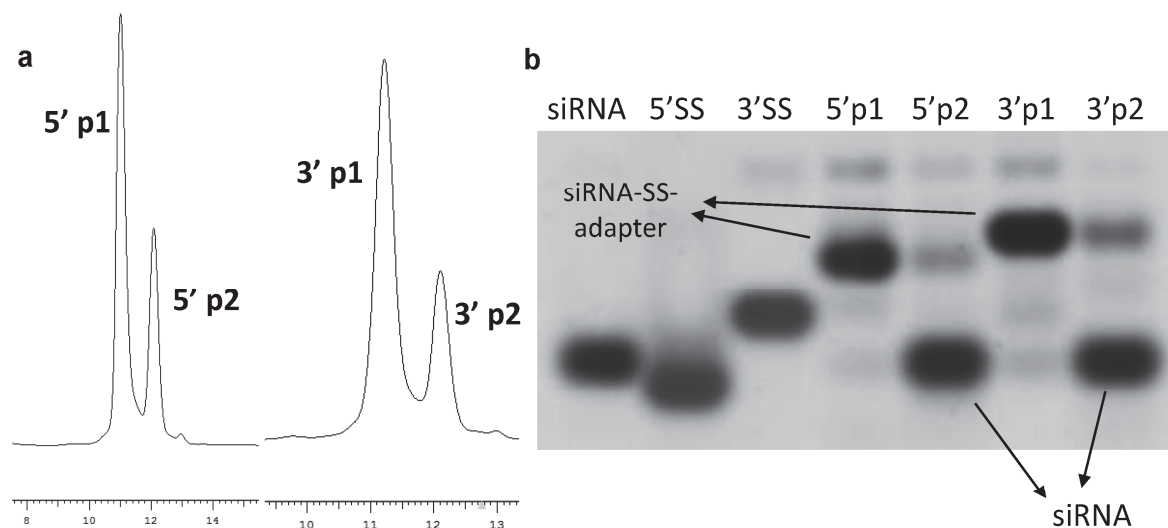


Figure 14. Purification and verification of the siRNA passenger strand–SS–DNA adaptor sequences. (a) Final purification was accomplished by HPLC. (b) The resulting peaks were analyzed with native PAGE. (5'SS: 5' thiolated DNA adaptor, 3'SS: 3' thiolated DNA adaptor, gel cropped)

The respective constructs from the previous experiments were assembled using the disulfide extended siRNA (SS-1bb1si/5'ov, SS-1bb1si/3'ov, SS-1bb2si) (Figure 15a). The verification of the disulfide conjugates and the assemblies was again performed with native PAGE (Figure 14b and Figure 15b).

All three structures showed a very efficient gene silencing activity similar to the one of 1bb2si (Figure 15c). In contrast to the previous experiments, all DNA extensions are attached to the 5' end of the siRNA passenger strand. The decreased silencing potential observed for the non-reducible 5' end extended construct could be overcome by incorporation of the disulfide linker. The passenger strand extended

constructs without backbone strand (SS-siRNA/3'ov, SS-siRNA/5'ov) outperformed their non-reducible equivalents.

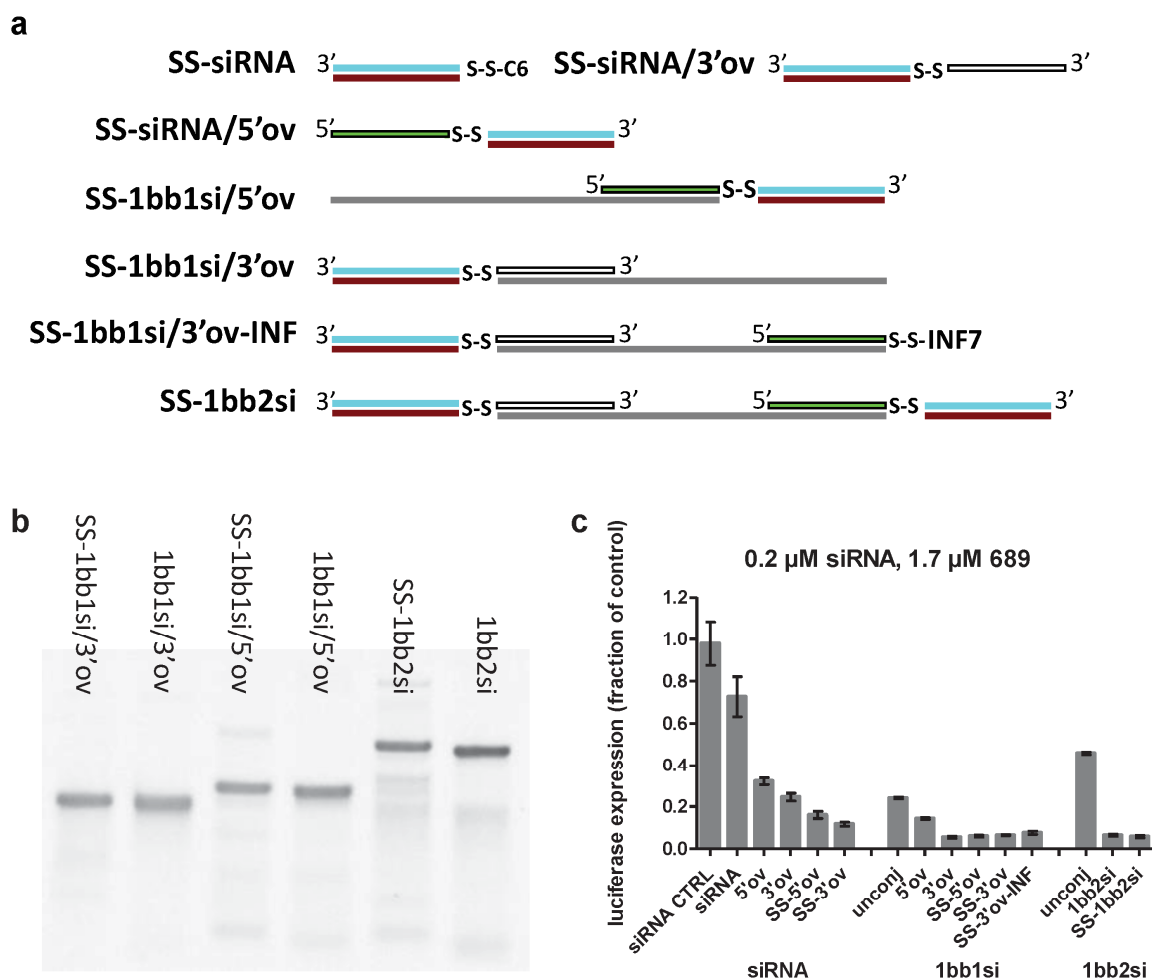


Figure 15. Bioreducible conjugation of the siRNA to the DNA backbone using disulfide chemistry. (a) Schematic representation of the structures from previous experiments with a disulfide linker introduced between the 5' passenger strand and the DNA extension. For SS-1bb1si/3'ov-INF, influenza peptide 7 is conjugated to the 5' DNA extension *via* its cysteine (see chapter 2.3.12). (b) Verification of correct assembly by native PAGE (gel cropped). (c) Transfection efficiency of the disulfide containing constructs. Adapted from [104].

The results for the substructures of 1bb2si, the star-shaped structures, the step-by-step extension and the bioreducible constructs could also be reproduced when performed at a constant N/P ratio of 6 (Appendix Figure 1).

3.1.8. Challenging the constructs

As the silencing for the outstanding structures had reached a level that made it hard to draw conclusions on the effect of the bioreducible attachment of the siRNA or the larger stepwise-extended structures, the best performing constructs were further compared by determining their EC₅₀ values (Figure 16). The polyplexes were formed at a siRNA concentration of 1 μM (corresponding to the previous transfections) and diluted stepwise in HBG. The siRNA concentration was plotted against luciferase expression, the x-axis was log₁₀ transformed and the linear range was determined. The EC-50 values were calculated *via* $EC_{50} = 10^{((0.5 - b) / a)}$.

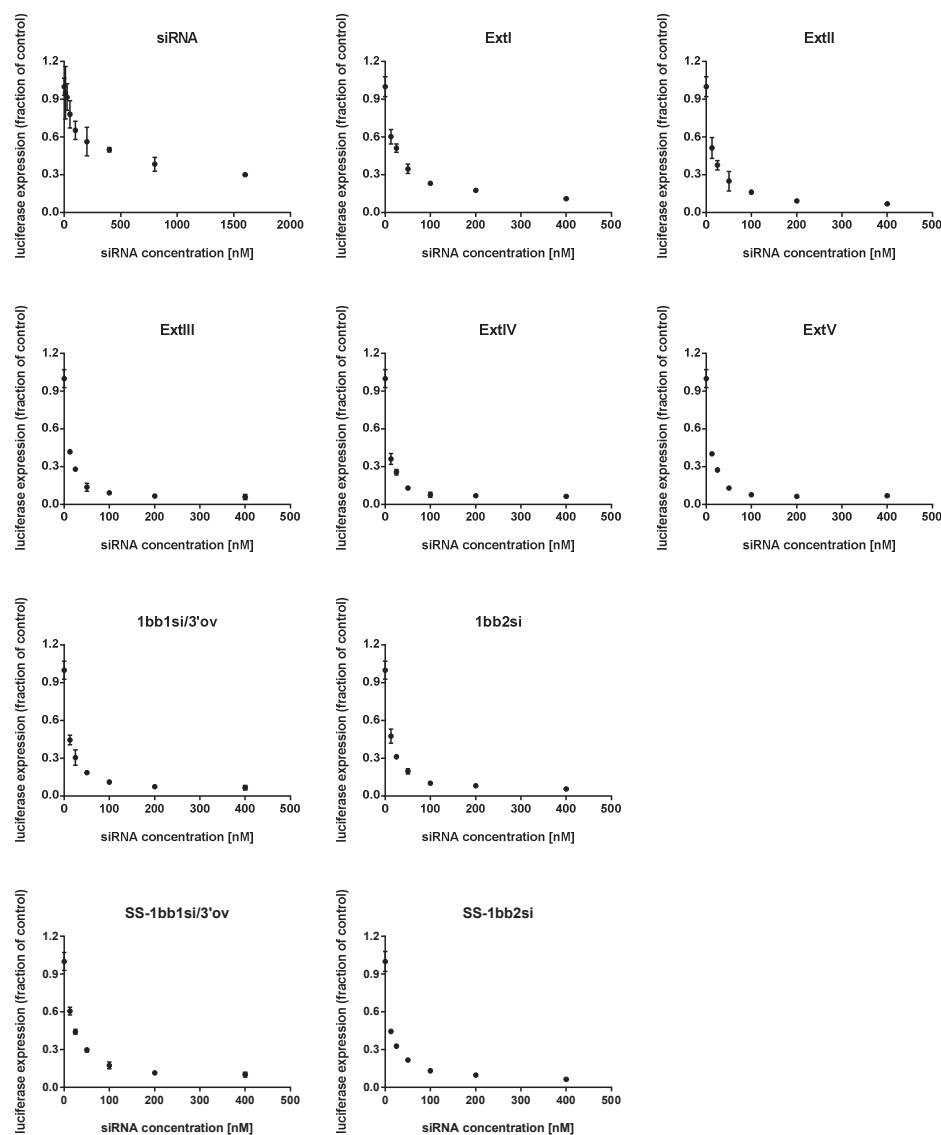


Figure 16. Dose-response curves for EC₅₀ value determination. Polyplexes were formed at a siRNA concentration of 1 μM and diluted in HBG before they were added to the cells (Incubation time on the cells: 1.5 h). Adapted from [104].

The difference between the structures remained non-significant with the following exceptions. The EC₅₀ value of SS-1bb1si/3'ov (19.9 nM) was *circa* two fold higher than the EC₅₀ value of the remaining structures containing the 79 nucleotides backbone strand. In case of the step-by-step extended siRNA, Ext IV (181 nucleotides, EC₅₀ of 4.4 nM) performed significantly better than Ext II (99 nucleotides, EC₅₀ of 11.7 nM) for which luciferase knock-down was already saturated at 0.2 μM siRNA (Figure 17).

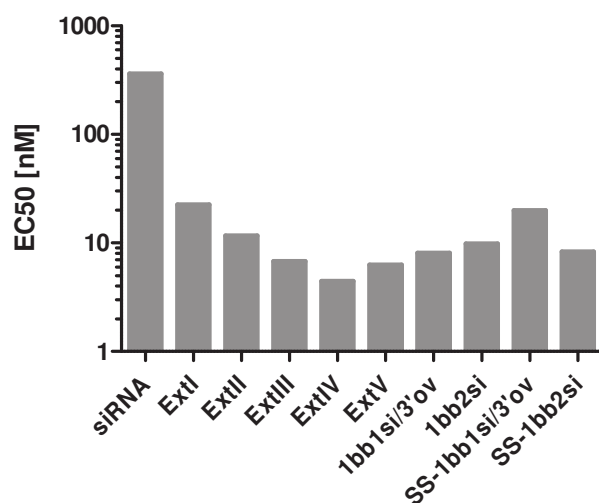


Figure 17. EC₅₀ values for best performing constructs with oligomer 689. For evaluation, the X-axis was log₁₀ transformed and the EC₅₀ value was determined from linear regression via $EC_{50} = 10^{((0.5 - b) / a)}$. Adapted from [104].

3.1.9. Luciferase knockdown is mediated by eGFP siRNA

To demonstrate that the reduced luciferase expression upon application of the DNA-extended constructs is really due to siRNA mediated mRNA downregulation, the following experiments were performed.

The metabolic activity of the cells after transfection was determined with a MTT assay (Figure 18). MTT is added to the cells and its reduction to purple formazan by cellular oxidoreductases can be regarded as a measure for metabolic activity. None of the structures led to a drastic decrease in formazan production as determined at a siRNA concentration of 0.2 μM with a MTT assay.

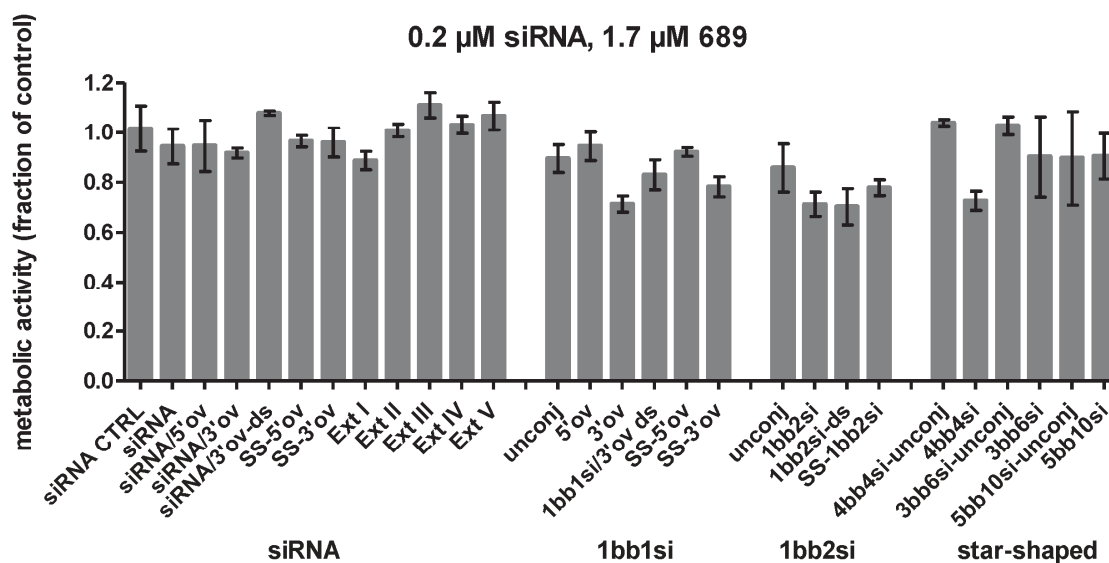


Figure 18. Metabolic activity assay with oligomer 689. Metabolic activity after transfection with oligomer 689 was evaluated for all constructs by a MTT assay at an oligomer concentration of 1.7 μ M and a siRNA concentration of 0.2 μ M. Adapted from [104].

To completely rule out unspecific effects, the eGFP siRNA was replaced by a control siRNA for the bioreducible constructs. Thiol modified CTRL siRNA was conjugated to the DNA extension *via* disulfide exchange, as for the eGFP siRNA. The bioreducible CTRL equivalents were assembled and directly compared to the eGFP siRNA nanostructures in a transfection experiment. Luciferase knockdown of the CTRL constructs remained insignificant (Figure 19).

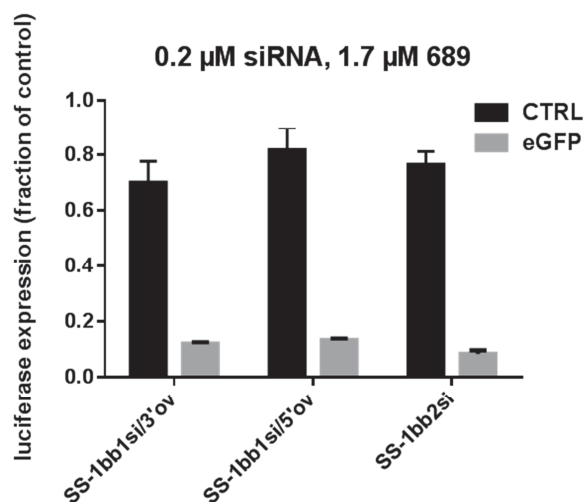


Figure 19. Knockdown of the eGFP-luciferase fusion protein by nanostructures containing a control siRNA instead of eGFP siRNA. SS-1bb1si/3'ov-CTRL, SS-1bb1si/5'ov-CTRL and SS-1bb2si-CTRL were synthesized and assembled similar to their eGFP siRNA equivalents. Adapted from [104].

Taken together with the results from the MTT assay, the reduced luciferase expression by transfection of the eGFP siRNA nanostructures can be attributed to RNA interference mediated knockdown.

3.1.10. Stability and particle sizes

Furthermore a stability analysis with a DNA/RNA binding assay was performed for all constructs (Figure 20). As all larger structures showed already complete complexation at an N/P ratio of 3, the ratio was further decreased down to 0.25 to challenge the polyplexes even more. For the most stable polyplexes, a minor amount remained in the pocket at N/P ratios down to 0.5. A slight decrease in stability could be observed for the star-like structure, siRNA/3'ov and the double-stranded constructs. Differences were non-significant for the step-by-step extended structures and the structures containing the 79 nucleotides backbone strand.

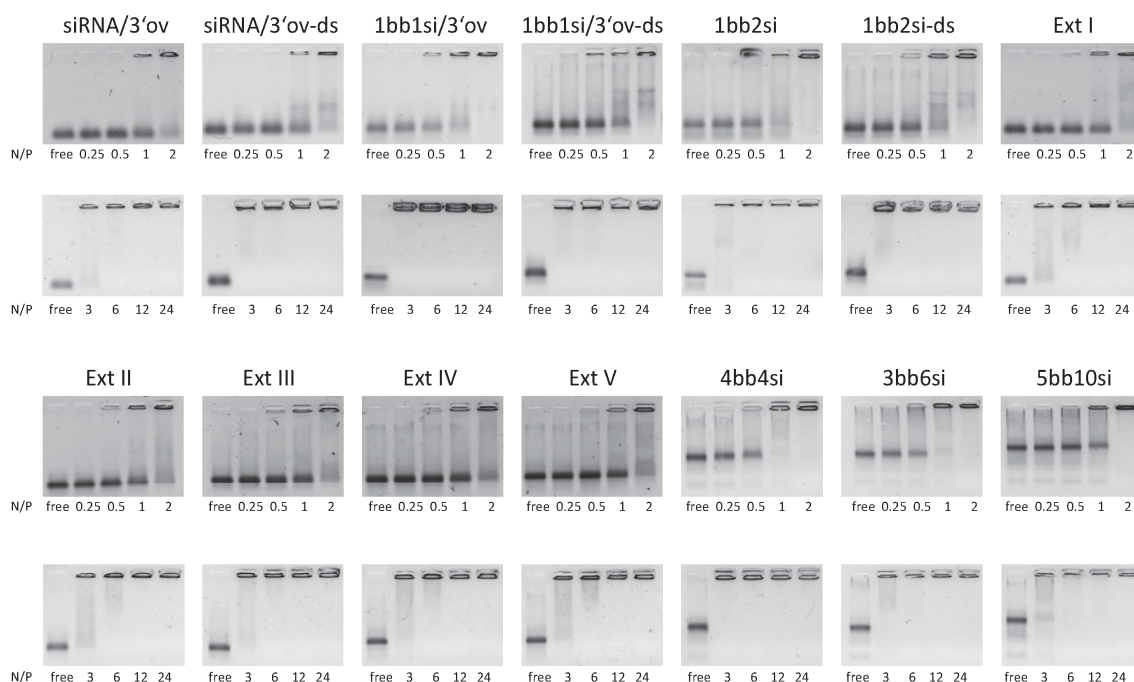


Figure 20. Polyplex stability for all constructs determined by a nucleic acid gel retardation assay. Migration into an agarose gel (1.5 %) was determined for polyplexes prepared at different N/P ratios (0.25 to 24) with oligomer **689**. Complexed DNA/RNA remains in the pocket, while free DNA/RNA migrates into the gel. Adapted from [104].

Dynamic light scattering measurements revealed that polyplexes of oligomer **689** and the siRNA constructs present heterogeneous populations of nanoparticles with sizes in the submicrometer range and high polydispersity indices (Table 1). Like for many related cationic carriers, probably multiple thousands of siRNAs are aggregated into the several hundred nanometer polyplexes. Thus the lack of significant size differences between the different siRNA constructs is not surprising. Results were comparable if a constant oligomer concentration or a constant N/P ratio was applied for polyplex formation.

Table 1. Particle size measurements by dynamic light scattering (adapted from [104])

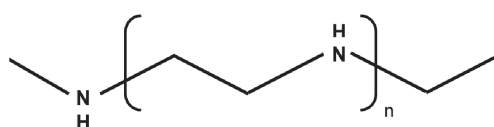
	constant N/P of 6		constant polymer amount*	
	number mean	PDI	number mean	PDI
siRNA	434.7 ± 5.5	0.09 ± 0.034	434.7 ± 5.5	0.09 ± 0.034
siRNA/3'ov	555.8 ± 13.0	0.142 ± 0.031	638.4 ± 11.3	0.196 ± 0.021
Ext I	861.6 ± 89.3	0.469 ± 0.031	976.2 ± 56.9	0.568 ± 0.032
Ext II	495.4 ± 167.0	1.00 ± 0	634.8 ± 92.0	0.907 ± 0.097
Ext III	631.9 ± 86.9	0.827 ± 0.103	744.5 ± 115.1	0.809 ± 0.128
Ext IV	410.8 ± 102.6	1.00 ± 0	272.8 ± 150.4	1.00 ± 0
Ext V	105.6 ± 84.2	1.00 ± 0	71.7 ± 24.7	1.00 ± 0
1bb1si/3'ov	694.7 ± 156.9	0.808 ± 0.185	698.6 ± 133.5	0.919 ± 0.096
1bb2si	412.9 ± 103.4	0.977 ± 0.040	950.6 ± 79.4	0.606 ± 0.062

*corresponding to N/P 6 for siRNA

3.1.11. Different polycations for siRNA transfection

So far, only oligomer **689** was used to test the effect of DNA extension of siRNA on transfection efficiency. It is also of interest if these findings hold true for more commonly used transfection agents like linear polyethylenimine (IPEI), or for lipid-containing formulations such as lipo-oligomer **454** (Figure 21). The latter contains six tyrosines and two oleic acid units which provide excellent stabilization through hydrophobic interactions and endosomal lysis through membrane destabilization. The fatty acid unit is connected to two identical arms consisting of two Stp units, three tyrosines for stabilization and a terminal cysteine [32].

Linear polyethylenimine



Oligomer 454

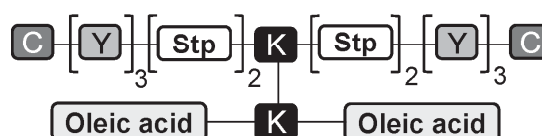


Figure 21. Alternative delivery reagents. Commonly used polyethylenimine (left) and sequence defined lipo-oligomer **454** (C: cysteine; T: tyrosine; Stp: succinoyl-tetraethylene pentamine; K: lysine, structure from N to C)

Hence, siRNA, 1bb2si and 1bb2si-unconj were complexed with IPEI and lipo-oligomer **454** at two different oligomer concentrations (corresponding to N/P 6 for siRNA and 1bb2si respectively) and tested for gene silencing efficiency and metabolic activity in N2A/eGFPluc cells (Figure 22).

Polyplexes formed with IPEI and canonical siRNA worked at neither concentration, while polyplexes formed with IPEI and 1bb2si mediated gene silencing to some extent (Figure 22a and b).

In contrast, if the well-stabilizing lipo-oligomer **454** was used for complexation, canonical siRNA already exhibited an efficient knockdown (82%) which could not be achieved by 1bb2si (60 %). Both constructs were compared at their optimum oligomer concentration (3.9 μ M for siRNA, 9.2 μ M for 1bb2si) (Figure 22c and d).

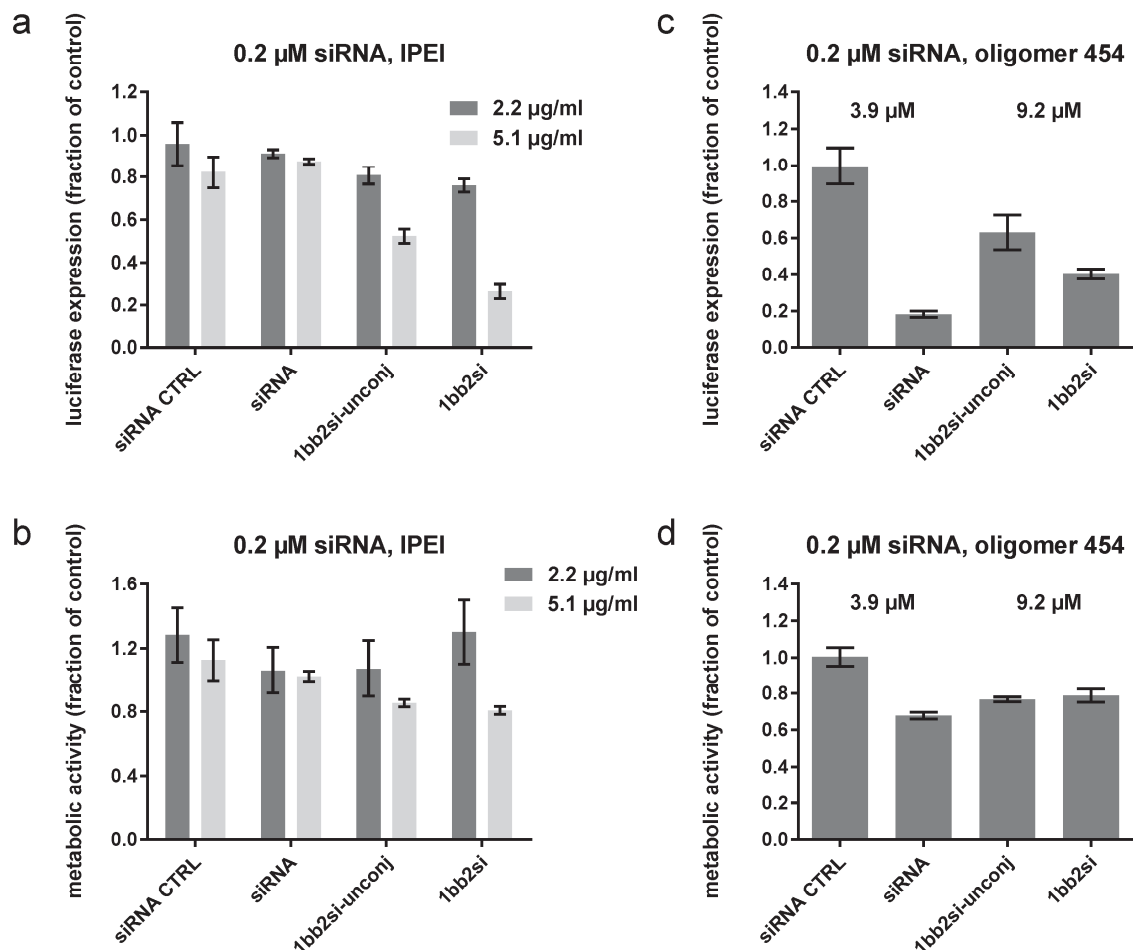


Figure 22. Transfection efficiency and metabolic activity after complexation with linear PEI and lipo-oligomer **454.** Transfection efficiency (a,c) and metabolic activity (b,d) of pure siRNA was compared to 1bb2si after complexation with (left) 2.2 μ g/ml or 5.1 μ g/ml linear PEI and (right) 3.9 μ M or 9.2 μ M oligomer **454**. Adapted from [104].

Consequently one can assume that the findings for oligomer **689** can be translated to other polycationic transfection agents such as IPEI, lacking lipidic moieties. For lipid containing delivery agents the additional stabilizing effect of the DNA extensions appears not to be necessary or may even be counterproductive.

3.1.12. Attachment of functional domains to siRNA

Stabilization of siRNA polyplexes is only one requirement for successful nucleic acid delivery. As mentioned in the introduction, receptor targeting for improved and specific intracellular uptake [36, 106] and transport across the endolysosomal barrier [107, 108] are additional steps where functionalization can be beneficial. Disulfide chemistry provides the option to attach functional units through the DNA backbone strand to the siRNA. INF7 is a lytic peptide known to promote endosomal escape [109]. It was coupled to the 3' thiol modified DNA extension sequence by the peptide's N-terminal cysteine. A construct containing one 5' passenger strand extended siRNA connected *via* the DNA backbone to INF7 was assembled as previously described (SS-1bb1si/3'ov-INF) (Figure 23a). As expected, after complexation with oligomer **689**, the inclusion of INF7 had no advantage over the respective construct without INF7 (SS-1si1bb/3'ov) (Figure 15c). The histidines of oligomer **689** already promote sufficient endosomal escape. Hence, oligomer **356**, lacking histidines, was used to verify a positive effect of INF7 as part of the nanostructure (Figure 23b). Oligomer **356** is a three armed oligomer of which two arms contain positively charged Stp and terminal cysteines for polyplex stabilization. The third arm contains 24 ethylene glycol units (PEG₂₄) for shielding and enhanced solubility and, in addition, folic acid to promote specific cellular uptake in folate receptor expressing cells [24].



Figure 23. INF7 siRNA conjugate via a DNA backbone strand and oligomer 356. (a) Schematic representation of SS-1bb1si/3'ov-INF (b) Oligomer **356** for complexation of SS-1bb1si/3'ov-INF (C: cysteine; Stp: succinyl-tetraethylene pentamine; K: lysine; PEG₂₄: polyethylene glycol consisting of 24 ethylene glycol units; FoIA: folic acid, structure from N to C). Adapted from [104].

The polyplexes were incubated on folate receptor positive KB/eGFPluc cells with an incubation time of 1 h and a siRNA concentration of 0.2 μ M (Figure 24).

Indeed, SS-1bb1si/3'ov-INF showed a great increase in silencing over SS-1bb1si/3'ov and canonical siRNA without reduction in metabolic activity, which could also be reproduced at a constant N/P ratio of 6, 12 and 24 (Appendix Figure 2).

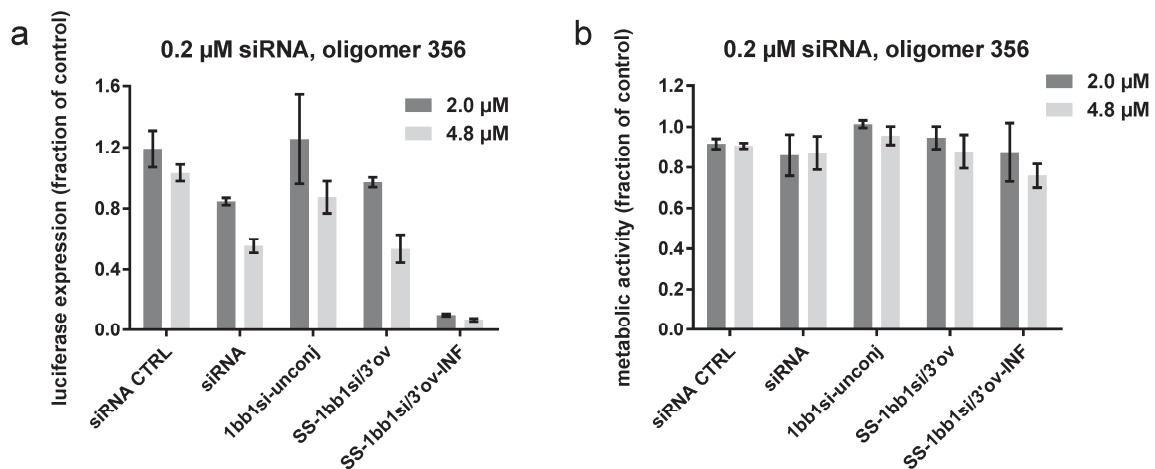


Figure 24. Transfection efficiency and metabolic activity of the INF7 siRNA conjugate. Comparison of siRNA hybridized to the DNA backbone strand with (SS-1bb1si/3'ov-INF) and without INF7 (1bb1si/3'ov). Incubation time was 1 h on KB/eGFPluc cells. Adapted from [104].

Folate-targeting was verified by including folate in the medium or using control oligomer **188**, which contains alanine instead of folate (Figure 25). In both cases the polyplex exerted no significant reduction in luciferase expression anymore.

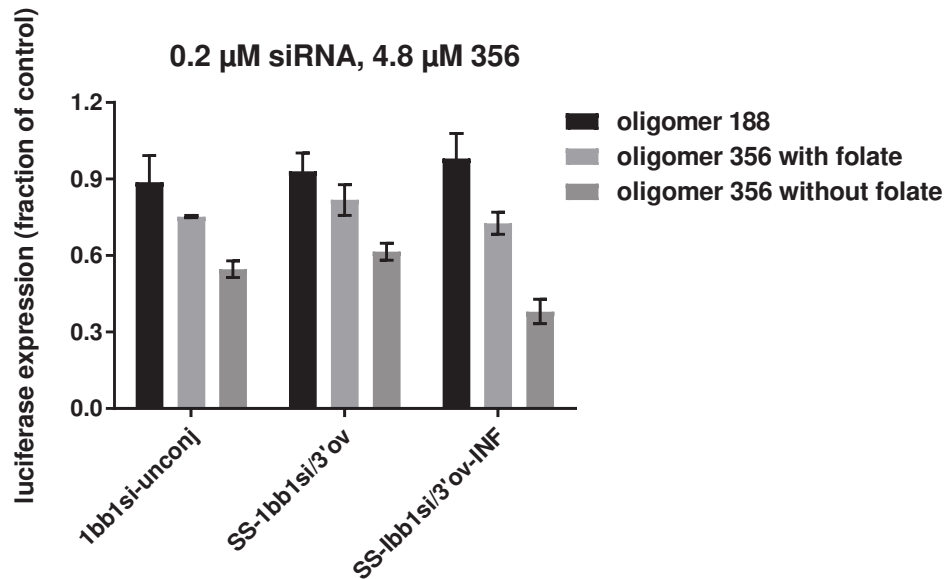


Figure 25. Folate receptor targeting of SS-1bb1si/3'ov-INF with oligomer 356. Folate targeting was verified by testing the formulation in a ligand competition assay, using both folate-containing medium ('with folate') and folate-free medium ('without folate'). In addition, lack of gene silencing by using ligand-free oligomer **188** (similar to oligomer **356**, but with folic acid ligand replaced by alanine) was evaluated. Adapted from [104].

Taken together these results, a highly functional polyplex out of DNA extended and INF7 functionalized siRNA and oligomer **356** could be formed. It harbours several domains to cope with the barriers for successful siRNA delivery. The DNA extension provides a high polyplex stability (Figure 26), PEG shields the nanoparticles from its environment, folate leads to receptor specific uptake and endosomal escape is guaranteed by INF7.

This proves that functional units can be attached to siRNA in a very simple way *via* a tunable DNA adaptor that improves polyplex stability itself.

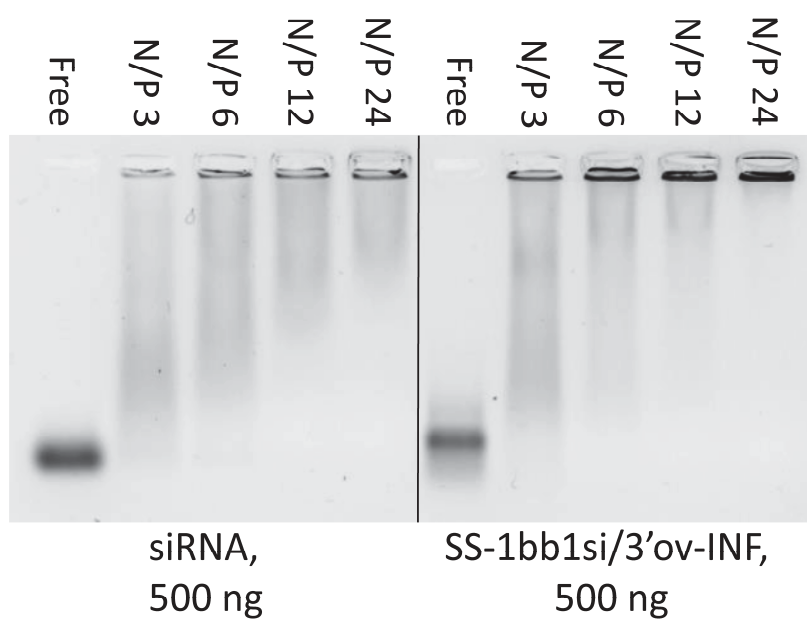


Figure 26. Binding assay for canonical siRNA and 1bb1si/3'ov-INF with oligomer 356. Complexed nucleic acids remain in the loading pocket while free nucleic acids migrate into the gel. Adapted from [104].

3.2. Localization and integrity of small single-stranded RNA

This chapter has been partly adapted from:

Philipp Heissig, Waldemar Schrimpf, Philipp Hadwiger, Ernst Wagner, Don C. Lamb, Monitoring integrity and localization of modified single-stranded RNA oligonucleotides by ultrasensitive fluorescence methods, PLOS ONE, in press.

3.2.1. Oligonucleotide Design

The model sequence is 23 nucleotides in length, with a thiol modification at its 5' and an amine modification at its 3' end. The sequence was originally selected as a putative antagomir against microRNA200c [94, 110], which is not present in the tested HeLa cell line in significant quantities [111]. HeLa cells were selected to rule out any sequence-specific interactions, as the current study focuses on the stability and localization of the RNAs irrespective of their effector function. Atto488 (excitation maximum: 501 nm; emission maximum: 523 nm, NHS-ester modified) and TMR (excitation maximum: 557 nm; emission maximum: 576 nm, maleimide modified) were selected as a FRET pair for dual labelling at the ends and attached to the 3' end *via* an amide bond and to the 5' end *via* formation of a thioether. This approach provided us with a very sensitive read-out as cleavage of a single nucleotide already leads to separation of the two dyes (Figure 27). Cleavage can be detected using FCS (through a reduction in the diffusion time), FCCS (*via* a loss in cross-correlation signal) and FRET (*via* a loss in FRET signal, which can be detected using either fluorescence intensity or fluorescence lifetime measurements). After the sequence is exposed to the cellular environment, cleavage is mediated by nucleases. RNase A and RNase T2 family members cleave single-stranded RNA with high specificity and affinity [83, 84].

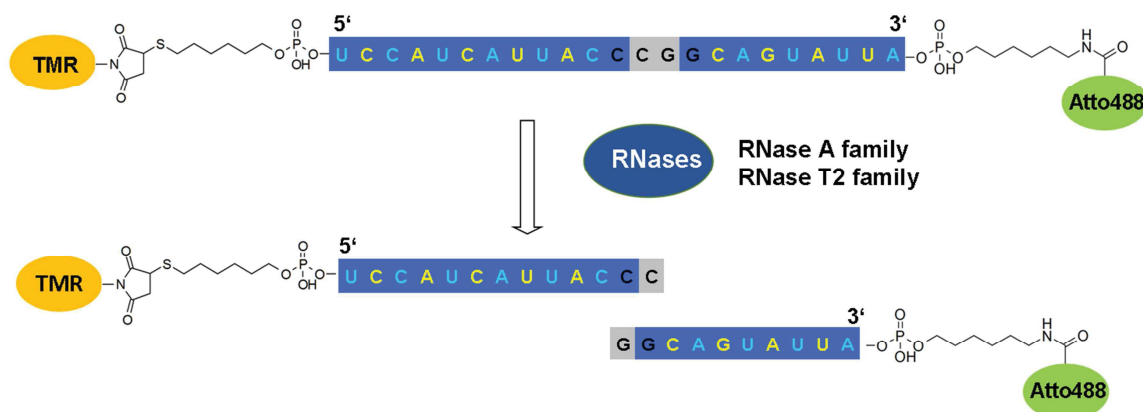


Figure 27. Design of the dual-labelled RNA oligonucleotide. (A) 23 nucleotides RNA oligonucleotide conjugated to tetramethylrhodamine (TMR) at its 5' end *via* a thioether bond and at its 3' end to Atto488 *via* an amide bond. Upon exposure to the cellular environment, the oligonucleotide can be degraded by various RNases.

Three different chemical backbone modifications were selected for this approach: natural phosphodiester bonds were replaced with phosphorothioate bonds (PS). RNA residues were replaced by 2'-modified analogues. 2'-Fluoro (2'-F) and 2'-O-Methyl (2'-O-Me) modifications were selected as these are widely used in RNAi and antisense applications.

As a stable control, a sequence consisting of a completely PS-modified backbone and alternating 2'-O-Me and 2'-F modifications was selected, since it was shown that this sequence provides adequate nuclease resistance [64]. Construct 1 is almost identical to the stable control with the exception of a single phosphodiester bond between nucleotide 10 and 11 counted from the 3' end surrounded by two non-modified nucleotides on each side (Figure 28). This provides a relatively stable sequence, which might still be susceptible to nucleolytic cleavage and can be used to investigate the intracellular location-specific RNase activity. Construct 2 has four PS and four 2'-O-Me modifications at the 5' and the 3' end, giving a stretch of 15 unmodified nucleotides in the middle. This should result in faster nucleolytic degradation, however, leaving the dyes attached to a four-nucleotide RNA strand. Hence, the cell treats the residual, labelled construct similar to unlabelled RNA even after degradation of the unmodified domain. As a second control, a completely unmodified RNA strand is included to confirm the effect of the modifications (Figure 28).

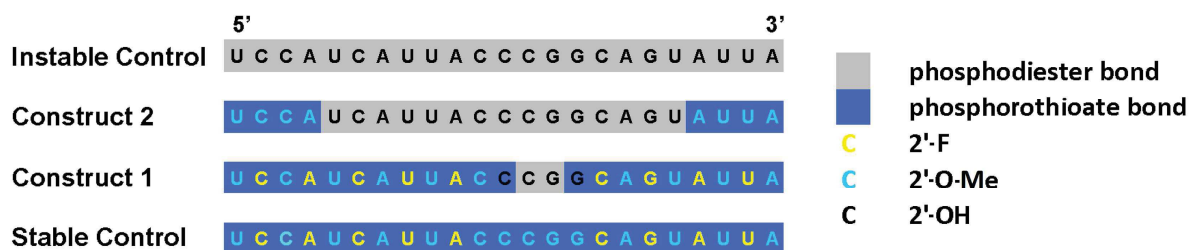


Figure 28. Modification patterns selected to monitor localization and integrity of the oligonucleotide. RNA backbone modifications to increase stability towards nucleolytic degradation: 2'-F, 2'-O-Me and phosphorothioate.

3.2.2. Stability evaluation in cell extracts

Initial experiments were conducted in cell extracts to get a first hint of the stabilizing effect of the modifications. 100 nM of RNA was incubated in HeLa whole-cell extracts at 37 °C. The time course of degradation was observed every 5 min with a confocal microscope and the concentration of cell extract was optimized to ensure an appropriate degradation rate for a measurement duration of 3 h (1/10 dilution). Evaluation was accomplished simultaneously using FCS, FCCS and FRET, providing us with distinct information about the behavior of the differently modified oligonucleotides.

3.2.2.1. Fluorescence correlation spectroscopy

The diffusion time of Atto488 or TMR containing particles through the focus was determined using the temporal auto-correlation analysis of the fluorescence intensity fluctuations (Figure 29a). Since pulsed interleaved excitation (PIE) was used [102], the influence of spectral crosstalk was removed resulting in correlation functions that are not biased by the presence of the other dye.

The diffusion coefficient inversely correlates with the particle size. This means that the diffusion coefficient of the dye conjugate increases when nucleotides are removed from the RNA construct over time. To quantify this degradation, an autocorrelation function (ACF) for two diffusing components was used to fit the data. In this simplified assumption, the slow component represents the full construct while the fast component corresponds to a digested dye-RNA fragment. The decrease in

the amplitude of the slow component was taken as a measure for oligonucleotide degradation.

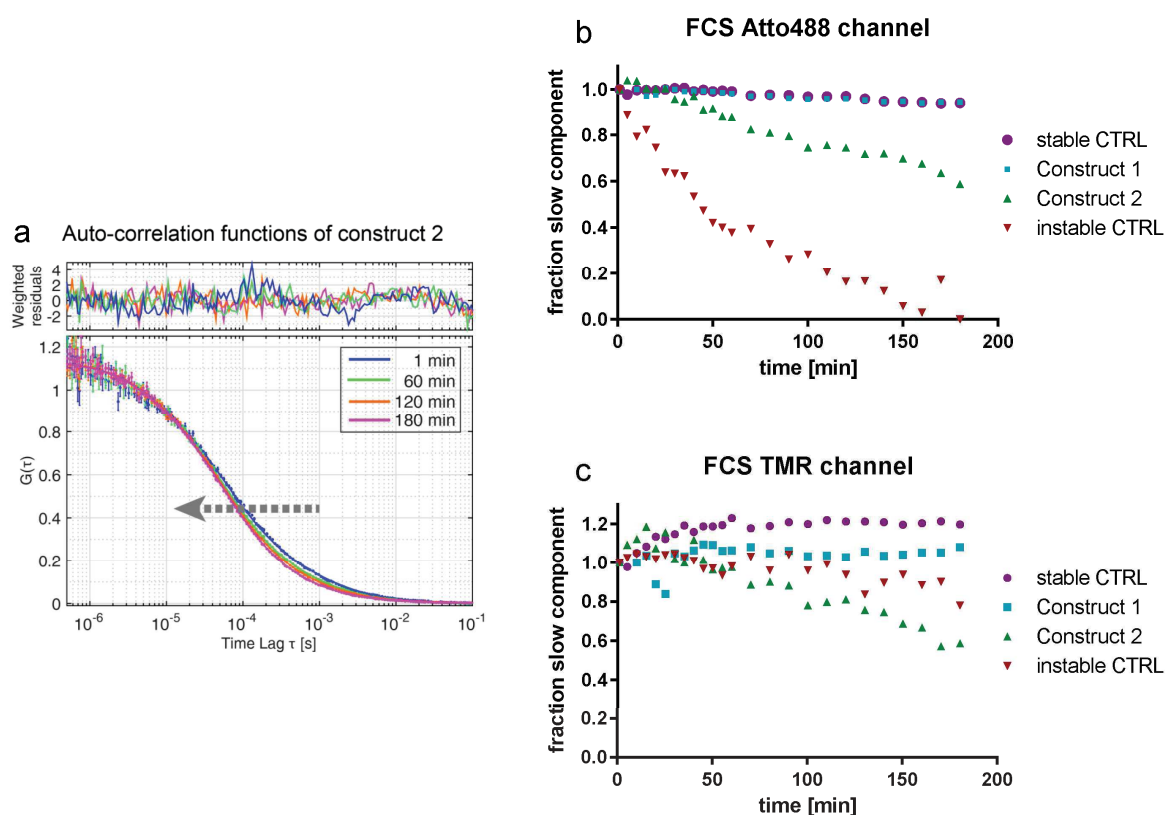


Figure 29. Monitoring degradation of the dual-labelled constructs in cell extracts using FCS. (a) The diffusion time is extracted from the autocorrelation function. Degradation of all four constructs over 200 min is analyzed by autocorrelation of the (b) Atto488 channel and the (c) TMR channel. The curves were normalized to 1 for the initial data-point. The measurements were performed by Waldemar Schrimpf (Department of Physical Chemistry, LMU).

The degradation dynamics of the different RNAs can be nicely observed from the FCS signal of Atto488. While no change in ACF was observed for the stable control and construct 1, the instable control and construct 2 degraded with time (Figure 29b). Assuming a monoexponential decay, the half-life of construct 2 was 4.7 times longer than for the instable control (construct 2: 220 min, instable control: 47 min) (Table 2). This stabilizing effect is attributed to the chemically modified ends of construct 2 (Figure 28). A single cleavage event at the unmodified position of construct 1 might not be recognized by this technique, as the dyes still contain a relatively long stretch of modified RNA which contributes to the slow component in the fit.

Analysis of the ACF from FCS measurements of TMR provided similar results with construct 1 and the fully modified RNA strand being more stable than construct 2 and

the unprotected RNA strand (Figure 29c). However, the change in the diffusion coefficient for the unprotected RNA strand was not as large as expected. This could be due to the association of the TMR with cellular proteins, as FCS measures only the mobility of the probe. The FCS measurements of TMR showed a high variation in diffusion coefficients of the slow component between the different constructs, suggesting that aggregation may play a crucial role. To avoid the complications of a purely FCS based analysis, a fluorescence cross-correlation analysis was performed on the same data.

Table 2. Half-lives of the differently modified constructs in HeLa cell extracts

	FCS (blue channel)	FCCS	FRET (lifetime)	FRET (intensity)
stable CTRL	> 1000 min	> 1000 min	401 min	564 min
Construct 1	> 1000 min	610 min	148 min	331 min
Construct 2	220 min	172 min	170 min	239 min
instable CTRL	47 min	89 min	103 min	128 min

3.2.2.2. Fluorescence cross-correlation spectroscopy

In FCCS, the fluorescence intensity fluctuations in one channel (corresponding to Atto488) are correlated to the fluctuations in the other channel (corresponding to TMR). Hence, when a RNA carries both labels, a cross-correlation signal will be observed. A single cleavage event leads to a complete loss in the cross-correlation amplitude, which makes this technique very sensitive (Figure 30a). By combining FCCS with PIE [102, 112] spectral cross-talk is removed, further increasing the sensitivity of the technique. This method is less biased towards cellular protein association compared to FCS, as the cross-correlation does not depend on the size of the construct. The FCCS results were consistent with FCS, with the exception that construct 1 revealed a slight degradation compared to the stable control, which is in accordance with the increased sensitivity of FCCS (half-life of 610 min). As determined by this technique, the half-life of construct 2 (172 min) was 1.9 times longer than the half-life of the instable control with 89 min (Figure 30b and Table 2).

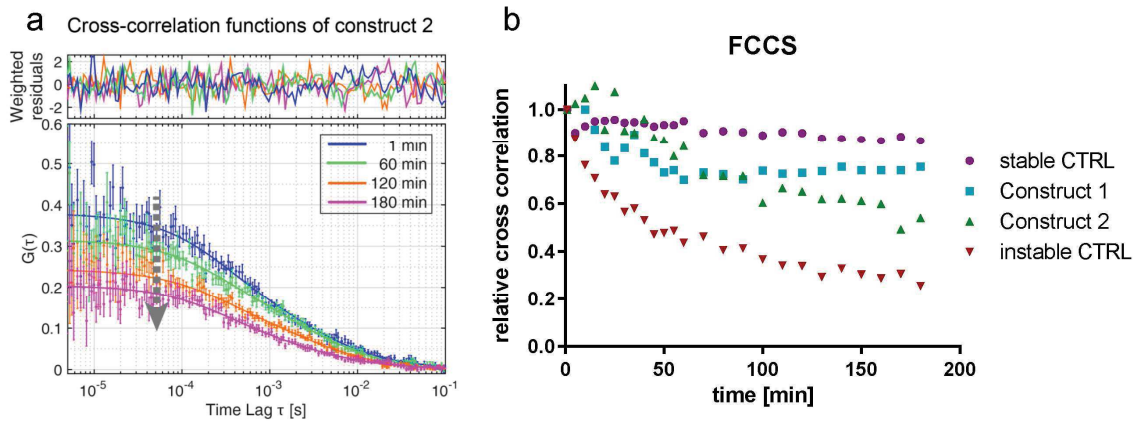


Figure 30. Monitoring degradation of the dual-labelled constructs in cell extracts using FCCS.

(a) The integrity of the constructs is extracted from the amplitude of the cross-correlation function. (b) Degradation of all four constructs over 200 min is analyzed by FCCS. The curves were normalized to 1 for the initial data-point. The measurements were performed by Waldemar Schrimpf (Department of Physical Chemistry, LMU).

3.2.2.3. Förster resonance energy transfer

Another measure of dual-labelled RNA integrity is FRET, which can be evaluated based on fluorescence intensity ratios or *via* the fluorescence lifetime of the donor dye. Non-radiative energy transfer from the donor to the acceptor dye depends on their spatial separation and can be observed for distances up to 10 nm. Hence, the intact double-labelled RNA should give a significantly higher emission in the red channel (TMR) and a reduced lifetime for the donor upon excitation of Atto488 than the cleaved construct (Figure 31a and b). Similar to FCCS, this technique is sensitive to a single cleavage event. Intensity based FRET is calculated from the ratio of the red signal after Atto488 excitation to the sum of red and green fluorescence after Atto488 excitation, corrected for spectral crosstalk of Atto488 into the acceptor channel and direct excitation of TMR. A parameter that was not accounted for was incomplete labelling of the RNA and possible degradation of the RNA before the experiment. However, since the RNA degradation in cell extracts was expected to be exponential, these parameters would only change the initial values and not affect the rate constants. FRET also provides information on the conformation of the RNAs. As transitions between coiled and stretched conformations change the distance between the dyes, the measured FRET efficiencies depend on the conformational state.

Furthermore, FRET measurements can be sensitive to artifacts from pH or aggregation dependent quenching of the dyes.

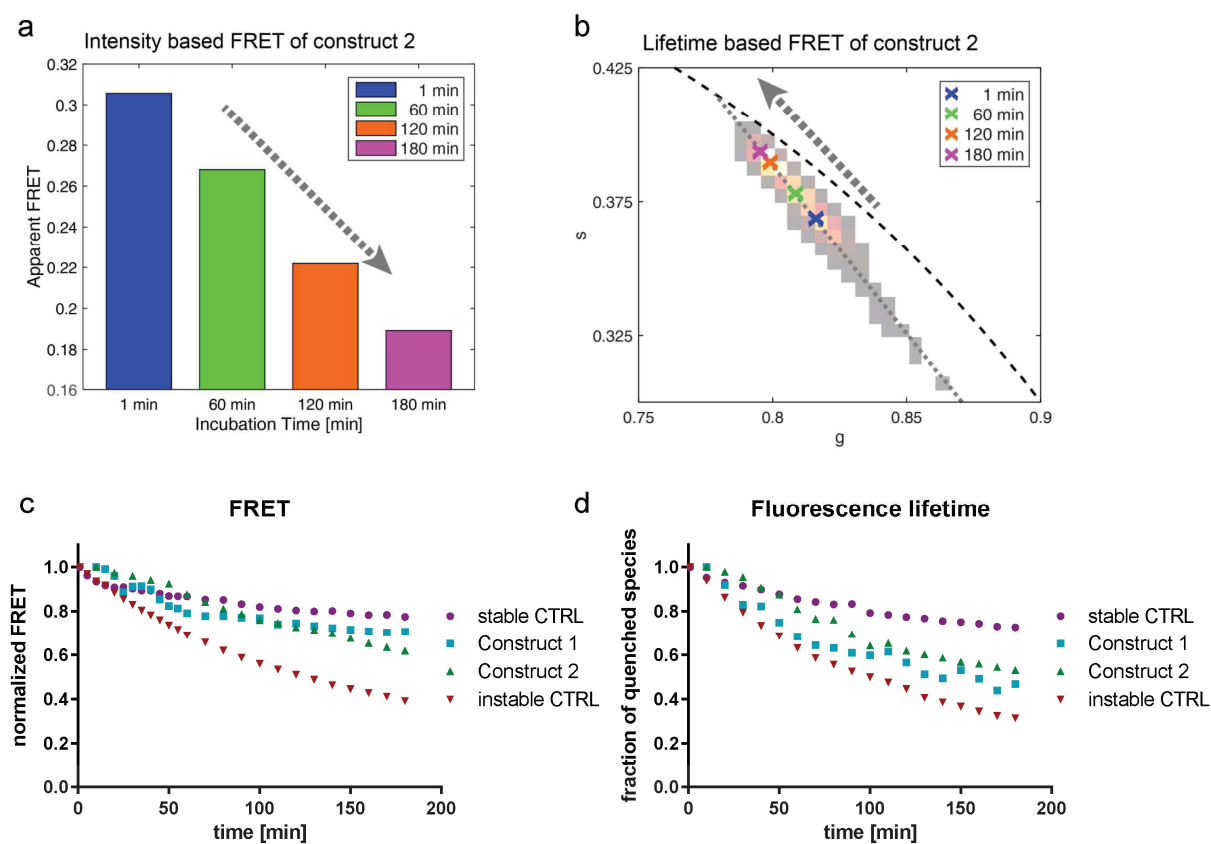


Figure 31. Monitoring degradation of the dual-labelled constructs in cell extracts using FRET.

FRET efficiency is determined from (a) the fluorescence intensities and (b) the donor fluorescence lifetime based FRET using a phasor analysis. Degradation of all four constructs over 200 min is analyzed by (c) intensity based FRET and (d) donor fluorescence lifetime based FRET. The curves were normalized to 1 for the initial data-point. The measurements were performed by Waldemar Schrimpf (Department of Physical Chemistry, LMU).

The results from the FRET experiments showed that the instable control was degraded the fastest with half-lives of 102 min and 128 min for measurements based on lifetime and intensity, respectively. As expected, construct 1 was more stable than construct 2 for the intensity measurements (half-life construct 1: 331 min, half-life construct 2: 239 min). For the lifetime based analysis, the stability-difference between the two constructs was insignificant (half-life construct 1: 149 min, half-life construct 2: 170 min). Interestingly, the stable control revealed a slight decrease in FRET efficiency over time (half-life: 401 min for lifetime based and 564 min for intensity based FRET) (Figure 31c and d, Table 2).

As no degradation is visible when evaluated by FCS or FCCS, this might be due to interactions with cellular components affecting the conformation of the construct or the lifetime of the Atto488.

Taken together, the results obtained from the different read-outs show that the extent of modification of the construct strongly correlates with its stability in cell extracts. Highly sensitive data for cleavage of just a single nucleotide can be obtained by FCCS. FRET provides additional information on the conformational state of the RNA while FCS detects association with cellular components. Applying only a single technique might lead to misinterpretation of the data, as artifacts like quenching, conformational changes and aggregation might be mistaken for stability related issues.

3.2.3. Measurements in cells

3.2.3.1. Transfection

After having elucidated the fate of the chemically modified oligonucleotides in cell extracts, the next question was if the results hold true when the RNAs are transfected directly into HeLa cells. The sequence defined cationic oligomer **278** [25, 30] was selected as a carrier, as it displays fast cellular uptake, which is indispensable for a time course degradation experiment. **278** is a U-shaped lipo-oligocation consisting of a protonable backbone of three succinoyl-tetraethylene pentamine (Stp) units for complexation of the nucleic acid. Terminal cysteines introduced for polyplex stabilization by disulfide formation are separated from the Stp units by branching lysines, which are connected to four linoleic acids which aid particle stabilization through hydrophobic interactions (Figure 32). Polyplexes were formed using oligomer **278** and the respective modified oligonucleotide and incubated on HeLa cells at a RNA concentration of 167 nM. After 15 min, non-bound polyplexes were washed away from the cells followed by an additional incubation at 37 °C. Biological processes were stopped at different time points by fixation with 4 % paraformaldehyde and the cells were examined under a confocal microscope.

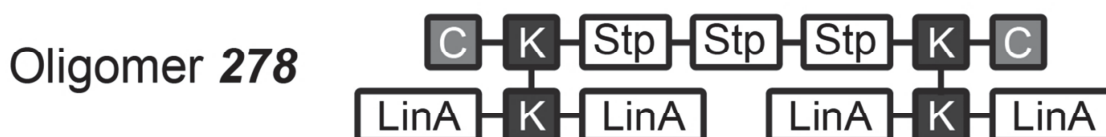


Figure 32. Oligomer 278 for transfection of the constructs into HeLa cells. U-shaped, sequence defined cationizable lipo-oligomer **278** for complexation of the dual-labelled RNAs (C: cysteine, K: lysine, Stp: succinoyl-tetraethylene pentamine, linA: linoleic acid, structure from N to C).

3.2.3.2. Fluorescence intensity

The fluorescence intensities of the four modification patterns were investigated after 15 min, 1 h, 6 h and 24 h (Figure 33a). The polyplexes were not immediately released after endosomal uptake. In fact, the RNA constructs continuously enter the cytosol over a longer time span. This accumulation is counteracted by RNA degradation and subsequent depletion from the cells. The fluorescence intensities that were observed for the four constructs at different time points reflect this balance (Figure 33b). In the measurements, the increase of the fluorescence intensity correlated with the extent of modification and, for the two most stable constructs, also with the duration of the incubation time after the transfection. For the less stable patterns, even a slight decrease in RNA concentration was observed over time. Especially the instable control showed very low fluorescence intensity at all time points. After the construct is taken up, it is almost immediately degraded by RNases. Since the dyes are no longer coupled to RNA, they are not retained in the cells, resulting in a low steady-state concentration.

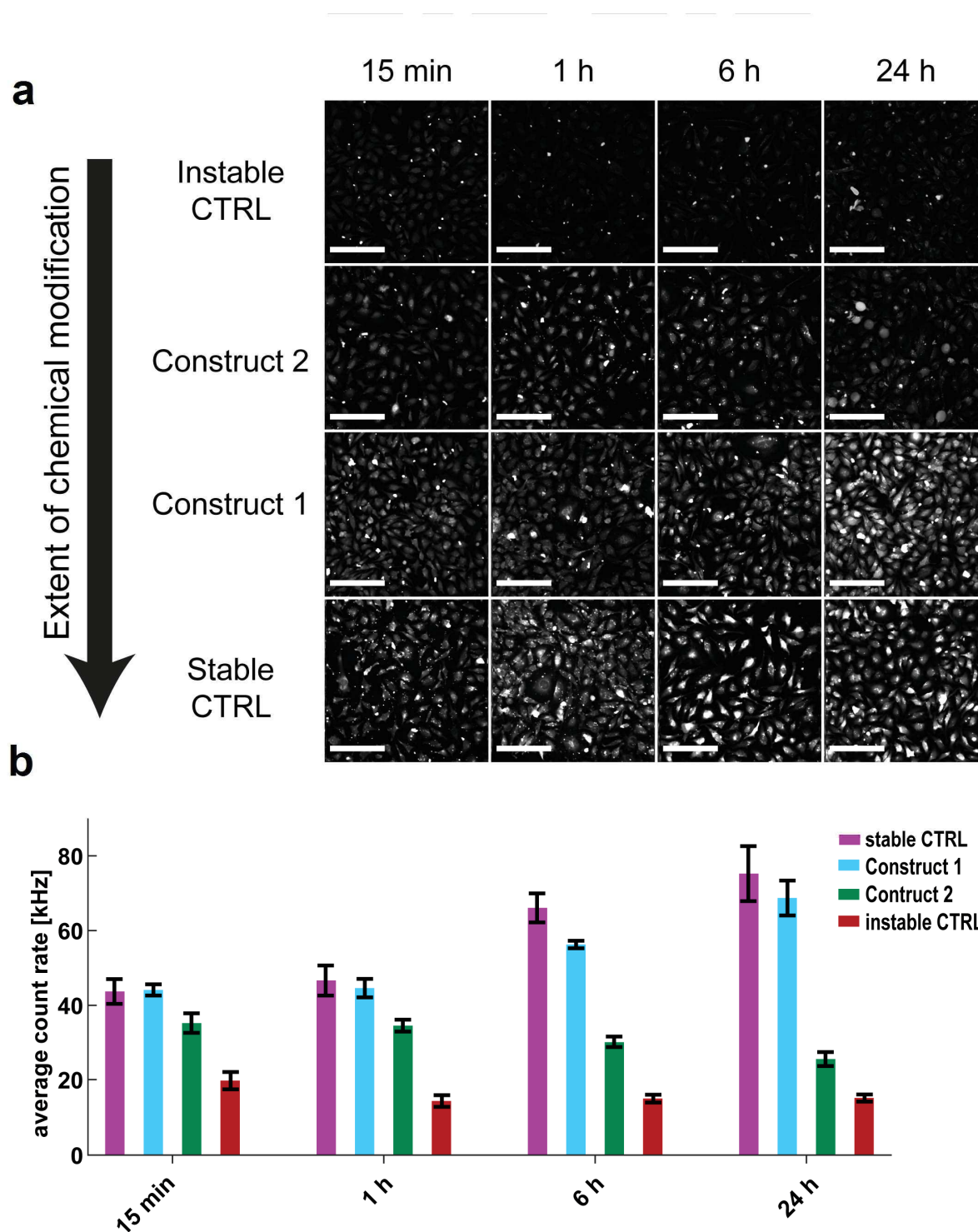


Figure 33. Fluorescence intensities of HeLa cells in culture after transfection with oligomer 278.

(a) Fluorescence intensity images of the HeLa cells 15 min, 1 h, 6 h and 24 h after transfection of the four different modification patterns. The contrast level is equal for all images. The scale bar represents 200 μm . (b) Average fluorescence count rate of the cells at the different conditions shown in (a). The error bars represent the standard deviation of three independent measurements. The measurements were performed by Waldemar Schrimpf (Department of Physical Chemistry, LMU).

Taking a closer look at the cells, one can distinguish between two populations: cells showing a high fluorescence intensity in the nucleus and cells showing a higher fluorescence intensity in the cytosol (Figure 34). The cells that show a strong nuclear translocation of the constructs also have a brighter total intensity. This nuclear translocation is not present for the instable control as degradation dominates over other cellular processes.

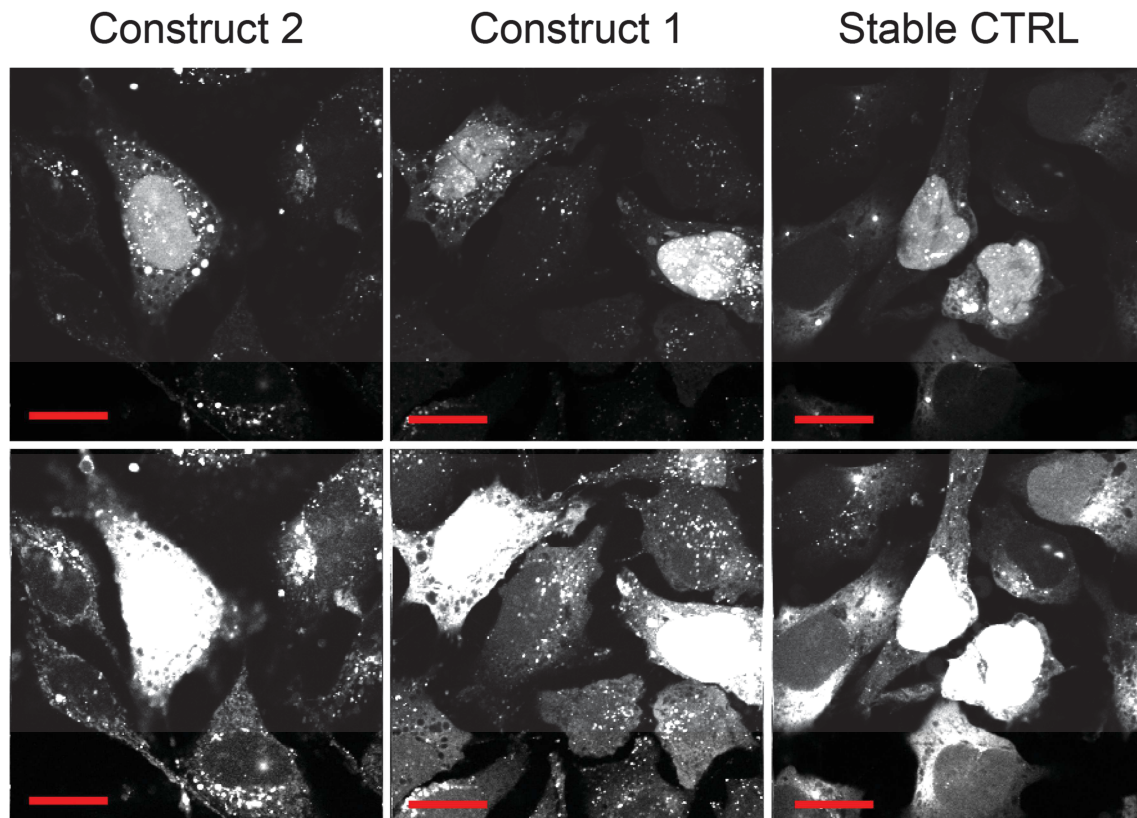


Figure 34. Nuclear translocation of the dual-labelled RNAs in HeLa cells. Cells with increased RNA concentrations in the nucleus show also an increased overall brightness for the different stabilized constructs. The upper and lower images are the same. The contrast for the upper images is set to allow observation of the bright cells whereas, on the bottom images, the contrast is set to better visualize the dim cells. The scale bar is 20 μm . The measurements were performed by Waldemar Schrimpf (Department of Physical Chemistry, LMU).

3.2.3.3. Fluorescence lifetime in cells

Using fluorescence lifetime imaging microscopy (FLIM), one can gather information regarding the integrity of the RNA constructs at different locations within the cells. Images were collected from cells that had been incubated at 37 °C for 15 min, 1 h, 6 h and 24 h after transfection using oligomer **278** as the carrier. Due to quenching *via* FRET, Atto488 in intact constructs shows a reduced fluorescence lifetime compared to that in cleaved RNA fragments. Thus, the lifetime can be used as a read-out for the progress of RNA degradation. The image is scanned pixel by pixel and the lifetime at each spot is determined using the phasor approach to FLIM (Figure 35 and Figure 37).

The phasor approach is a fit-free way of analyzing lifetime data in the Fourier space by utilizing certain rules that simplify the analysis [113, 114]. The first of these rules is the fact that all purely mono-exponential decays lie on the universal circle centered at (0.5,0) with a radius of 0.5. The exact position on the circle is determined by the fluorescence lifetime, with short decays lying close to the (1,0) point while long lifetimes are closest to the origin. The second important rule is that mixtures of different lifetime species result in a phasor that is a linear combination of the two species. The vector is intensity-weighted meaning that any mixture of two lifetimes will lie on a straight line connecting the phasors of the pure species. Knowing the end positions of this line makes it possible to calculate the fractional contributions for any unknown mixture.

In the phasor plot, the combined FLIM data of all measurements and patterns show a distribution along a line connecting the mono-exponential decays at 4.1 ns (corresponding to unquenched Atto488) and at 1.25 ns (corresponding to the intact construct showing FRET) (Figure 37).

However, there are other sources of fluorescence quenching that need to be considered. The first one is quenching in densely packed particles (vesicles or polyplex aggregates). These regions are recognizable as small bright spots in the images and form a tail towards very short lifetimes in the phasor plot, as shown for the stable control construct with and without the acceptor dye (TMR) 24 h after transfection (Figure 35).

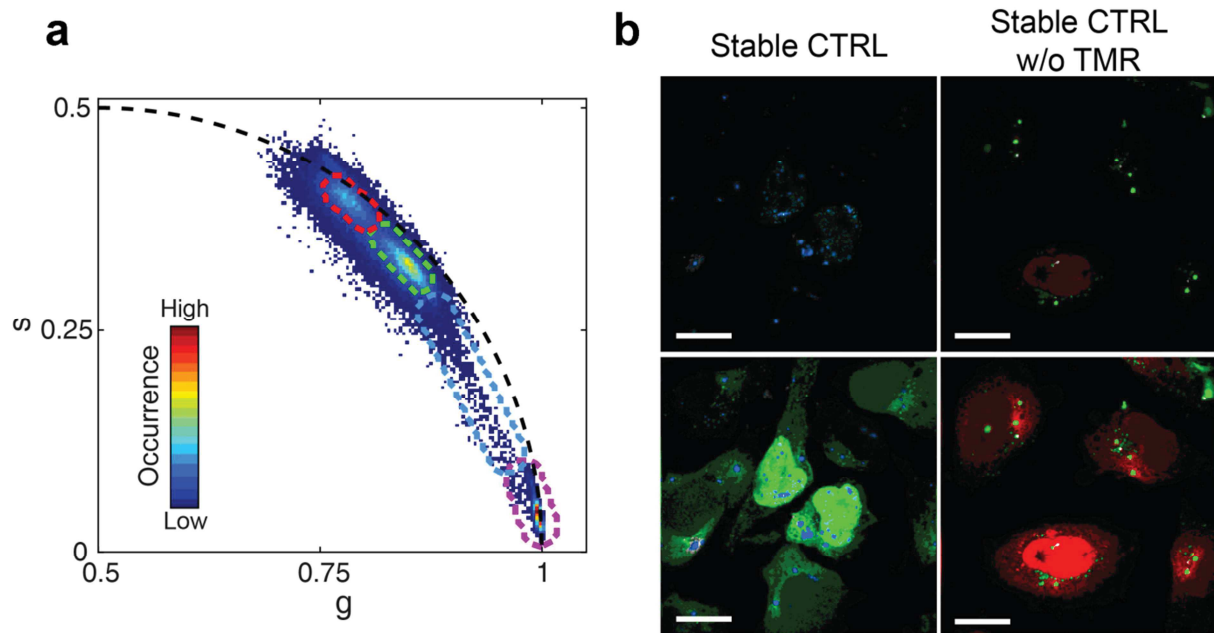


Figure 35. Quenching in polyplexes. (a) Phasor histogram of the FLIM images shown in panel b. The red, green and blue dotted ellipsoids were used to color code the individual pixels in panel b. The magenta ellipsoid highlights the phasor of pure polyplexes (made with the stable control RNA) measured *in vitro*. (b) FLIM images of the stable control both with (left) and without (right) the acceptor dye (TMR) after 24 h incubation (upper panels). The contrast is set to visualize the shorter lifetime of the bright polyplex aggregates in the cells (lower panels). The image contrast was scaled to better visualize the cells. The scale bar is 20 μm . The measurements were performed by Waldemar Schimpf (Department of Physical Chemistry, LMU).

In the control construct without the acceptor dye, quenching in these spots is still noticeable, but much reduced. This suggests that increased FRET between the densely packed RNAs is the main quenching source, but that self-quenching by the dyes or quenching from the carrier oligomer may also play a role. This is also noticeable with intensity based FRET (Figure 36). Using an upper intensity threshold, these aggregates can be easily filtered out and removed from further analysis.

A second source of lifetime changes that do not depend on the integrity of the constructs are conformational changes of the free RNAs as FRET is highly sensitive to the distance between the donor-acceptor dye pair.

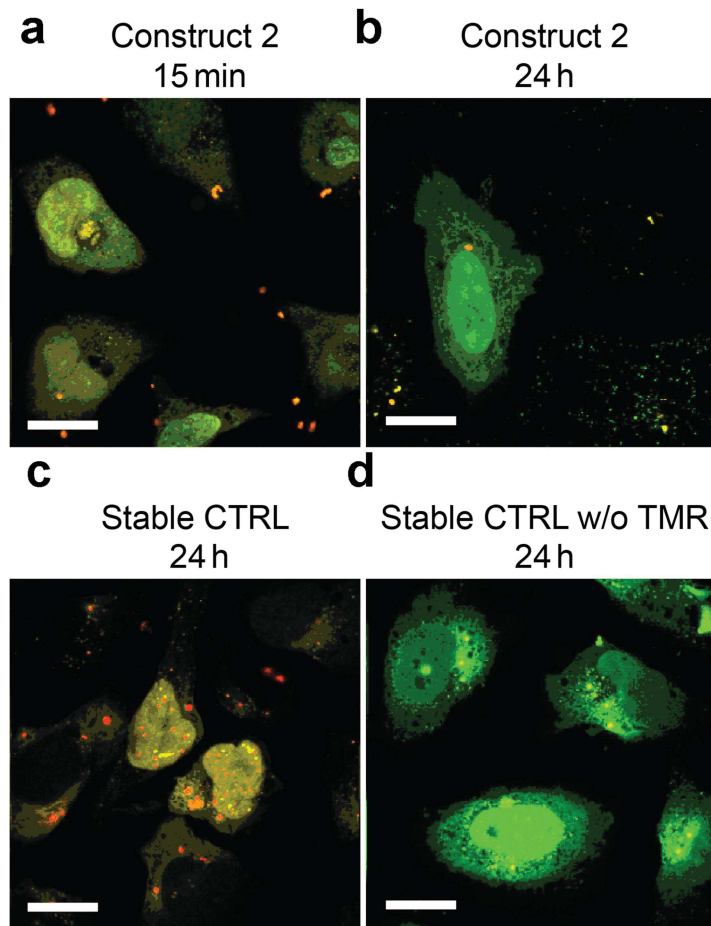


Figure 36. Intensity based FRET images. Donor (green) and acceptor (red) signal after donor excitation is shown 15 min (a) and 24 h (b) after transfection for construct 2 and 24 h after transfection for the stable control with (c) and without (d) acceptor dye (TMR). The scale bar is 20 μm . The measurements were performed by Waldemar Schrimpf (Department of Physical Chemistry, LMU).

In order to investigate the degradation of the RNAs, the distribution of the pixels of the different patterns at different time points were plotted (Figure 37 and Figure 38a-d) and the average value was extracted using a Gaussian fit (Figure 38e). The pixel positions along the line (i.e. the average pixel lifetimes) can also be depicted in the images using a color code (Figure 37). Blue represents a short fluorescence lifetime corresponding to an intact construct. Red represents a long lifetime indicating a degraded oligonucleotide.

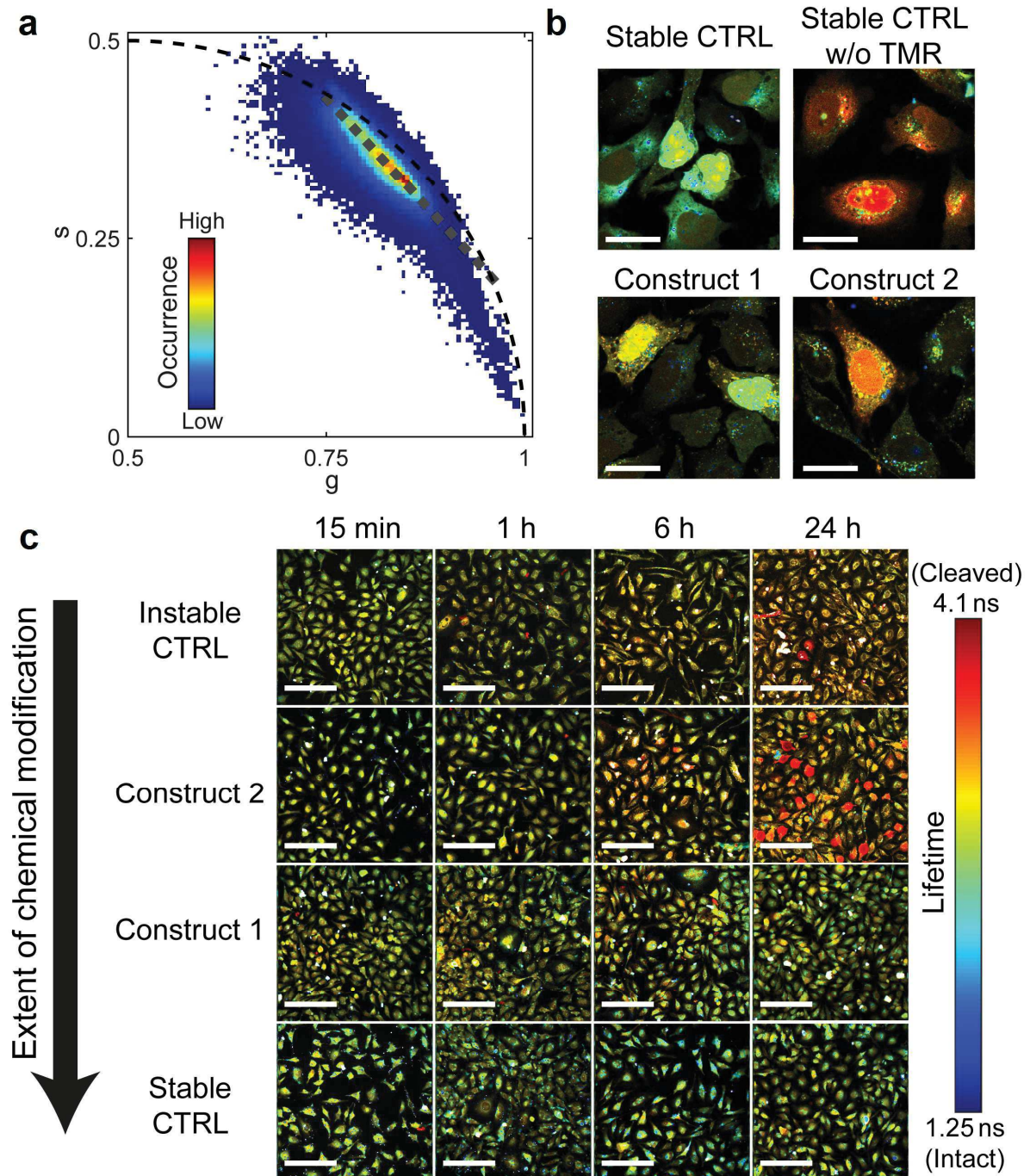


Figure 37. Phasor FLIM analysis in cultured HeLa cells. (a) The phasor histogram of images shown in panel b and c. The grey dotted line indicates the axis used for color-coding the FLIM images in b and c. (b) FLIM images 24 h after transfection of the stable control RNA, construct 1, construct 2 and the stable control RNA without TMR in cultured HeLa cells. The scale bar is 30 μm . (c) FLIM images for all measured constructs and time points. These measurements are the same as those shown in Figure 33. The scale bar is 200 μm . The measurements were performed by Waldemar Schrimpf (Department of Physical Chemistry, LMU).

The dual-labelled stable control and construct 1 do not show any change in lifetime over the whole time course of 24 h (Figure 37c rows 3 and 4). This lack of degradation also explains the strong accumulation of the constructs within the cells. However, taking into account the fact that construct accumulation is a little stronger for the stable control, one can assume that there is a slight degradation of construct 1, which increases the ability of the cells to dispose of the oligonucleotide. Considering the fact that the cells are constantly fed with intact constructs from endosomes and aggregates, it is not surprising that the lifetime experiment reveals no significant differences (Figure 38a and b) as, at any point, the amount of degraded RNAs is negligible compared to that of the intact constructs. Construct 2 nicely shows an increase in lifetime over the time course, corresponding to degradation of the construct. Especially highly fluorescent cells have a long lifetime, originating from accumulation of the degraded oligonucleotide (Figure 37c row 2). For the instable control, the observed fluorescence lifetime increases slower than for the more stable construct 2 (Figure 38 c and d). However, considering the very low fluorescence intensity of the control, it is most likely that the oligonucleotides are degraded and depleted from the cells so fast that the lifetime values mostly originate from intact constructs that have just been released into the cytosol. In contrast, construct 2 Atto488 still has a stabilized four nucleotides stretch of RNA attached, which is not as easily expelled from the cells as free dye. This is supported by the fact that the fluorescence intensity of construct 2 images is significantly higher than that of the instable control images.

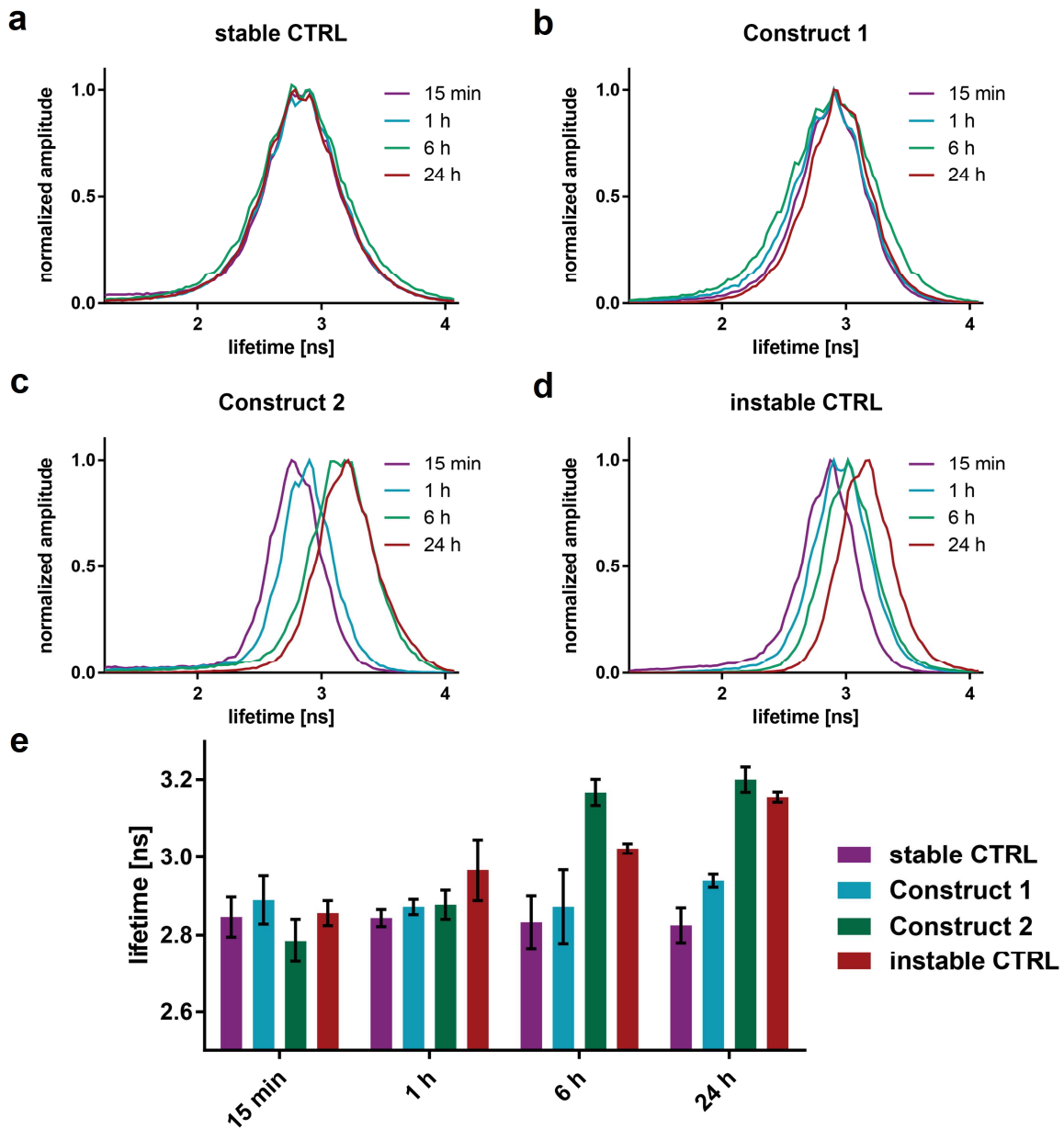


Figure 38. Quantification of the fluorescence lifetime measurements. (a-d) Distribution of the pixels along the line connecting the mono-exponential decays at 4.1 ns and at 1.25 ns in the phasor plot for the four modification patterns. (e) Summary of the average fluorescence lifetimes of the cell populations shown in panels a-d using a Gaussian fit to the distribution. The error bars represent the standard deviations of three independent measurements. The measurements were performed by Waldemar Schimpf (Department of Physical Chemistry, LMU).

Short lifetimes that originate from FRET and represent a high construct integrity can be distinguished from unspecific quenching effects by testing also the control sample where the stable control pattern was conjugated only to Atto488. Since no FRET can occur, any differences in lifetime observed are due to unspecific quenching. As

expected, the fluorescence lifetime was long in the cytosol as well as the nucleus after 1 h and 24 h (Figure 39).

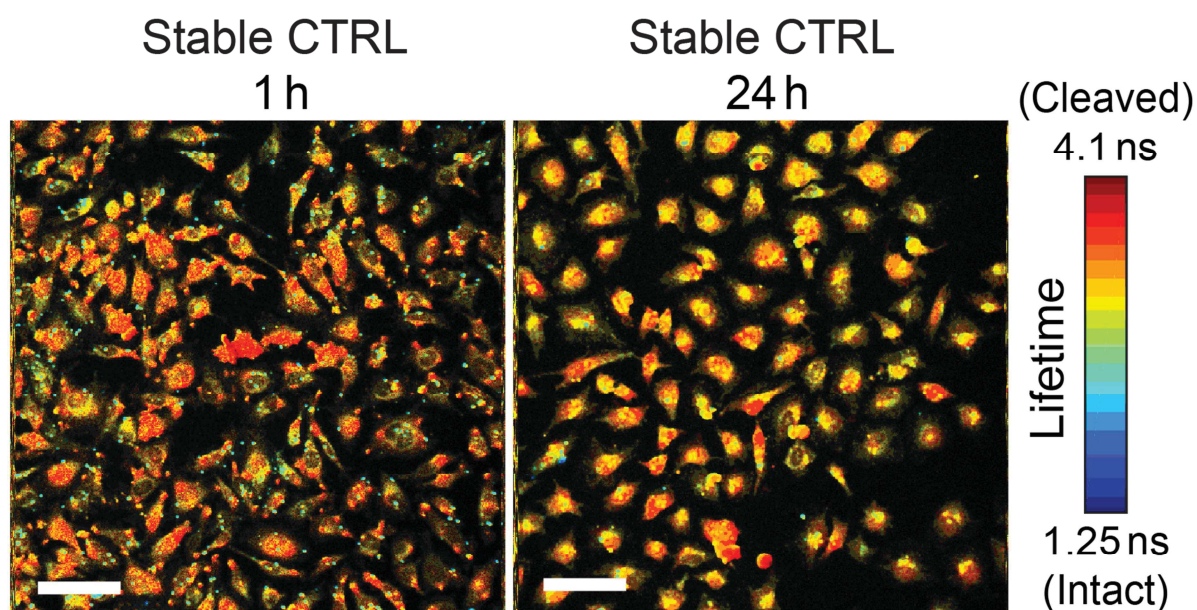


Figure 39. Fluorescence lifetime imaging microscopy of the completely stabilized oligonucleotide conjugated to Atto488 only. The fluorescence lifetime was measured 1 h and 24 h after transfection to HeLa cells. The scale bar is 100 μm . The measurements were performed by Waldemar Schrimpf (Department of Physical Chemistry, LMU).

The small bluish dots in the cytosol are visible for all constructs and most probably possess a high density of Atto488 leading to quenching through aggregation (Figure 35 and Figure 36). Possible sources are endosomes that have not yet released the constructs or polyplexes that have not disassembled. Consequently, as soon as the oligonucleotides are liberated into the cytosol or the nucleus, a decreased lifetime can be assigned to FRET originating from an intact construct.

In general, the measured lifetime values can be explained by a balance originating from the release of intact RNA, its degradation and subsequent depletion from the cells. Longer stretches of nucleotides accumulate in the cells and are transported into the nucleus when the cells are transfected with high efficiency. With decreasing length of the stabilized RNA stretch, depletion from the cells is favored.

4. Conclusions

4.1. DNA as a tunable adaptor for siRNA polyplex stabilization and functionalization

This chapter has been partly adapted from:

Philipp Heissig, Philipp M. Klein, Philipp Hadwiger, Ernst Wagner, DNA as tunable adaptor for siRNA polyplex stabilization and functionalization, Molecular Therapy Nucleic Acids (2016), 5, e288

This study demonstrates how siRNA can be extended by DNA adaptors to improve complex formation with sequence defined cationic oligomers, resulting in improved gene silencing efficiency. Several DNA/siRNA nanostructures ranging from DNA extension of one siRNA up to structures where two to ten siRNA units are merged into one construct were tested. Delivery could be improved remarkably after complexation with the three-armed cationic oligomer **689**. Interestingly, the larger structures containing multiple siRNAs were less potent than the simple ones with one or two siRNA units. A possible reason for this is that a linear structure conjugated to only one siRNA is easier accessible by the RISC complex. The observed key criterion for efficacy was the simple extension of siRNA with DNA to provide a sufficient number of negative charges.

However, larger structures might have advantages over the linear constructs when delivered without a transfection agent. Without complexation with cationic oligomers, the linear structures are prone to degradation by nucleases. The compact organization of origamis or polyhedrons makes the constructs less accessible for nucleases due to steric hindrance.

A step-by-step extension of a single siRNA could show that a prolongation of up to 181 DNA nucleotides results in a significant improvement of transfection efficiency with oligomer **689**. In polyplexes with other transfection agents, the siRNA might have a different optimal DNA extension length. But as the canonical siRNA format is constrained to 21 to 23 base pairs, it is unlikely that this represents the optimum. Therefore DNA extension of siRNA might have advantages in many formulations.

The optimal extension length however has to be evaluated for each delivery agent separately.

An additional finding was that a 3' DNA extended siRNA passenger strand is advantageous over a 5' extended one. Probably 5' DNA extension disturbs RISC loading or passenger strand removal. An influence of differences in secondary structure formation of the 3' and the 5' extension being responsible for this effect is unlikely, as the benefit of the 3' extended structures is also present when the extension is hybridized to a DNA backbone strand. So when conjugating siRNA to DNA, the 3' end of the passenger strand should be chosen as attachment site. Figuring out the reason behind this would go beyond the scope of this work.

The differences between 3' and 5' passenger strand extension indicates that steric hindrance is an issue to consider even for the simple structures, which carry only an 18 nucleotides extension. To overcome this limitation a reducible disulfide linker was introduced between the 5' siRNA passenger strand and the DNA extension that should liberate the siRNA from the DNA adaptor in the cytosol. With this strategy, it was possible to enhance the performance of the 5' extension constructs to the level of their 3' counterparts. Hence, if siRNA should be modified on both ends of the passenger strand a reducible conjugation should be considered for the 5' terminus. However, including bioreducible disulfides comes along with a possible destabilization during therapeutical application. Even before the nanoparticle has entered the cell, extracellular Glutathione might promote disulfide reduction and exchange [115]. Furthermore, disulfides have to be handled with care during synthesis as they are instable in a reducing environment.

Eventually we could lift the findings to a more general level as DNA extension of siRNA is also beneficial when using linear PEI as transfection agent. This is well in agreement with the previous finding that showed enhanced activity of linear PEI when using sticky siRNA [52].

It was assumed that the dominating reason for an improved transfection efficiency of the nanostructures is their better complexation with polycations. Consequently the question was asked if this finding can be reproduced for oligomers which form already stable particles with canonical siRNA. Lipo-oligomer **454** containing fatty acids and tyrosines for polyplex stabilization was used as a model [32]. Transfection efficiency could not be further improved by DNA extension of siRNA. The already

known high siRNA polyplex stability apparently makes an additional stabilizing effect by DNA extension dispensable.

Importantly, it was also shown that a DNA backbone strand cannot only be used for extension or connection of multiple siRNAs, but also to include other functional domains in a very simple way. Thiolated DNA extensions can be conjugated to any thiol containing functional molecule. Through hybridization with the DNA backbone strand the functional unit can be linked to siRNA. As a proof of concept, the endosomolytic peptide INF7 was conjugated *via* a 79 nucleotides DNA adaptor to a siRNA. The INF7-modified DNA backbone strand, which can be further optimized in terms of length and structure for each application, improved transfection efficiency and polyplex stability with the multifunctional oligomer **356**.

This strategy resulted in a straightforward construction of defined folate-receptor targeted siRNA polyplexes containing all key elements for functional delivery, including particle surface shielding by polyethylene glycol, bioreversible stabilization by disulfide bonding, folate as receptor-targeting ligand, and INF7 for endosomal escape. The advantage of this strategy is the simplicity of how complex structures can be assembled out of building blocks. Synthesis is facilitated as the building blocks are constructed independently from each other (in this case the siRNA and the INF7 peptide). Various combinations of the functionalized DNA strands can be achieved simply by designing the sequences of the backbone. Assembly requires nothing but mixing the building blocks and the backbone, heating and slowly cooling the solution to room temperature, which makes a final purification dispensable.

Even though this work is providing an overview over extending siRNA for better polyplex stabilization, plenty of possibilities still remain to be examined.

This includes for example the effect of replacing the DNA adaptors with RNA. RNA is structurally more flexible than DNA, which could have an impact on complexation with polycations. Furthermore, RNA is degraded faster than DNA which might improve intracellular siRNA availability, but decrease extracellular nanostructure stability. It would also be interesting to investigate if secondary structure of the single-stranded extensions influences polyplex formation. The difference between stretches containing a single base unable to hybridize could be compared with strands that form extensive secondary structures.

In summary, the current work emphasizes that designing polyplexes for siRNA delivery can not only be accomplished by optimization of the cationic carrier, but also by modification of the siRNA itself. DNA is a highly suitable backbone for improving stability of the polyplexes and for functionalization of the siRNA.

4.2. Localization and integrity of small single-stranded RNA

This chapter has been partly adapted from:

Philipp Heissig, Waldemar Schrimpf, Philipp Hadwiger, Ernst Wagner, Don Lamb, Monitoring integrity and localization of modified single-stranded RNA oligonucleotides by ultrasensitive fluorescence methods, PLOS ONE, in press.

The stability of short single-stranded RNA oligonucleotides modified with phosphorothioates, 2'-O-Me and 2'-F was compared in cellular extracts and in cultured cells. By evaluating the degradation with FCS, FCCS and FRET (both intensity and fluorescence lifetime based) in cell extracts, it was concluded that each methodology provides distinct information on the behavior of the two-dye labelled constructs, which is indispensable to understand the fate of those RNAs. With FCCS, the integrity of the connection between the two dyes is monitored with very high sensitivity. Additional information on interactions with cellular components is detected by FCS, but at the expense of sensitivity for RNA degradation. FRET is not only sensitive towards construct cleavage, but can also detect conformational changes as FRET efficiency depends on the distance between the two dyes. All techniques were necessary to minimize biases in the analysis from unspecific effects like aggregation, interactions with cellular components, quenching or conformational changes. Taking the results from the four techniques together, the non-modified oligonucleotide was on average degraded 2.2 times faster than the construct with the modified ends (construct 2) and 8.3 times faster than the almost completely modified construct 1. A completely stabilized stable control was not degraded in cell extracts. These findings are in good agreement with previous works on chemically modified RNAs [116].

Fluorescence lifetime measurements in cells in culture revealed interesting information on modification dependent integrity and localization of the oligonucleotides. It was concluded that non-stabilized single-stranded RNA oligonucleotides are degraded before a significant accumulation of the constructs can occur. For the stabilized constructs, on the other hand, intracellular fluorescence intensity increased with the extent of modification. Construct 2, with only a few modifications, showed no continuous increase in fluorescence intensity, but the equilibrium concentration was significantly higher than for the instable control. For construct 1 and the stable control, however, the release of the constructs into the cytosol far exceeded their degradation and depletion, leading to an accumulation over time. The short, non-modified region in construct 1 slightly decelerated the accumulation within the cells. Furthermore, in cells displaying a high fluorescence intensity, the oligonucleotides were transported into the nucleus. A high transfection rate is a prerequisite for the domination of the nuclear translocation mechanism over the depletion mechanism.

The lifetime of the constructs in living cells can be explained by a balance between release of the intact constructs from endosomes and polyplexes, degradation by RNases and subsequent depletion of the fluorophores from the cells. The difference of construct 1 and the stable control observed for the fluorescence intensities has no significant effect on the lifetime measurements, since the small contribution of the cleaved constructs is drowned out by the majority of intact RNAs. Construct 2 transfected cells reached a plateau in lifetime after 6 h with a mean fluorescence lifetime that is ca. 0.35 ns longer than for the stable control. The slower increase in the fluorescence lifetime over time for the instable control can be attributed to the fast complete degradation and depletion of the dyes from the cells directly after their release into the cytosol. The lifetime values mostly originated from the few intact constructs immediately after their liberation.

Taken together considering also the results from the cell extract measurements, it was concluded that a fully PS modified backbone and alternating 2'-O-Methyl and 2'-Fluoro modifications provide complete resistance towards nuclease activity for single-stranded oligonucleotides under the experimental conditions. A single unmodified region accelerates degradation and slightly reduces accumulation, but still shows highly increased RNase resistance when compared to non-modified RNA. Stability

decreases with the length of the stretch of unmodified nucleotides as demonstrated by the difference between construct 1 and construct 2.

With FLIM, information on the endosomal release, liberation from polyplexes and localization dependent stability of any double-labelled construct after its transfection was obtained. Hence, this technique can be a useful tool to understand more about the behavior of transfected oligonucleotides and their dependency on different chemical modification patterns. The information on localization-dependent integrity and availability can be used to figure out the bottlenecks of oligonucleotide delivery and help to specifically improve the functionality of a carrier.

5. Summary

Over the last decades, various potential RNA therapeutics have been developed. Even though their mechanism of action is mostly directed by complementary base pairing, the applications are versatile. What makes the approach so powerful is that one can interfere with almost any cellular process by simply selecting the appropriate sequence. The most prominent examples are double-stranded siRNAs or microRNAs which downregulate mRNA through the RNA interference mechanism. However, also single-stranded nucleic acids can act as antisense oligonucleotides and disturb almost any stage of mRNA processing coding for the protein of interest.

The difficulty that comes along with nucleic acid therapeutics is the functional delivery to the intracellular site of action. A promising approach is the complexation of the negatively charged nucleic acids with cationic oligomers, which not only neutralize the charge of the complex, but can be used to incorporate shielding, targeting and endosomolytic domains. The carrier can be optimized with respect to stability and functionality according to its application. However also the oligonucleotide offers a level for fine-tuning the nanoparticle, as it can easily be extended, chemically modified or functionalized by itself.

The first part examined how DNA can be used to extend and functionalize siRNA for improved polyplex stability and transfection efficiency with the three-armed cationic oligomer **689**. Already an 18 nucleotides DNA extension increased polyplex stability and silencing potential significantly. Joining several siRNAs into one construct did not increase reporter protein downregulation compared to the single siRNA containing equivalents. Gradually extending siRNA with double-stranded DNA enhanced the transfection efficiency until a plateau at 181 nucleotides. The beneficial effect of the extensions was reproduced with linear polyethylenimine as transfection agent. In contrast, with lipo-oligomer **454** the DNA extensions had no positive effect, as the fatty acid-induced stabilization of the polyplexes is already sufficient with canonical siRNA. Lastly, siRNA was successfully functionalized with the endosomolytic peptide INF7 *via* a DNA adaptor. This proved that the direct modification of siRNA with DNA is a very useful tool for polyplex stabilization and functionalization, as it can be easily optimized by varying the length, structure and conjugated functional units.

The second part focused on the stability and localization of small RNAs after exposure to cellular environment. More precisely, the behavior of four single-stranded dual-fluorophore labelled RNA oligonucleotides, which were chemically stabilized to a different extent, was tested. Firstly, the degradation of those constructs was monitored in HeLa cell extracts with different ultrasensitive fluorescence methods like fluorescence correlation spectroscopy, fluorescence cross-correlation spectroscopy and Förster resonance energy transfer. The extent of chemical modification correlated with the degradation rate. Considering only one technique leads to misinterpretation of the results due to unspecific effects like quenching, aggregation or conformational changes. Secondly, the localization dependent integrity of the four oligonucleotides was examined in HeLa cells with fluorescence lifetime imaging microscopy after transfection with a cationic transfection agent. The extent of chemically stabilizing RNA modification correlated with integrity and an increased cellular accumulation. Especially the cells that were transfected with high efficiency transported the oligonucleotides into the nucleus. Overall, the observed lifetime values can be explained by a balance between uptake of the constructs from endosomes, degradation by cellular nucleases and depletion from the cells, which is favored when the RNA is removed from the dyes.

6. Appendix

6.1. Abbreviations

2'-F	2'-Fluoro
2'-O-Me	2'-O-Methyl
ACF	Autocorrelation function
Ago	Argonaute
bb	Backbone
bp	Base pair
CTRL	Control
DMEM	Dulbecco's modified eagle medium
DMSO	Dimethylsulfoxide
DNA	Desoxyribonucleic acid
ds	Double-stranded
DTNB	5,5'-Dithiobis-(2-nitrobenzoic acid
DTT	Dithiothreitol
EC50	Half maximal effective concentration
EDTA	Ethylenediamine tetraacetic acid
eGFP	Enhanced green fluorescent protein
EtOH	Ethanol
FBS	Fetal bovine serum
FCS	Fluorescence correlation spectroscopy
FCCS	Fluorescence cross-correlation spectroscopy
FDA	Food and drug administration
FLIM	Fluorescence lifetime imaging microscopy
FoIA	Folic acid
FRET	Förster resonance energy transfer
HBG	HEPES buffered glucose
HEPES	4-(2-Hydroxyethyl)-1-piperazineethanesulfonic acid
HPLC	High performance liquid chromatography
INF7	Endosomolytic peptide #7 derived from influenza HA2
IRF	Instrument response function
KCl	Potassium chloride

LinA	Linoleic acid
IPEI	Linear polyethylenimine
miRNA	microRNA
mRNA	Messenger RNA
MTT	3-(4,5-dimethylthiazol-2-yl)-2,5-diphenyltetrazolium bromide
N/P ratio	Amine/phosphate ratio
NA	Numerical aperture
NaCl	Sodium chloride
NHS	N-hydroxysuccinimid
nt	Nucleotides
ov	Overhang
PAGE	Polyacrylamide gel electrophoresis
pcv	Packed cell volume
PEG	Polyethylene glycol
PEI	Polyethylenimine
PIE	Pulsed interleaved excitation
PMSF	Phenylmethanesulfonyl fluoride
PNPase	Polynucleotide phosphorylase
PS	Phosphorothioate
RISC	RNA induced silencing complex
RNA	Ribonucleic acid
RNAi	RNA interference
Rnase	Ribonuclease
RPMI medium	Roswell Park Memorial Institute medium
RT	Room temperature
siRNA	Small interfering RNA
ss	Single-stranded
SS	Disulfide
Stp	Succinoyl-tetraethylene pentamine
TBE	Tris/borate/EDTA
TCEP	Tris(2-carboxyethyl)phosphine
TEMED	Tetramethylethylenediamine
TMR	Tetramethylrhodamine
UTR	Untranslated region

6.2. Additional methods

6.2.1. Intensity FRET analysis

For the intensity based FRET analysis, the FRET efficiency E was calculated according to equation S1:

$$E = \frac{(I_{GR} - \beta \cdot I_{GG} - \alpha \cdot I_{RR})}{\gamma \cdot I_{GG} + (I_{GR} - \beta \cdot I_{GG} - \alpha \cdot I_{RR})} \quad (S1)$$

where I_x denotes the fluorescence intensity in channel x . The individual channels were GG and GR for the green and red fluorescence after excitation with the 475 nm laser, respectively, and RR for the red signal after 565 nm excitation. α represents the direct excitation of tetramethylrhodamine at 475 nm excitation and β stands for the spectral cross-talk of Atto488 into the red channel. Using single dye controls, these values were determined to be 7.4 % for α and 13 % for β for the setup and measurement parameters used for this manuscript. γ , the parameter accounting for the different detection efficiency in the green and the red channels, could not be determined for the setup and was assumed to be equal to unity. However, varying the parameter within a reasonable range showed no significant effect on the measured degradation times. The FRET efficiency was calculated in 5 min intervals for the first hour and subsequently in 10 min intervals. The data was normalized to the initial data point.

6.2.2. Lifetime FRET analysis

For analyzing fluorescence lifetime based FRET, the phasor approach was used [113, 114]. Calculations were performed using the home written software package PAM. Here, each 10 min of the signal in the green channel was divided into 2500 individual segments and, for each segment, the phasor coordinates were calculated. To account for the instrument response function, the data were referenced using an Atto488 carboxylic acid solution. The division into 2500 was done in order to be able to remove the influence of bright aggregates on the measured fluorescence lifetime.

In order to be able to extract the fraction of molecules from the phasor positions, a simple two-component system was assumed. The first component consists of intact RNA exhibiting FRET and therefore a reduced fluorescence lifetime for the donor molecule, while the degraded RNA fragments constitute the second species showing no FRET signal and a longer fluorescence lifetime. During the experiment, ongoing degradation changes the ratio between the two components but the individual lifetimes stay the same. In the phasor plot, such a shift in fraction results in a straight line connecting the two base components. The relative contribution of the individual species can then be extracted from the exact position on this line.

In practice, the lifetimes of both the intact and degraded species were not known *a priori*. To get these values, a line was extrapolated from the trajectory of the phasor coordinates during the measurement. The two intersects of this line with the universal circle were assumed to be the phasors of the base components. The lifetimes associated with these components varied slightly between the different species, but were generally around 1.2 ns for the cleaved species and 3.5 ns for the intact species. The later corresponds well to the lifetime measured for the control with just the donor fluorophore. From the center position of the 2500 segments, the relative photon contribution of these components was calculated. Finally, this photon contribution was further corrected for the reduced brightness of the intact species due to FRET resulting in the fraction of intact RNA. The relative brightness was estimated from the ratio of the fluorescence lifetime.

6.2.3. FCS and FCCS analysis

The auto- and cross correlation curves were calculated from the photon traces using the software package PAM. In the first hour of the measurement, correlation curves were calculated for every 5 min, afterwards for every 10 min.

The auto-correlations were fit with a two-component free diffusion model, assuming a 3D Gaussian shape:

$$G_{ACF}(\tau) = \left(1 + \frac{T}{1-T} \cdot e^{-\frac{\tau}{t_T}}\right) \cdot \frac{\gamma}{(N_{Fast} + \varepsilon \cdot N_{Slow})^2} \cdot \left(\frac{N_{Fast}}{\left(1 + \frac{\tau}{t_{Fast}}\right) \cdot \sqrt{1 + \frac{\tau}{p^2 \cdot t_{Fast}}}} + \frac{\varepsilon^2 \cdot N_{Slow}}{\left(1 + \frac{\tau}{t_{Slow}}\right) \cdot \sqrt{1 + \frac{\tau}{p^2 \cdot t_{Slow}}}} \right) + G(\infty) \quad (S2)$$

Here, T and t_T denote the dark state fraction and correlation time, respectively. N_i represents the average number of molecules in the focus for the slow or the fast component, while t_i denotes their diffusion times. γ is the shape factor of a 3D Gaussian profile and corresponds to 0.35355. The parameter p is the ratio between the axial and lateral focus size. To relate the amplitudes of the two components into number of molecules, the difference in molecular brightness of the two species has to be taken into account. Thus, the relative brightness ε caused by quenching of the intact construct due to FRET needs to be used. It is estimated as the ratio of the lifetimes of the quenched and the unquenched states as given by the lifetime FRET analysis mentioned above.

The slow component was assumed to represent the intact construct, while the fast component corresponds to the degraded fragments. Based on the N_i , the fraction of intact RNA was calculated for the green channel (GG) and the red channel after 565 nm excitation (RR).

The cross-correlation curves were fit with a simplified model using only a single component and no dark state term:

$$G_{CCF}(\tau) = \frac{\gamma}{N_{cc}} \cdot \frac{1}{\left(1 + \frac{\tau}{t}\right) \cdot \sqrt{1 + \frac{\tau}{p^2 \cdot t}}} + G(\infty) \quad (\text{S3})$$

Based on the N_i from the auto- and cross-correlation functions, the fraction of intact RNA was calculated according to:

$$F_{slow} = \frac{\sqrt{(N_{fast,GG} + N_{slow,GG}) \cdot (N_{fast,RR} + N_{slow,RR})}}{\varepsilon \cdot N_{cc}} \quad (\text{S4})$$

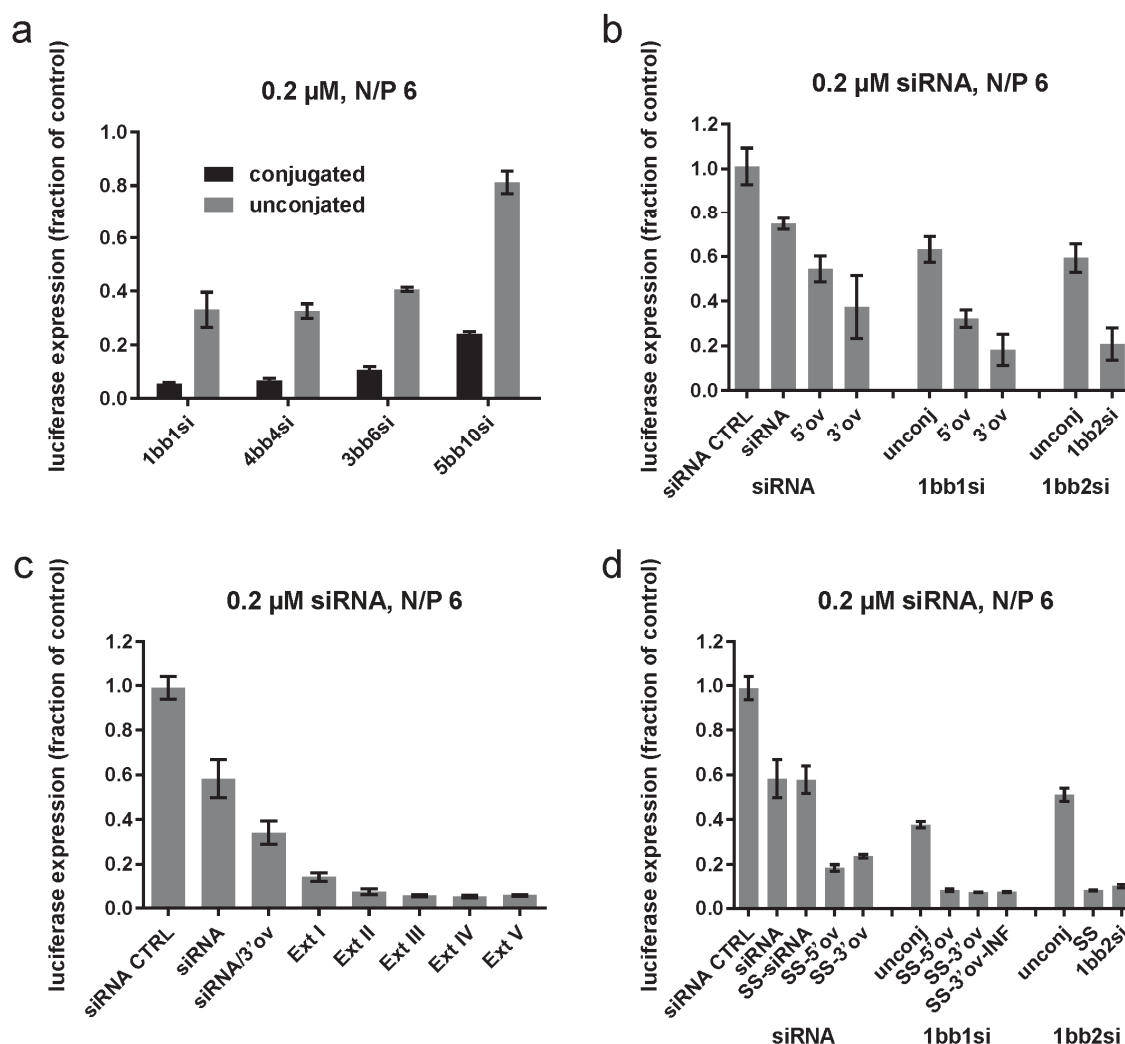
The parameter ε again corrects for the decreased brightness of the intact species.

6.2.4. FLIM analysis

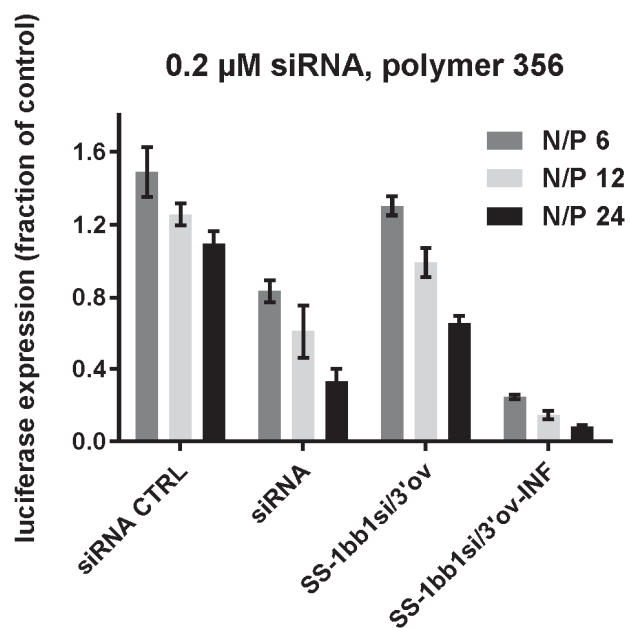
The phasor analysis for experiments on fixed cells was done in much the same way as for the lifetime based FRET measurements in cellular extracts. Pixels with intensities below a threshold of 200 photons were omitted from further analysis, thus eliminating the influence of the regions around the cells and limiting the influence of

auto-fluorescence. An upper threshold of 1000-2000 photons was also applied to remove RNA aggregates from the analysis. As described above, a line connecting the phasors of the degraded and the intact species was extrapolated. A histogram was generated from the positions of the individual pixel along that line (Figure 38a-d) that was subsequently fit with a Gaussian curve to extract the average lifetime (Figure 38e).

6.3. Appendix figures



Appendix Figure 1. Reproduction of the luciferase knockdown experiments at a constant N/P ratio of 6 with oligomer 689. The (a) star-shaped structures, the (b) substructures of 1bb2si, the (c) step-by-step extended structures and the (d) bioreducible structures were transfected with oligomer 689 at a constant N/P ratio of 6.



Appendix Figure 2. Reproduction of the luciferase knockdown experiments at a constant N/P ratio with oligomer 356. The effect of INF7 on transfection efficiency was examined at a constant N/P ratio of 6, 12 and 24.

6.4. Publications

Heissig P, Klein PM, Hadwiger P, Wagner E, *DNA as a Tunable Adaptor for siRNA Polyplex Stabilization and Functionalization*. Mol Ther Nucleic Acids, 2016, 5: p. e288.

Müller K, Klein PM, **Heissig P**, Roidl A, Wagner E, *EGF receptor targeted lipopolyplexes for antitumoral siRNA and miRNA delivery*. Nanotechnology, 2016, 27(46): p. 464001.

Heissig P, Schrimpf W, Hadwiger P, Wagner E, Lamb DC, *Monitoring integrity and localization of modified single-stranded RNA oligonucleotides using ultrasensitive fluorescence methods*, PLOS ONE, in press.

6.5. Poster presentations

Multifunctional RNA nanoagents as miR sensors and effectors; **Heissig P**, Schrimpf W, Müller K, Lamb DC, Wagner E, SFB 1032 meeting, München, Germany, January 2016

microRNA-200c and molecular nanoagents; **Heissig P**, Schrimpf W, Müller K, Lamb DC, Wagner E, SFB 1032 meeting, Altötting, Germany, February 2015

microRNA responsive switches via chemically modified microRNA target sequence conjugates, **Heissig P**, Schrimpf W, Lamb DC, Wagner E, Nanosciences: Great Adventures on Small Scales, CeNS Workshop, Venice, Italy, September 2013

Molecular nanoagents utilizing the intracellular microRNA machinery for switching functions in cells; **Heissig P**, Müller K, Wagner E; SFB 1032 retreat, February 2013

7. References

1. Lee, R.C., R.L. Feinbaum, and V. Ambros, *The C. elegans heterochronic gene lin-4 encodes small RNAs with antisense complementarity to lin-14*. Cell, 1993. **75**(5): p. 843-54.
2. Reinhart, B.J., et al., *The 21-nucleotide let-7 RNA regulates developmental timing in Caenorhabditis elegans*. Nature, 2000. **403**(6772): p. 901-6.
3. Lagos-Quintana, M., et al., *Identification of novel genes coding for small expressed RNAs*. Science, 2001. **294**(5543): p. 853-8.
4. Fire, A., et al., *Potent and specific genetic interference by double-stranded RNA in Caenorhabditis elegans*. Nature, 1998. **391**(6669): p. 806-11.
5. Elbashir, S.M., et al., *Duplexes of 21-nucleotide RNAs mediate RNA interference in cultured mammalian cells*. Nature, 2001. **411**(6836): p. 494-8.
6. Hammond, S.M., et al., *An RNA-directed nuclease mediates post-transcriptional gene silencing in Drosophila cells*. Nature, 2000. **404**(6775): p. 293-6.
7. Hutvagner, G., et al., *A cellular function for the RNA-interference enzyme Dicer in the maturation of the let-7 small temporal RNA*. Science, 2001. **293**(5531): p. 834-8.
8. Carthew, R.W. and E.J. Sontheimer, *Origins and Mechanisms of miRNAs and siRNAs*. Cell, 2009. **136**(4): p. 642-55.
9. Tomari, Y., et al., *A protein sensor for siRNA asymmetry*. Science, 2004. **306**(5700): p. 1377-80.
10. Guo, L. and Z. Lu, *The fate of miRNA* strand through evolutionary analysis: implication for degradation as merely carrier strand or potential regulatory molecule?* PLoS One, 2010. **5**(6): p. e11387.
11. Liu, J., et al., *Argonaute2 is the catalytic engine of mammalian RNAi*. Science, 2004. **305**(5689): p. 1437-41.
12. Lee, Y., et al., *The nuclear RNase III Drosha initiates microRNA processing*. Nature, 2003. **425**(6956): p. 415-9.
13. Lund, E., et al., *Nuclear export of microRNA precursors*. Science, 2004. **303**(5654): p. 95-8.
14. Lewis, B.P., C.B. Burge, and D.P. Bartel, *Conserved seed pairing, often flanked by adenosines, indicates that thousands of human genes are microRNA targets*. Cell, 2005. **120**(1): p. 15-20.
15. Wittrup, A. and J. Lieberman, *Knocking down disease: a progress report on siRNA therapeutics*. Nat Rev Genet, 2015. **16**(9): p. 543-52.
16. Vicentini, F.T., et al., *Delivery systems and local administration routes for therapeutic siRNA*. Pharm Res, 2013. **30**(4): p. 915-31.
17. Ng, E.W., et al., *Pegaptanib, a targeted anti-VEGF aptamer for ocular vascular disease*. Nat Rev Drug Discov, 2006. **5**(2): p. 123-32.
18. Bobbin, M.L. and J.J. Rossi, *RNA Interference (RNAi)-Based Therapeutics: Delivering on the Promise?* Annu Rev Pharmacol Toxicol, 2016. **56**: p. 103-22.
19. Judge, A.D., et al., *Sequence-dependent stimulation of the mammalian innate immune response by synthetic siRNA*. Nat Biotechnol, 2005. **23**(4): p. 457-62.
20. Kariko, K., et al., *Small interfering RNAs mediate sequence-independent gene suppression and induce immune activation by signaling through toll-like receptor 3*. J Immunol, 2004. **172**(11): p. 6545-9.
21. Boussif, O., et al., *A versatile vector for gene and oligonucleotide transfer into cells in culture and in vivo: polyethylenimine*. Proc Natl Acad Sci U S A, 1995. **92**(16): p. 7297-301.
22. Lachelt, U., et al., *Fine-tuning of proton sponges by precise diaminoethanes and histidines in pDNA polyplexes*. Nanomedicine, 2014. **10**(1): p. 35-44.
23. Akinc, A., et al., *Exploring polyethylenimine-mediated DNA transfection and the proton sponge hypothesis*. J Gene Med, 2005. **7**(5): p. 657-63.
24. Dohmen, C., et al., *Nanosized multifunctional polyplexes for receptor-mediated siRNA delivery*. ACS Nano, 2012. **6**(6): p. 5198-208.

25. Frohlich, T., et al., *Structure-activity relationships of siRNA carriers based on sequence-defined oligo (ethane amino) amides*. J Control Release, 2012. **160**(3): p. 532-41.
26. Yu, H., V. Russ, and E. Wagner, *Influence of the molecular weight of bioreducible oligoethylenimine conjugates on the polyplex transfection properties*. AAPS J, 2009. **11**(3): p. 445-55.
27. Jackson, A.L., et al., *Position-specific chemical modification of siRNAs reduces "off-target" transcript silencing*. RNA, 2006. **12**(7): p. 1197-205.
28. Wagner, E., *Polymers for siRNA delivery: inspired by viruses to be targeted, dynamic, and precise*. Acc Chem Res, 2012. **45**(7): p. 1005-13.
29. Salcher, E.E., et al., *Sequence-defined four-arm oligo(ethanamine)amides for pDNA and siRNA delivery: Impact of building blocks on efficacy*. J Control Release, 2012. **164**(3): p. 380-6.
30. Schaffert, D., et al., *Solid-phase synthesis of sequence-defined T-, i-, and U-shape polymers for pDNA and siRNA delivery*. Angew Chem Int Ed Engl, 2011. **50**(38): p. 8986-9.
31. Scholz, C., P. Kos, and E. Wagner, *Comb-like oligoaminoethane carriers: change in topology improves pDNA delivery*. Bioconjug Chem, 2014. **25**(2): p. 251-61.
32. Troiber, C., et al., *Stabilizing effect of tyrosine trimers on pDNA and siRNA polyplexes*. Biomaterials, 2013. **34**(5): p. 1624-1633.
33. Klein, P.M. and E. Wagner, *Bioreducible Polycations as Shuttles for Therapeutic Nucleic Acid and Protein Transfection*. Antioxidants & Redox Signaling, 2014. **21**(5): p. 804-817.
34. Mao, S., et al., *Influence of polyethylene glycol chain length on the physicochemical and biological properties of poly(ethylene imine)-graft-poly(ethylene glycol) block copolymer/SiRNA polyplexes*. Bioconjug Chem, 2006. **17**(5): p. 1209-18.
35. Whitehead, K.A., R. Langer, and D.G. Anderson, *Knocking down barriers: advances in siRNA delivery*. Nat Rev Drug Discov, 2009. **8**(2): p. 129-38.
36. Dohmen, C., et al., *Defined Folate-PEG-siRNA Conjugates for Receptor-specific Gene Silencing*. Mol Ther Nucleic Acids, 2012. **1**: p. e7.
37. Abourbeh, G., et al., *PolyIC GE11 polyplex inhibits EGFR-overexpressing tumors*. IUBMB Life, 2012. **64**(4): p. 324-30.
38. Zhang, W., et al., *Combination of sequence-defined oligoaminoamides with transferrin-polycation conjugates for receptor-targeted gene delivery*. J Gene Med, 2015. **17**(8-9): p. 161-72.
39. Wagner, E., et al., *Influenza virus hemagglutinin HA-2 N-terminal fusogenic peptides augment gene transfer by transferrin-polylysine-DNA complexes: toward a synthetic virus-like gene-transfer vehicle*. Proc Natl Acad Sci U S A, 1992. **89**(17): p. 7934-8.
40. Scholz, C. and E. Wagner, *Therapeutic plasmid DNA versus siRNA delivery: common and different tasks for synthetic carriers*. J Control Release, 2012. **161**(2): p. 554-65.
41. Tam, D.Y. and P.K. Lo, *Multifunctional DNA Nanomaterials for Biomedical Applications*. Journal of Nanomaterials, 2015: p. doi:10.1155/2015/765492.
42. Seeman, N.C., *Nucleic acid junctions and lattices*. J Theor Biol, 1982. **99**(2): p. 237-47.
43. Rothemund, P.W., *Folding DNA to create nanoscale shapes and patterns*. Nature, 2006. **440**(7082): p. 297-302.
44. Douglas, S.M., et al., *Rapid prototyping of 3D DNA-origami shapes with caDNAno*. Nucleic Acids Res, 2009. **37**(15): p. 5001-6.
45. Zadeh, J.N., et al., *NUPACK: Analysis and design of nucleic acid systems*. J Comput Chem, 2011. **32**(1): p. 170-3.
46. Chang, M., C.S. Yang, and D.M. Huang, *Aptamer-Conjugated DNA Icosahedral Nanoparticles As a Carrier of Doxorubicin for Cancer Therapy*. ACS Nano, 2011. **5**(8): p. 6156-6163.
47. He, Y., et al., *Hierarchical self-assembly of DNA into symmetric supramolecular polyhedra*. Nature, 2008. **452**(7184): p. 198-U41.
48. Goodman, R.P., R.M. Berry, and A.J. Turberfield, *The single-step synthesis of a DNA tetrahedron*. Chemical Communications, 2004. **12**(12): p. 1372-1373.
49. Andersen, E.S., et al., *Self-assembly of a nanoscale DNA box with a controllable lid*. Nature, 2009. **459**(7243): p. 73-U75.

50. Sacca, B. and C.M. Niemeyer, *DNA Origami: The Art of Folding DNA*. Angewandte Chemie-International Edition, 2012. **51**(1): p. 58-66.
51. de Vries, J.W., F. Zhang, and A. Herrmann, *Drug delivery systems based on nucleic acid nanostructures*. J Control Release, 2013. **172**(2): p. 467-83.
52. Bolcato-Bellemin, A.L., et al., *Sticky overhangs enhance siRNA-mediated gene silencing*. Proc Natl Acad Sci U S A, 2007. **104**(41): p. 16050-5.
53. Lee, S.H., et al., *Dual gene targeted multimeric siRNA for combinatorial gene silencing*. Biomaterials, 2011. **32**(9): p. 2359-2368.
54. Mok, H., et al., *Multimeric small interfering ribonucleic acid for highly efficient sequence-specific gene silencing*. Nature Materials, 2010. **9**(3): p. 272-278.
55. Brunner, K., et al., *Cell-penetrating and neurotargeting dendritic siRNA nanostructures*. Angew Chem Int Ed Engl. **54**(6): p. 1946-9.
56. Allison, S.J. and J. Milner, *RNA Interference by Single-and Double-stranded siRNA With a DNA Extension Containing a 3' Nuclease-resistant Mini-hairpin Structure*. Molecular Therapy-Nucleic Acids, 2014. **3**: p. e141.
57. Nakashima, Y., et al., *Branched RNA nanostructures for RNA interference*. Chemical Communications, 2011. **47**(29): p. 8367-8369.
58. Hong, C.A., et al., *Self-assembled DNA nanostructures prepared by rolling circle amplification for the delivery of siRNA conjugates*. Chemical Communications, 2014. **50**(86): p. 13049-13051.
59. Hong, C.A., et al., *Dendrimeric siRNA for Efficient Gene Silencing*. Angewandte Chemie-International Edition, 2015. **54**(23): p. 6740-6744.
60. Chang, C.I., et al., *Enhanced intracellular delivery and multi-target gene silencing triggered by tripodal RNA structures*. Journal of Gene Medicine, 2012. **14**(2): p. 138-146.
61. Lee, H., et al., *Molecularly self-assembled nucleic acid nanoparticles for targeted in vivo siRNA delivery*. Nature Nanotechnology, 2012. **7**(6): p. 389-393.
62. Kocabey, S., et al., *Cellular Uptake of Tile-Assembled DNA Nanotubes*. Nanomaterials, 2014. **5**(1): p. 47-60.
63. Yu, D.B., et al., *Single-Stranded RNAs Use RNAi to Potently and Allele-Selectively Inhibit Mutant Huntingtin Expression*. Cell, 2012. **150**(5): p. 895-908.
64. Lima, W.F., et al., *Single-Stranded siRNAs Activate RNAi in Animals*. Cell, 2012. **150**(5): p. 883-894.
65. Chorn, G., et al., *Single-stranded microRNA mimics*. RNA. **18**(10): p. 1796-804.
66. Elsner, M., *Single-stranded siRNAs for in vivo gene silencing*. Nat Biotechnol, 2012. **30**(11): p. 1063.
67. Chan, J.H., S. Lim, and W.S. Wong, *Antisense oligonucleotides: from design to therapeutic application*. Clin Exp Pharmacol Physiol, 2006. **33**(5-6): p. 533-40.
68. Inoue, H., et al., *Sequence-dependent hydrolysis of RNA using modified oligonucleotide splints and RNase H*. Nucleic Acids Symp Ser, 1987(18): p. 221-4.
69. Disterer, P., et al., *Development of therapeutic splice-switching oligonucleotides*. Hum Gene Ther, 2014. **25**(7): p. 587-98.
70. Hammond, S.M. and M.J. Wood, *Genetic therapies for RNA mis-splicing diseases*. Trends Genet, 2011. **27**(5): p. 196-205.
71. Lu, Q.L., S. Cirak, and T. Partridge, *What Can We Learn From Clinical Trials of Exon Skipping for DMD?* Mol Ther Nucleic Acids, 2014. **3**: p. e152.
72. Porensky, P.N., et al., *A single administration of morpholino antisense oligomer rescues spinal muscular atrophy in mouse*. Hum Mol Genet, 2012. **21**(7): p. 1625-38.
73. Siva, K., G. Covello, and M.A. Denti, *Exon-skipping antisense oligonucleotides to correct missplicing in neurogenetic diseases*. Nucleic Acid Ther, 2014. **24**(1): p. 69-86.
74. Bennett, C.F. and E.E. Swayze, *RNA targeting therapeutics: molecular mechanisms of antisense oligonucleotides as a therapeutic platform*. Annu Rev Pharmacol Toxicol, 2010. **50**: p. 259-93.

75. Li, Z. and T.M. Rana, *Therapeutic targeting of microRNAs: current status and future challenges*. Nat Rev Drug Discov, 2014. **13**(8): p. 622-38.
76. Krutzfeldt, J., et al., *Silencing of microRNAs in vivo with 'antagomirs'*. Nature, 2005. **438**(7068): p. 685-689.
77. Obad, S., et al., *Silencing of microRNA families by seed-targeting tiny LNAs*. Nat Genet, 2011. **43**(4): p. 371-8.
78. Ottosen, S., et al., *In vitro antiviral activity and preclinical and clinical resistance profile of miravirsin, a novel anti-hepatitis C virus therapeutic targeting the human factor miR-122*. Antimicrob Agents Chemother, 2015. **59**(1): p. 599-608.
79. Chu, R.S., et al., *CpG oligodeoxynucleotides act as adjuvants that switch on T helper 1 (Th1) immunity*. J Exp Med, 1997. **186**(10): p. 1623-31.
80. Krieg, A.M., *Therapeutic potential of Toll-like receptor 9 activation*. Nat Rev Drug Discov, 2006. **5**(6): p. 471-84.
81. Houseley, J. and D. Tollervey, *The many pathways of RNA degradation*. Cell, 2009. **136**(4): p. 763-76.
82. Sorrentino, S., *The eight human "canonical" ribonucleases: molecular diversity, catalytic properties, and special biological actions of the enzyme proteins*. FEBS Lett, 2010. **584**(11): p. 2194-200.
83. Rosenberg, H.F., *RNase A ribonucleases and host defense: an evolving story*. J Leukoc Biol, 2008. **83**(5): p. 1079-87.
84. Luhtala, N. and R. Parker, *T2 Family ribonucleases: ancient enzymes with diverse roles*. Trends Biochem Sci, 2010. **35**(5): p. 253-9.
85. Houseley, J., J. LaCava, and D. Tollervey, *RNA-quality control by the exosome*. Nat Rev Mol Cell Biol, 2006. **7**(7): p. 529-39.
86. Kulkarni, M., S. Ozgur, and G. Stoecklin, *On track with P-bodies*. Biochem Soc Trans, 2010. **38**(Pt 1): p. 242-51.
87. Nagarajan, V.K., et al., *XRN 5'-->3' exoribonucleases: structure, mechanisms and functions*. Biochim Biophys Acta, 2013. **1829**(6-7): p. 590-603.
88. Eckstein, F., *Phosphorothioate oligodeoxynucleotides: What is their origin and what is unique about them?* Antisense & Nucleic Acid Drug Development, 2000. **10**(2): p. 117-121.
89. Deleavey, G.F. and M.J. Damha, *Designing Chemically Modified Oligonucleotides for Targeted Gene Silencing*. Chemistry & Biology, 2012. **19**(8): p. 937-954.
90. Shukla, S., C.S. Sumaria, and P.I. Pradeepkumar, *Exploring Chemical Modifications for siRNA Therapeutics: A Structural and Functional Outlook*. Chemmedchem, 2010. **5**(3): p. 328-349.
91. Manoharan, M., et al., *Unique gene-silencing and structural properties of 2'-fluoro-modified siRNAs*. Angew Chem Int Ed Engl, 2011. **50**(10): p. 2284-8.
92. Pallan, P.S., et al., *Unexpected origins of the enhanced pairing affinity of 2'-fluoro-modified RNA*. Nucleic Acids Res, 2011. **39**(8): p. 3482-95.
93. Smart, N., P.J. Scambler, and P.R. Riley, *A rapid and sensitive assay for quantification of siRNA efficiency and specificity*. Biol Proced Online, 2005. **7**: p. 1-7.
94. Kopp, F., et al., *miR-200c sensitizes breast cancer cells to doxorubicin treatment by decreasing TrkB and Bmi1 expression*. PLoS One, 2012. **7**(11): p. e50469.
95. Velu, C.S. and H.L. Grimes, *Utilizing antagomiR (antisense microRNA) to knock down microRNA in murine bone marrow cells*. Methods Mol Biol, 2012. **928**: p. 185-95.
96. Fisher, T.L., et al., *Intracellular disposition and metabolism of fluorescently-labeled unmodified and modified oligonucleotides microinjected into mammalian cells*. Nucleic Acids Res, 1993. **21**(16): p. 3857-65.
97. Lorenz, P., et al., *Phosphorothioate antisense oligonucleotides induce the formation of nuclear bodies*. Mol Biol Cell, 1998. **9**(5): p. 1007-23.
98. Chen, A.K., M.A. Behlke, and A. Tsourkas, *Sub-cellular trafficking and functionality of 2'-O-methyl and 2'-O-methyl-phosphorothioate molecular beacons*. Nucleic Acids Res, 2009. **37**(22): p. e149.

99. Reif, R., F. Haque, and P. Guo, *Fluorogenic RNA nanoparticles for monitoring RNA folding and degradation in real time in living cells*. *Nucleic Acid Ther*, 2012. **22**(6): p. 428-37.
100. Krutzfeldt, J., et al., *Specificity, duplex degradation and subcellular localization of antagomirs*. *Nucleic Acids Res*, 2007. **35**(9): p. 2885-92.
101. Hirsch, M. and M. Helm, *Live cell imaging of duplex siRNA intracellular trafficking*. *Nucleic Acids Res*, 2015. **43**(9): p. 4650-60.
102. Muller, B.K., et al., *Pulsed interleaved excitation*. *Biophys J*, 2005. **89**(5): p. 3508-22.
103. Hendrix, J., et al., *Pulsed interleaved excitation fluctuation imaging*. *Biophys J*, 2013. **105**(4): p. 848-61.
104. Heissig, P., et al., *DNA as Tunable Adaptor for siRNA Polyplex Stabilization and Functionalization*. *Mol Ther Nucleic Acids*, 2016. **5**: p. e288.
105. Kos, P., et al., *Histidine-rich stabilized polyplexes for cMet-directed tumor-targeted gene transfer*. *Nanoscale*, 2015. **7**(12): p. 5350-5362.
106. Lachelt, U. and E. Wagner, *Nucleic Acid Therapeutics Using Polyplexes: A Journey of 50 Years (and Beyond)*. *Chem Rev*, 2015: p. doi:10.1021/cr5006793.
107. Wagner, E., *Effects of membrane-active agents in gene delivery*. *Journal of Controlled Release*, 1998. **53**(1-3): p. 155-158.
108. Boeckle, S., et al., *Melittin analogs with high lytic activity at endosomal pH enhance transfection with purified targeted PEI polyplexes*. *Journal of Controlled Release*, 2006. **112**(2): p. 240-248.
109. Plank, C., et al., *The Influence of Endosome-Disruptive Peptides on Gene-Transfer Using Synthetic Virus-Like Gene-Transfer Systems*. *Journal of Biological Chemistry*, 1994. **269**(17): p. 12918-12924.
110. Rio, D.C., et al., *Preparation of cytoplasmic and nuclear RNA from tissue culture cells*. *Cold Spring Harb Protoc*, 2010. **2010**(6): p. pdb prot5441.
111. Barad, O., et al., *MicroRNA expression detected by oligonucleotide microarrays: system establishment and expression profiling in human tissues*. *Genome Res*, 2004. **14**(12): p. 2486-94.
112. Foo, Y.H., et al., *Factors affecting the quantification of biomolecular interactions by fluorescence cross-correlation spectroscopy*. *Biophys J*, 2012. **102**(5): p. 1174-83.
113. Clayton, A.H., Q.S. Hanley, and P.J. Verveer, *Graphical representation and multicomponent analysis of single-frequency fluorescence lifetime imaging microscopy data*. *J Microsc*, 2004. **213**(Pt 1): p. 1-5.
114. Digman, M.A., et al., *The phasor approach to fluorescence lifetime imaging analysis*. *Biophys J*, 2008. **94**(2): p. L14-6.
115. Brulisauer, L., et al., *Tracking the bioreduction of disulfide-containing cationic dendrimers*. *Angew Chem Int Ed Engl*, 2012. **51**(50): p. 12454-8.
116. Corey, D.R., *Chemical modification: the key to clinical application of RNA interference?* *J Clin Invest*, 2007. **117**(12): p. 3615-22.

8. Acknowledgments

There are many people who contributed to my thesis on the scientific and social level. I can frankly say that I enjoyed going to the AK Wagner lab each morning.

First of all I want to thank Prof. Ernst Wagner for the opportunity to do my PhD in his working group and for encouraging me to follow up new projects. I highly appreciated his support, guidance and valuable advises during the years.

Further thanks go to Prof. Don C. Lamb and Dr. Waldemar Schrimpf for the fruitful collaboration on RNA stability.

Thanks to the whole AK Wagner group for the scientific support and the nice atmosphere. I could find new friends here, what helped me a lot to get settled in Munich.

In particular I want to thank the SFB colleagues: Philipp for the good ideas with DNA nanostructures, his oligomers and his willingness to have coffee with me and my seat neighbour Katharina for her helpfulness.

Gratitude also goes to: Wolfgang for fixing all our devices, Martina for her commitment in group events and practical courses, Dongsheng for oligomer synthesis, Philipp Hadwiger for oligonucleotide synthesis, Ursula, Anna, Miriam and Markus for keeping the lab running, Dr. Florian Kopp for introducing me into the lab and “Andi’s group” for scientific advises and always being welcome to the PhD room.

Although the scientific overlaps were only minor, my thanks go to Sören, Ruth, Claudia and Stephan for the coffee break conversations and after work activities.

Finally I want to thank Antonia for the best distraction from work that I could imagine and my parents and grandparents for their support in every respect over the years.